Strong Primary Contribution to Brown Carbon Light Absorption in Tibet and Urban Areas: Insights based on in situ measurements

Wenhui Zhao[1,2], Weiwei Hu[1,3,4*], Zhaoce Liu[1,2], Tianle Pan[1,2], Tingting Feng[1,2], Jun Wang [1,2], Yiyu Cai[1,2], Lin Liang[5,6], Shan Huang[5,6*], Bin Yuan[5,6], Nan Ma[5,6], Min Shao[5,6], Guohua Zhang[1,3,4], Xinhui Bi[1,3,4], Xinming Wang[1,3,4], Pengfei Yu[5,6]

1. State Key Laboratory of Advanced Environmental Technology, Guangzhou Institute of Geochemistry, Chinese Academy of Sciences, Guangzhou, 510640, China;

2. University of Chinese Academy of Sciences, Beijing 100049, China;

3. Guangdong–Hong Kong–Macao Greater Bay Area Environmental Pollution Research and Control Joint Laboratory, Guangzhou Institute of Geochemistry, Chinese Academy of Sciences, Guangzhou 510640, China;

4. Guangdong Key Laboratory of Environmental Resource Utilization and Protection, Guangzhou Institute of Geochemistry, Chinese Academy of Sciences, Guangzhou 510640, China;

5. College of Environment and Climate, Jinan University, Guangzhou 511443, China;

6. Guangdong–Hongkong–Macau Joint Laboratory of Collaborative Innovation for Environmental Quality, Guangzhou 511443, China

*Correspondence to: Weiweihu@gig.ac.cn; shanhuang_eci@jnu.edu.cn

Abstract

To investigate optical properties, sources, and radiative effects of brown carbon (BrC), we conducted synchronous field campaigns in the Qinghai–Tibet Plateau (Yangbajing) and urban Guangzhou in July 2022, using multi-wavelength Aethalometer (AE33) and aerosol mass spectrometer (AMS) measurements. Total aerosol and BrC light absorption coefficients at 370 nm (Abs_{total}: 1.6 ± 1.6 M m^{-1}; BrC: 0.2 ± 0.3 M m^{-1}) in Tibet were an order of magnitude lower than Guangzhou, attributed to extremely low aerosol/organic aerosol (OA) mass concentrations. However, BrC fractions in Abs_{total} (15 % vs. 21 % at 370 nm) correlated with primary OA (POA) ratios, highlighting anthropogenic emission impacts even in this clean background. Diurnal variations (morning/evening peaks) of source–specific BrC absorption were regulated by local emissions (e.g., biomass burning, traffic emission) and regional secondary formation. Source apportionment revealed primary sources (biomass burning OA (BBOA), hydrocarbon-like OA (HOA)) dominated BrC absorption (> 75 %). The mass absorption cross–section (MAC) of HOA (2.08 m^2 g^{-1} in Tibet; 2.57 m^2 g^{-1} in Guangzhou) was comparable to that of BBOA (1.11–2.54 in Tibet; 1.91 m^2 g^{-1} in Guangzhou), indicating the high light absorption capacity of BrC from fossil fuel. Integrated "simple forcing efficiency" (370–660 nm) showed primary emissions contributed > 98 % of total radiative forcing at both sites. This study advances understanding of BrC dynamics and sources in diverse environments, underscores primary sources' critical role in BrC absorption, and emphasizes the need for source–specific OA optical parameterization.

Keywords:

Brown carbon; Source apportionment; Multiple linear regression; Optical properties; Radiative forcing

1. Introduction

Light absorbing components of atmospheric aerosols comprise black carbon (BC) and light absorbing organic aerosols, known as brown carbon (BrC). The BrC exhibits significant absorption in the near-ultraviolet (300–400 nm) and visible ranges (Andreae and Gelencsér, 2006; Kirchstetter and Thatcher, 2012; Laskin et al., 2015), but it remains largely overlooked in most climate models (Chung et al., 2012). Feng et al. (2013) found that accounting for the strong absorption of BrC in model could shift the global mean direct radiative forcing of OA at the top of the atmosphere from a cooling of −0.08 Wm^{-2} to a warming of +0.025 Wm^{-2}, emphasizing the significant role of BrC in global and regional direct radiative forcing of carbonaceous aerosols. Wang et al. (2025) revealed that dark BrC, emitted by wildfires and agricultural burning, strongly absorbs solar radiation, thereby generating a radiative effect of +0.02 to +0.68 Wm^{-2}, which contributed comparable warming as BC. ~~A portion of organic aerosols (OA), categorized as "Brown Carbon (BrC)", exhibits a significant capacity to absorb radiation within the near-ultraviolet (300–400 nm) and visible range (Andreae and Gelencsér, 2006; Kirchstetter and Thatcher, 2012; Laskin et al., 2015).~~ Current ~~Global~~ global model simulation studies have demonstrated that the impact of BrC can contribute ~~contributing~~ 12–50 % of the total positive radiative forcing from

light-absorbing atmospheric aerosols~~of the total positive radiative forcing~~ and can be regionally different, which emphasizes the spatially dynamic variation of BrC and its important role in atmospheric warming (Li et al., 2025; Brown et al., 2018; Feng et al., 2013; Wang et al., 2018; Xu et al., 2024),.

In general, the source of atmospheric BrC can be categorized by direct emission (primary BrC) and secondary generation (secondary BrC) (Laskin et al., 2015). Over the past decade, primary BrC was found to be dominated by biomass burning, and the absorption capacity of BrC from fossil fuel is often neglected (Saleh, 2020)~~by non-fossil biomass burning, and the OA from fossil fuel is non-absorbing (Saleh, 2020)~~. However, more and more recent studies have shown that fossil fuels (vehicle emissions and coal combustions) are also important contributors to the BrC, which have been previously underestimated (Du et al., 2014; Kasthuriarachchi et al., 2020a; Xie et al., 2017; Huang et al., 2022; Tang et al., 2020). Wang et al. (2022b) conducted a comprehensive review of the relationship between the source and light absorption characteristics of BrC based on the measurement results in China, positing that the emission and light absorption capacity of BrC from fossil fuel combustion might be comparable to or even exceed those induced by biomass burning. This finding raises the question of how much primary fossil and non-fossil sources contribute to ambient BrC. Regarding secondary BrC, its formation involves complex gaseous, particulate, and liquid-phase reactions from diverse precursors (Laskin et al., 2015)~~This finding raises the question about how much the primary fossil and non-fossil sources contribute to the BrC in the ambient air. For secondary BrC, its formation is complex due to the complicated gaseous, particulate, and liquid phase reactions of diverse precursors (Laskin et al., 2015)~~. E.g., the nitro compounds formed through NO_3 oxidation or OH oxidation under high NO_x chemistry can lead to a significant enhancement in light absorption within the ultraviolet–visible (UV–Vis) range (Li et al., 2020; Jiang et al., 2019). Aqueous reactions of carbonyl groups with reduced nitrogenous organic compounds, such as organic amines and ammonium, are also found to be important BrC sources (Powelson et al., 2014; Tang et al., 2022).~~Aqueous reactions of carbonyl groups with reduced nitrogenous organic compounds, such as organic amines and ammonium, are also found to be important BrC sources as well (Powelson et al., 2014; Tang et al., 2022).~~

The complex sources and multi–forming pathways of BrC make its global simulation a great challenge, e.g., mass absorption cross–section (MAC), which serves as a crucial optical parameter in simulating the BrC light absorption and further its radiative forcing, is still not clear due to the impact of multiple factors. E.g., various studies have demonstrated that the BrC light absorption properties are susceptible to the sources (Tang et al., 2020), photochemical aging (Yu et al., 2016; Wong et al., 2017; Lee et al., 2014; Zhao et al., 2015), humidity (Kasthuriarachchi et al., 2020b), acidity of aerosols (Mo et al., 2017; Phillips et al., 2017), and structure of chromophores (Laskin et al., 2014; Hems and Abbatt, 2018). In general, the MAC of secondary BrC was found to be generally lower than primary sources in ambient BrC (Qin et al., 2018; Zhang et al., 2022b). Smog chamber experiments also show that the MAC of aged coal combustion emission (0.14 ± 0.08 m^2 g^{-1}) was much lower than that of primary emissions (0.84 ± 0.54 m^2 g^{-1}) (Ni et al., 2021). If the impact of the atmospheric aging on MAC is not considered in the model, the simulated BrC light absorption may be overestimated by 45 % to 128 % (Li et al., 2025). In addition, Li et al. (2025) pointed out that the uncertainty in the effective MAC of primary BrN (i.e., absorptive nitrogenous component of BrC) from anthropogenic and biomass burning has the greatest

impact (reaching ±76 % uncertainty) on the simulated BrN light absorption, highlighting the key role of source–specific MAC in the global simulation of BrC light absorption. Further clarification of the MAC of BrC from different sources in the ambient air is imperative, which can greatly help to improve the understanding of BrC light absorption and the model simulation. However, the total contribution to ambient BrC from SOA and POA and their source–specific MAC values is still ambiguous due to varied regions and circumstances, which warrants further study.

Due to the complexity and diversity of BrC, in conjunction with black carbon (BC)~~BC~~, which share similar combustion sources and complex mixture states (Bond and Bergstrom, 2006; Cappa et al., 2012; Cappa et al., 2019), it remains challenging to measure the source–specific BrC light absorption in the ambient air directly. The field measurement on ambient BrC begins with filter–based offline methods using solvent (water or organic solvent) extraction (Bond and Bergstrom, 2006). One of the limits of the offline technique is the low time resolution (usually 12–24 hours), which cannot reflect the dynamic variation of BrC during a day. As measurement techniques have developed, online methods for aerosol light absorption at different wavelengths have become available (Lack et al., 2014). The most widely used instruments include multi–wavelength Aethalometers (AE31/AE33) (Drinovec et al., 2015) and three–wavelength multi-pass Photo Acoustic Spectroscopy (PAS) (Lack et al., 2012). The online measurements can provide dynamic variations in BrC light absorption at high time resolution (1 minute). Together with source apportionment techniques, source contribution to BrC at high time resolution can be obtained, which can greatly aid in understanding the dynamic characteristics of ambient BrC and its sources.

Currently, most of the field studies focusing on ambient BrC and its sources are conducted in urban areas (Qin et al., 2018; Sun et al., 2021; Wang et al., 2019b; Zhong et al., 2023), while the BrC contribution in regional background areas is still limited. The Qinghai–Tibet Plateau (QTP) region, spanning approximately 2.5 million square kilometers, is acknowledged as the world's highest plateau (Yao et al., 2012). The atmosphere in QTP can substantially influence the climate in the world. E.g., the light–absorbing carbonaceous aerosols have been identified as one of the main factors causing the accelerated glacier retreat across the QTP (Usha et al., 2022; Kang et al., 2019; Chelluboyina et al., 2024). Compared to the southern and northern regions of the QTP, anthropogenic BC is the dominant driver of glaciers melt in the central QTP, whose radiative forcing can be up to 17 times greater than that in the southern QTP (Li et al., 2017; Ming et al., 2013). Moreover, a portion of the glaciers in central QTP are situated in the headwaters of the Yangtze River, thus, the melting directly impacts the livelihoods of millions of people downstream. The melt sensitivity of these glaciers to light-absorbing impurities (such as OA, BC and mineral dust) is not only higher than that of their southern counterparts but also carries greater regional ecological and social significance (Li et al., 2017). Although BrC is an important light-absorbing OA, limited studies on its variation and sources have been conducted in the central QTP, and most have focused on the edge of the southern region (Wang et al., 2019a; Zhang et al., 2021; Tian et al., 2023)~~Limited studies on BrC variation and its sources have been conducted in QTP, and mostly focused on the edge of the southern region of QTP (Wang et al., 2019a; Zhang et al., 2021; Tian et al., 2023)~~. We found that cross-border transport of biomass burning from South Asia was responsible for a significantly higher BrC light absorption contribution in the southern QTP than in the central and northeastern regions.

However, OA in the central QTP not only originated from long-range transport (Xu et al., 2018), but anthropogenic activities also have a significant impact on the OA sources, such as local biomass burning and fossil fuels (Xiang et al., 2024). Field measurements in the central QTP can improve our understanding of how human activities in remote regions impact light-absorbing aerosols and, consequently, glacial melting and radiative forcing.~~A cross-border transport of biomass burning from South Asia, which was responsible for a significantly higher light absorption contribution from BrC in the southern region of the QTP compared to the central and northeastern regions, was found.~~ In central QTP, only one source apportionment of the light absorption of offline water–soluble BrC was reported (Zhu et al., 2024), which showed a large contribution of biomass burning (29 %), fossil fuel combustion (17 %) and secondary contribution (54 %) to the total BrC light absorption. Further clarification is still needed. In addition, although ~~despite~~ the online BrC data have been ~~was~~ reported in the Tibet region, the dynamic variation of BrC and its source contribution is seldom ~~seldomly~~ shown (Zhang et al., 2021; Wang et al., 2024; Chen et al., 2024; Wang et al., 2019a; Tian et al., 2023; Zhu et al., 2021; Zhu et al., 2017). The investigation of~~investigation on~~ the dynamic variation of BrC, e.g., diurnal variation, can greatly promote the understanding of BrC fate in the ambient air, which shall be further studied.

In this study, the real–time measurement of OA and light absorption of aerosols was carried out in the background site of central QTP. For comparison, a concurrent campaign was also carried out during the same period in a typical megacity of China, Guangzhou. The comparison results from distinct two environments at the same time can help better understand the light absorption capacity of BrC in QTP. In both campaigns, an online multi–wavelength Aethalometer (AE33) was applied to characterize the dynamic variation of BrC. The positive matrix factorization (PMF) method together with aerosol mass spectrometer (AMS) data was used to apportion the sources of OA. The multiple linear regression (MLR) was used to explore the possible dynamic source contribution to BrC in two representative regions. Finally, source–specific BrC to light absorption and the radiative forcing in remote and urban areas was shown.

2. Methodology

2.1. Sampling sites

The field campaigns were simultaneously conducted from July 3 to August 3, 2022 in Tibet, and from July 16 to August 5, 2022 in urban Guangzhou, as depicted in Fig. 1. The Yangbajing site (YBJ site; 30.2°N, 90.45°E; 4,300 m above sea level [a.s.l.]) serves as a background location situated in the central QTP, approximately 90 km northwest of Lhasa City. With a permanent population of around 6,000, YBJ was supposed to be influenced by mixed plumes of regional transportation, while local anthropogenic emissions (e.g., light traffic flow and/or fuel combustion for domestic heating or cooking activities) were also found (Liu et al., 2021; Xiang et al., 2024). The urban site (GIG site; 23.1 °N, 113.4°E; 53 m a.s.l.) is set on the campus of the Guangzhou Institute of Geochemistry, Chinese Academy of Sciences (CAS), located in the downtown area of Guangzhou (permanent population: ~20 million). The GIG site is surrounded by transportation, commercial, and residential areas (Chen et al., 2021). During the whole campaigns, lower temperature and Relative Humidity (RH) were observed in the YBJ site (13.4 ± 4.6 °C, 52.1 ± 21.9 %) than those in the GIG site (29.5 ± 2.8 °C, 82.9 ± 12.7 %), which is expected due to the high altitude of Yangbajing (4,300 m) compared to Guangzhou (53 m). Southeast and north winds were

dominant throughout the observation period at the YBJ site with an average wind speed of 2.3 ± 1.6 m s^{-1}, while the GIG site was dominated by south and southwest winds at a speed of 2.2 ± 0.9 m s^{-1}, as shown in Fig. 1. The date and time used in this study are reported using Beijing Time (BJT: UTC +8h).

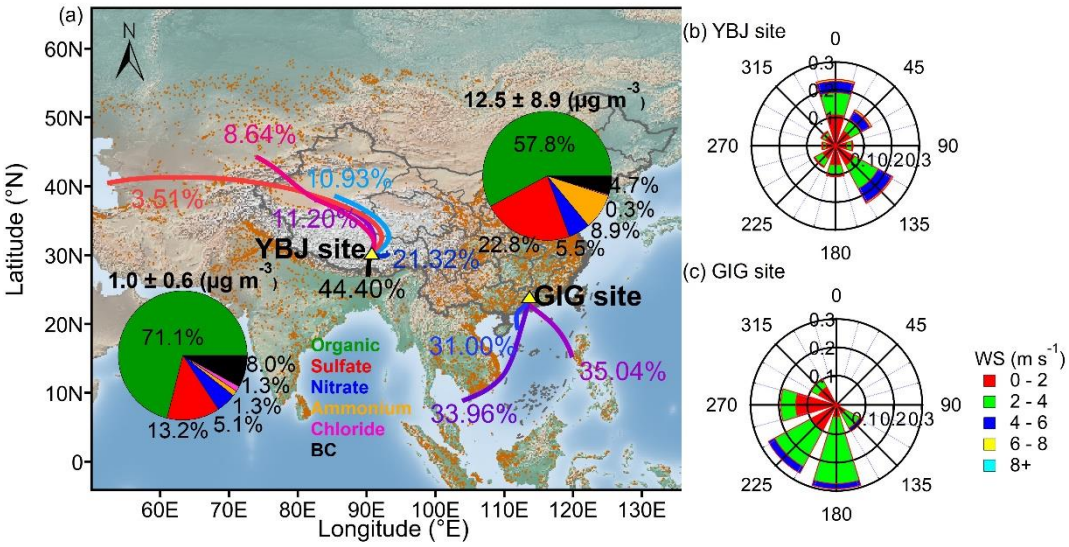

Figure 1. (a) Map of the locations of Yangbajing (YBJ) and Guangzhou (GIG~~GZ~~) sites (yellow triangles). Solid colored lines represent the average back trajectory clusters during the whole campaign and the corresponding contributions plotted using the MeteoInfo version 2.2.6 developed by Wang (2019) (download from *http://www.meteothink.org*, last access time: 23 June 2025). The orange dots on the map indicate the location of the fire spot (download from *Active Fire Data Earthdata (nasa.gov)*, last access time: 14 December 2023). The pie charts represent the chemical compositions of submicron particulate matter (PM_1) along with their contributions at both sites during this campaign. The rose plots colored by wind speed (WS) at (b) the YBJ site and (c) the GIG site are also shown.

2.2. Light absorption coefficient measurement

The aerosol light absorption coefficients at both sites were measured by multi–wavelength Aethalometer (Model AE33, Magee Scientific Corp., Berkeley, CA, USA) at seven wavelengths (370, 470, 520, 590, 660, 880, 950 nm) with a high time resolution of 1 minute (Drinovec et al., 2015). Ambient aerosols were introduced into AE33 through a $PM_{2.5}$ cyclone at a flow rate of 5 L min^{-1}. The AE33 collected aerosols via continuous pumping to a specific location on the filter belt. It then measured the transmitted light that passed through this sample–containing spot and a corresponding blank filter film spot. The instantaneous light–absorbing aerosols were determined by analyzing the variation in the attenuation rate of the transmitted light across the particulate–loaded filter membrane. To accurately reflect the real optical absorption coefficients of airborne aerosols, a real–time compensation parameter (k value) and a fixed filter multiple scattering parameter (C_{ref} = 1.57 for tetrafluoroethylene (TFE)–coated glass filter) are required to correct the optical attenuation coefficient measured on the filter membrane. For the k value, the "dual–point" measurement technique of AE33 avoids the "aerosol loading" effect during single filter tape membrane sampling, enabling real–time calculation corrections for load compensation parameters (Drinovec et al., 2015). Multiple studies have shown that the C value (2.8–7.8) varies with different wavelengths and observation locations (Qin et al., 2018; Collaud Coen et al., 2010; Tian et al., 2023; Zhang et al., 2021). In this study, the C_{final} values of 3.34 (2.23* C_{ref}) for the YBJ site and 3.6 (2.3*1.57) for the GIG site were applied based on the previous studies in Tibet (Zhang et al., 2021) and Guangzhou (Cai et al., 2024), also using the AE33 instrument.

2.3. OA measurement and source apportionment

The main chemical compositions of submicron aerosols including OA, nitrate, sulfate, ammonium, and chloride were measured using a soot particle time–of–flight aerosol mass spectrometer (SP–AMS; Aerodyne Research Inc., Billerica, MA, USA) (Onasch et al., 2012) at YBJ site ~~(Onasch et al., 2012)~~ and a time–of–flight aerosol chemical speciation monitor (ToF–ACSM; Aerodyne Research Inc., Billerica, MA, USA) (Fröhlich et al., 2013) at GIG site. During this campaign, both the SP–AMS and ToF–ACSM shared the same sampling inlet with co–located AE33. The setup diagram can be found in Fig. S1. ~~The detailed principle of SP–AMS can refer to Onasch et al. (2012) and ToF–ACSM to Fröhlich et al. (2013).~~ The time resolution of SP–AMS and ToF–ACSM was 1 min and 40 s, respectively. For SP-AMS, dual vaporization mode and tungsten-only V mode were alternatively applied every 4 minutes. In this study, tungsten-only mode, which resembled the traditional HR-ToF-AMS, was applied. The ionization efficiency (IE) calibration was done using monodispersed NH_4NO_3 aerosols before and after campaigns. The relative ionization efficiency (RIE) of sulfate and ammonium is 1.26 and 4.24 for SP–AMS and 1.22 and 3.39 for ACSM, while a default RIE of 1.4 was used for OA. A constant collection efficiency (CE) of 0.5 was used for YBJ measurement due to the quite low mass fraction of ammonium nitrate (< 40 %), while the composition-dependent collection efficiency (average CDCE = 0.52) (Middlebrook et al., 2012) was applied in GIG measurement. The SP–AMS data were processed using SQUIRREL (v1.65) and PIKA (v1.25A), embedded in Igor Pro (v6.37; WaveMetrics, Inc., Lake Oswego, OR, USA), while ToF–ACSM data were processed using Tofware 3.2.4 (Tofwerk AG, Thun, Switzerland).

The positive matrix factorization (PMF) (Ulbrich et al., 2009; Zhang et al., 2011) was applied to the OA spectral matrix to resolve the sources of OA at both sites. More detailed information can be found in Text S1 and Table S2. The final OA source apportionment at the YBJ site and GIG site are shown in Fig. S4. At the YBJ site, five OA factors were finally resolved using free PMF with PMF3.05 (Ulbrich et al., 2009), including hydrocarbon–like OA (HOA, 11 %) mainly from traffic emissions, biomass burning OA (BBOA, 9 %), biofuel–OA (13 %), less–oxidized oxygenated OA (LO–OOA, 42 %), and more–oxidized oxygenated OA (MO–OOA, 25 %). At the GIG site, OA was resolved based on Multilinear Engine 2 (ME–2; SoFi 6.8) (Canonaco et al., 2013), and the standard BBOA mass spectra (Hu et al., 2016; Hu et al., 2013) were introduced as an external constraint to fully constrain (a value = 0) BBOA factor at the GIG site. Finally, five factors were chosen with MO–OOA (49 %) and LO–OOA (22 %) dominating the total OA, followed by cooking–related OA (COA, 13 %), BBOA (8 %), and HOA (8 %).

2.4. Calculation of BC and BrC light absorption coefficients

The Absorption Ångström exponent (AAE) method was widely used to distinguish BC and BrC light absorption coefficients measured by Aethalometer (Lack and Langridge, 2013). Previous studies demonstrated that the aerosol light absorption at 880 nm was entirely dominated by BC (Kirchstetter et al., 2004). The absorption coefficients of BrC at shorter wavelengths (370, 470, 520, 590, and 660 nm) can be calculated by combining the AAE (Lack and Langridge, 2013) with BC light absorption at 880 nm, using the following Equations:

$$\mathrm{Abs_{BC}}(\lambda) = \mathrm{Abs}(880) \times \left(\frac{880}{\lambda}\right)^{\mathrm{AAE_{BC}}} \quad (1)$$

$$Abs_{BrC}(\lambda) = Abs(\lambda) - Abs_{BC}(\lambda) \quad (2)$$

Here, $Abs_{BC}(\lambda)$ and $Abs_{BrC}(\lambda)$ (M m^{-1}) represent light absorption coefficients of BC and BrC at wavelength λ (nm), respectively. $Abs(\lambda)$ represents the total aerosol light–absorbing coefficients at the wavelength λ, which can be calculated by the mass concentration of BC (μg m^{-3}) multiplied by mass absorption cross–section (MAC; m^2 g^{-1}) at wavelength λ, denoted as $Abs(\lambda) = BC(\lambda) \times MAC(\lambda)$. In this study, default MAC values for BC (18.47, 14.54, 13.14, 11.58, 10.35, and 7.77 m^2 g^{-1} for 370, 470, 520, 590, 660, and 880 nm, respectively) were used (Drinovec et al., 2015). AAE_{BC} denotes the wavelength dependence of pure BC particles, which was usually assumed as 1 to calculate the light absorption coefficient of BC (Tian et al., 2023; Zhang et al., 2022b). However, due to the multiple effects (e.g., lensing effect) caused by the mixing of non–BC/coating materials and BC during atmospheric evolution, the light absorption of BC can be enhanced (Jacobson, 2001; Liu et al., 2017; Peng et al., 2016). Moreover, AAE_{BC} was also found to be varied as a function of absolute wavelength values (Luo et al., 2022), which was suggested as 0.8–1.4 for BC particles (Lack and Langridge, 2013; Kasthuriarachchi et al., 2020a; Zhai et al., 2022; Corr et al., 2012). We summarized the AAE_{BC} values from the literatures in Table S3, and found all the actually used values are between 1 – 1.18. E.g., within one campaign (Kasthuriarachchi et al., 2020), 93% of directly measured AAE from ambient core BC in Singapore was found to be less than 1.1. An AAE_{BC} of 1.4 represents a typical high value, considering the mixing of non-absorbing material with BC in the extreme case (Lack and Langridge, 2013). For our study, we found ~82% of data was negative value when the AAE_{BC} of 1.4 was applied, which is unrealistic to apply here. ~~In this study, the value of AAE 1.4 lead to most of the BrC light absorption coefficient to be negative values, which is not applicable to this study.~~ Thus, to investigate the uncertainty of BrC estimated here, AAE_{BC} of 0.8 to 1.2 was applied, which results in 2–13 % and 4–14 % of BrC contribution to total light absorption from 370 to 660 nm for the YBJ site and GIG site, respectively.

2.5. Sources contribution to BrC light absorption based on multiple linear regression (MLR)

To further understand the sources of BrC light absorption, a multiple linear regression (MLR) was used to apportion the BrC light absorption to different components resolved by the source apportionment of OA (Kasthuriarachchi et al., 2020a; Qin et al., 2018; Tian et al., 2023; Zhang et al., 2021), using the following Equations:

$$Abs_{BrC}(\lambda) = \sum(a \times Factor) + \text{intercept} \quad (3)$$

Here, $Abs_{BrC}(\lambda)$ (M m^{-1}) represents the BrC light absorption coefficient at a wavelength of λ (370, 470, 520, 590 and 660 nm); *a* represent the regression coefficients of different OA components, which can be regarded as MAC (m^2 g^{-1}) values (Kasthuriarachchi et al., 2020a); *Factor* (μg m^{-3}) represents the mass concentration of OA from different sources (see Sect. 2.3).

2.5.1. Uncertainty analyses for the MLR method

Multicollinearity is an important factor leading to inaccurate estimation of regression coefficients in the MLR model. To estimate the uncertainty of the MLR method, we tested different scenarios with varied PMF factor combinations based on their correlation. To compare with other published results and simplify the calculation process, the MLR uncertainty at 370 nm was estimated. In general, four cases

were chosen for the YBJ campaign, and three cases were chosen for the GIG campaign by combining or excluding collinear factors. The detailed information can be found in Text S2 and Table ~~S2~~S5. All the cases yield similar low coefficients for the SOA factor and high coefficient values for the POA factors, suggesting the validity of MLR analysis shown here.

With each solution, the uncertainty of the regression coefficient (i.e., MAC) for the individual OA components input into the MLR model was evaluated using Monte Carlo simulations. For the Monte Carlo calculation input, the uncertainty of the PMF factor mass concentration needs to be evaluated. A bootstrap analysis (100 iterations; (Ulbrich et al., 2009) was applied, which shows a 9–36 % uncertainty for the PMF factors at the YBJ site and 3–9 % at the GIG site, as shown in Table ~~S3~~S6. The uncertainty for the coefficient of BrC at 370 nm was estimated to be 43 % for the YBJ site and 36 % for the GIG site based on the lower (0.8) and upper limit of (1.2) previously reported AAE_{BC} range. The total uncertainties of each coefficient for each PMF factor were then calculated by Monte Carlo with 10,000 simulations.

Considering that biomass burning is widely reported as an important source of BrC light absorption and regarded as a warming agent affecting global climate (Wang et al., 2025), we consider all biomass burning related contributing sources when run the MLR model in the case of eliminating the collinearity problem in this study. As previously reported in the literature (Kasthuriarachchi et al., 2020a; Qin et al., 2018), the MAC of COA is nearly zero, thus, the light absorption by COA at GIG site was not considered in this study. We finally combined the BBOA factor and Biofuel–OA factor as BBOA (case 3) for the YBJ site and included BBOA, HOA as input (case 3) for the GIG site (Table 1). The SOA (LO-OOA and MO-OOA) at GIG site were not inputted here due to the collinearity with BBOA, the light absorption contribution and MAC values (case 3) at GIG site will be lower limits for SOA. For its upper limits, Case 2 in the supporting information (Text S2; Table ~~S2~~S5) was also shown (Fig. ~~S8~~S9). At the YBJ site, the MAC uncertainty of BBOA (26.4 %), HOA (20.8 %), LO–OOA (56.3 %), and MO-OOA (57.9%) was found, as shown in Table ~~S4~~S7. For the GIG site, the MAC uncertainty of HOA (5.8 %), BBOA (6.8 %), and intercept (21.6 %) was estimated. With the final solution, the total light absorption calculated from the predicted regression coefficients (i.e., MAC) showed strong agreement with the measured values, as indicated by the slopes (YBJ: 0.9; GIG: 0.9) and Pearson correlation coefficients (YBJ: R = 0.8; GIG: R = 0.7). These results suggest the robustness of the regression analyses. However, a notable intercept (0.37 M m^{-1}, representing 13 % of the total light absorption) was observed in the MLR model at the GIG site. This intercept indicates a portion of BrC light absorption that could not be explained by the OA factors, potentially due to uncertainties associated with the MLR method. The detailed discussion of MAC and BrC light absorption contributions is shown in Sect.3.2.

Table 1. Regression coefficients (MAC) of the final case of multiple linear regression (MLR) at 370, 470, 520, 590, and 660 nm at the YBJ site and GIG site. Note that the SD represents the Standard deviation purely calculated from the MLR model.

YBJ site					
	Wavelength (nm)				
MAC (Average ± SD)	370nm	470nm	520nm	590nm	660nm
biofuel–OA	1.11 ± 0.11	0.42 ± 0.05	0.11 ± 0.03	0.11 ± 0.02	0 ± 0.03
HOA	2.08 ± 0.3	1.11 ± 0.14	0.18 ± 0.10	0.16 ± 0.06	0 ± 0.07
LO–OOA	0.15 ± 0.08	0.14 ± 0.03	0.07 ± 0.02	0.04 ± 0.02	0.01 ± 0.02
MO–OOA	0.18 ± 0.18	0.19 ± 0.08	0 ± 0.06	0.02 ± 0.04	0 ± 0.04

Intercept	0 ± 0.02	0.02 ± 0.01	0.04 ± 0.01	0.02 ± 0	0.03 ± 0
GIG site					
			Wavelength (nm)		
MAC (Average ± SD)	370nm	470nm	520nm	590nm	660nm
BBOA	1.91 ± 0.21	0.90 ± 0.10	0.35 ± 0.06	0.40 ± 0.04	0.20 ± 0.02
HOA	2.57 ± 0.28	1.40 ± 0.13	0.72 ± 0.07	0.38 ± 0.06	0.13 ± 0.03
Intercept	0.37 ± 0.17	0.18 ± 0.08	0.42 ± 0.04	0.17 ± 0.03	0.11 ± 0.02

2.6. Calculation of radiative forcing

The estimation of the direct radiative forcing caused by BrC was conducted using a model known as the "simple forcing efficiency (SFE)", which can provide a radiative forcing (W g^{-1}) based on a given mass of aerosols. Although the resulting value of SFE is lower than that projected by climate models, it still serves as a valuable tool for gauging the sensitivity of various input parameters (Bond et al., 2006; Chylek and Wong, 1995). In this study, we used a modified version of the wavelength-dependent SFE without considering mass scattering and expressed it as follows (Tian et al., 2023; Zhang et al., 2020a; Zhang et al., 2022b): ~~In this study, we used a modified version of wavelength–dependent SFE without considering the mass scattering can be expressed as follows (Tian et al., 2023; Zhang et al., 2020a; Zhang et al., 2022b):~~

$$SFE(\lambda) = \frac{S(\lambda)}{4} \times \tau_{atm}^2 \times (1 - F_c) \times 4\alpha_s \times MAC(\lambda) \quad (4)$$

Here, $S(\lambda)$ (W g^{-1} nm^{-1}) is the wavelength–dependent solar irradiance based on the ASTM G173–03 Reference Spectra (https://www.nrel.gov/grid/solarresource/spectra–am1.5.html); τ_{atm} represents atmospheric transmission (0.79); F_c is the cloud fraction (0.6); α_s is the surface albedo (global average 0.19) (Chen and Bond, 2010). $MAC(\lambda)$ (m^2 g^{-1}) is the mass absorption cross–section of different OA components at wavelength λ at a 1 nm resolution. The MAC(λ) can be calculated according to the power–law fitting results between the MAC from each OA component at different wavelengths (370 to 660 nm) in this study. Note that the SFE represents a straightforward calculation designed to ascertain the relative significance of diverse optical properties of radiative forcing. However, to accurately determine forcing efficiency, a comprehensive radiative transfer model is still necessary (Efremenko and Kokhanovsky, 2021).

3. Results and discussion

3.1. Overview of Aerosol light absorption

The summarized total aerosol light absorption coefficients (Abs_{total}) -as a function of wavelength at two sites are shown in Fig. 2 and Table ~~S5~~S8. The more detailed temporal evolutions of Abs_{total} at two sites are displayed in Fig. ~~S6~~S7, In general, the average Abs_{total} ranged from 0.6 to 1.6 M m^{-1} (370 to 950 nm) at the YBJ site, while the 7–8 times higher Abs_{total} (4.2–13.2 M m^{-1}) was observed at the GIG site (Fig. 2a and Table ~~S5~~S8). This discrepancy was primarily attributed to the much higher aerosol mass concentration in urban Guangzhou (PM_1: 12.5 ± 8.8 μg m^{-3}) compared to the background Tibetan region (PM_1: 1.0 ± 0.6 μg m^{-3}) (Figs. 2a and 2b). The campaign-averaged ~~campaign-averaged of~~ BrC light absorption coefficients (Abs_{BrC}) and its contribution to total aerosol light absorption increased with decreasing wavelength at both sites (AAE of BrC is 2.6 for YBJ and 3.2 for GIG; Figs. 2c, 3b, and 3d),

indicating strong BrC light absorption at shorter wavelengths. At 370 nm, where BrC contributes the most to the total light absorption, Abs_{BrC} in Tibet (0.2 ± 0.3 M m^{-1}) was found to be a factor of 13 lower than that in Guangzhou (2.9 ± 2 M m^{-1}). This finding is consistent with the much lower OA mass concentrations (by a factor of ~10) at the YBJ site (OA: 0.7 ± 0.4 μg m^{-3} vs 6.9 ± 5.8 μg m^{-3} at GIG; Figs. 2b and 2c). ~~For 370 nm, where BrC contributes most to the total light absorption, a factor of 13 lower of Abs_{BrC} in Tibet (0.2 ± 0.3 M m^{-1}) than Guangzhou (2.9 ± 2 M m^{-1}) was found, consistent with the much lower OA mass concentrations (a factor of ~ 10) in YBJ (OA: 0.7 ± 0.4 μg m^{-3} vs 6.9 ± 5.8 μg m^{-3} at GIG; Figs. 2b and 2c).~~ A positive correlation between BrC light absorption and OA mass concentration was also observed across different field studies (Fig.2d; Table ~~S1~~S4). This relationship aligns with the findings of Wang et al. (2022a), who reported that BrC light absorption at 365 nm positively correlates with OA mass concentration across various sources.

To facilitate a visual comparison with previous studies, the literature–reported BrC light absorption results at 365 or 370 nm are summarized in Fig. 3e and Table ~~S1~~S4. This wavelength was chosen due to its higher BrC abundance across different wavelengths, which leads to less uncertainty. At the YBJ site, the campaign-averaged Abs_{BrC} at 370 nm (0.2 M m^{-1}; 0.03–0.6 M m^{-1} for 5–95 % range; Table ~~S1~~S4) was lower than the values reported across the Qinghai–Tibet Plateau (QTP) (0.6–14.9 M m^{-1}), e.g., the BrC light absorption at YBJ site (central QTP) was much lower than those observed at the edges of the QTP, such as Ngari (5.9–10.7 M m^{-1}), Qomolangma Station (QOMS, 4.4 M m^{-1}), and Gaomeigu (12.3 M m^{-1}), where elevated values are primarily influenced by the cross–border transport of biomass burning plumes during pre–monsoon or post–monsoon period (Zhang et al., 2021; Tian et al., 2023; Zhu et al., 2017). The low BrC light absorption at YBJ can be attributed to the extremely low mass loading of OA (0.7 ± 0.5 μg m^{-3}), which is influenced by wet deposition from precipitation and specific atmospheric circulation patterns during July, a monsoon period (Xu et al., 2018; Zhao et al., 2013). In addition, the absolute BrC light absorption coefficient at YBJ was comparable to levels measured in certain remote regions, such as the Arctic (0.04–0.2 M m^{-1} at 365 nm) (Barrett and Sheesley, 2017; Yue et al., 2022; Yue et al., 2019), highlighting the relatively clean atmospheric conditions at YBJ as a background site in Tibet. In general, BrC light absorption in urban areas tends to be higher or comparable to that in QTP regions due to typically higher OA mass concentrations (Fig. 2d).

Although a relatively large discrepancy in the absolute light absorption coefficient of BrC was observed between the YBJ and GIG sites, the contribution of BrC to total aerosols ($Fraction_{BrC}$) was comparable at both sites (15 % vs. 21 %), highlighting the significant role of BrC in light absorption at both locations. We summarized $Fraction_{BrC}$ across different studies and regions, as shown in Fig. 3e and Table ~~S1~~S4, which reveals that $Fraction_{BrC}$ values generally fall within a range of 8–58 %. Notably, the $Fraction_{BrC}$ in the Qinghai–Tibet Plateau (QTP) is comparable to that in urban areas. Furthermore, a clear trend shows that $Fraction_{BrC}$ at the edges of the northeastern (such as Qinghaihu Lake) and south QTP (such as Ngari) tends to be higher than in the central QTP (such as Beiluhe, Namco, and YBJ site), and the $Fraction_{BrC}$ in Northern China is generally higher than in Southern China. To better understand the factors driving the $Fraction_{BrC}$, we investigated the relationship between the contribution of primary organic aerosol (POA) and secondary OA (SOA) to total OA and the $Fraction_{BrC}$. As illustrated in the inset plot of Fig. 3e, a positive correlation was observed, suggesting that the enhanced POA contribution

will increase the BrC light absorption contribution in carbonaceous aerosol. For sites at the edges of the QTP and in northern Chinese cities, where the $Fraction_{BrC}$ is higher, OA is significantly influenced by the combustion of solid fuels, including coal and biomass, particularly during winter. This finding signifies the importance of POA in contributing to ambient BrC light absorption.

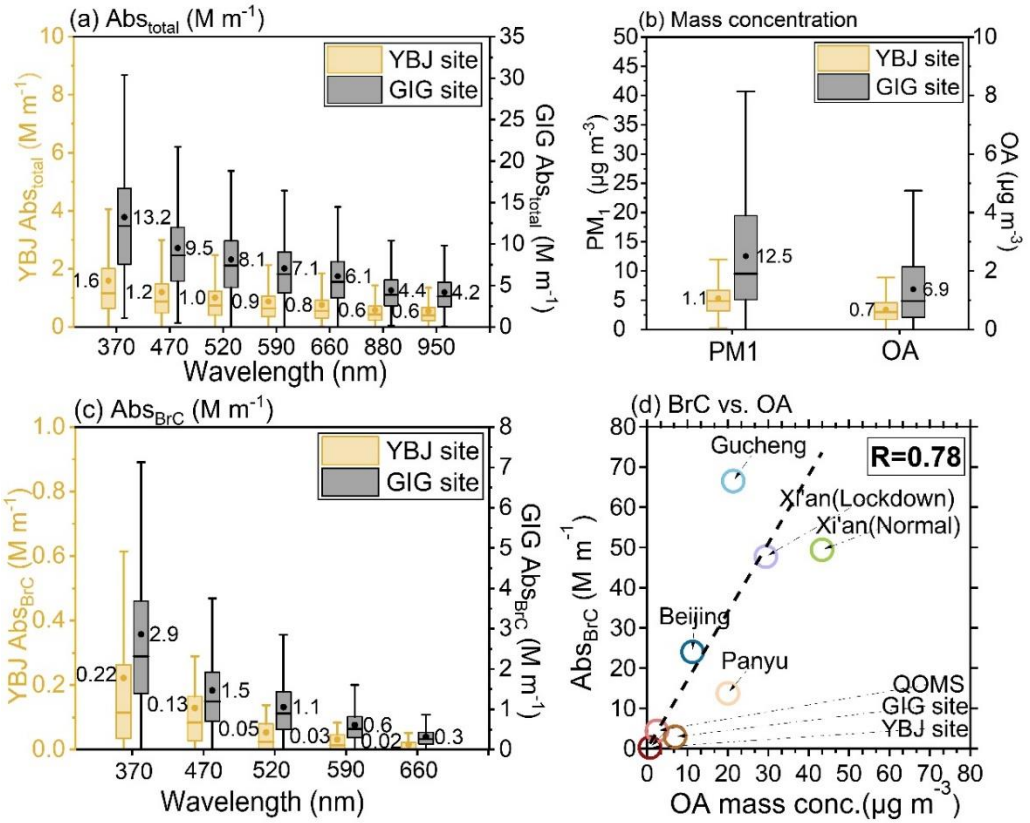

Figure 2. Box plot of the light absorption coefficient of total aerosols (Abs_{total}) (a) and BrC (Abs_{BrC}) (c) from 370nm to 950nm at YBJ (left Y axis) and GIG (right Y axis) sites. The Abs_{BrC} was separated from the Abs_{total} based on Eq. (1) and (2) using AAE_{BC}=1, (b) Box plot of PM_1 and OA mass concentrations at the YBJ site and GIG site. The whiskers indicate the 90th and 10th percentiles, the upper and lower boundaries of boxes indicate the 75th and 25th percentiles, the lines in the boxes indicate the median values, and the markers for the mean values. (d) Scatter plot of the BrC absorption coefficient as a function of OA concentration (data from the literature (Table ~~S1~~S3)).

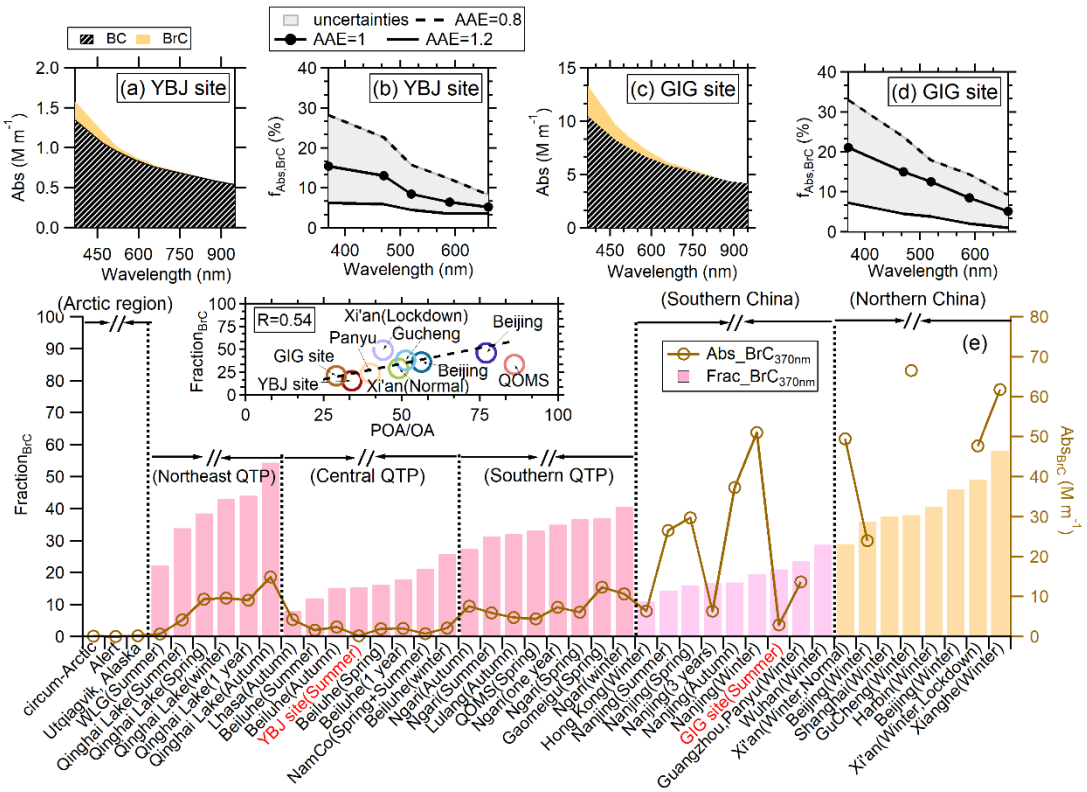

Figure 3. The absolute light absorption coefficients of BC (Abs_{BC}) and BrC (Abs_{BrC}) at wavelengths from 370 to 880 nm at the (a) YBJ site and (c) GIG site, respectively. The BrC was calculated based on the AAE of BC (AAE_{BC})=1. The contribution of BrC light absorption at wavelengths from 370 to 660 nm at the (b) YBJ site and (d) GIG site, respectively. The grey–filled area represents variations in the BrC light absorption fraction caused by the AAE_{BC} from 0.8 (dashed line) to 1.2 (solid line). The circle makers are the average value estimated based on AAE_{BC}=1. (e) The summary of BrC light absorption coefficients (the brown circles) and their contributions to total light absorption coefficients at 370 nm from the literature results. The results were categorized according to the locations of their observation sites (Arctic region, Qinghai–Tibet Plateau (QTP region), Southern China, and Northern China). The inset plot represents the relationship between the BrC light absorption fraction and the contribution of primary OA to total OA. The detailed information is provided in Table ~~S1~~S4.

To further elucidate the dynamic evolution of BrC light absorption, the diurnal variations of $Abs_{BC,370}$ and $Abs_{BrC,370}$ were displayed in Fig. 4 (Abs_{total} at different wavelengths was shown in Fig. ~~S7~~S8). $Abs_{BC,370}$ and $Abs_{BrC,370}$ at both sites peaked simultaneously, indicating combustion source for BC are also important contributor to the BrC in both studies. At the YBJ site, the peaks at 08:00 and 22:00 align with the NO_x ($NO + NO_2$) and CO, which were due to the local or regional anthropogenic emissions (such as vehicle emissions and other combustion activities) in Tibet. In other periods, a background ~~-~~$Abs_{BrC,370}$ value of 0.19 M m^{-1} was found at YBJ site. The diurnal patterns of $Abs_{BC,370}$ and $Abs_{BrC,370}$ at the GIG site, which showed an enhancement at 10:00 and a stronger peak at 21:00, were slightly different from those at the YBJ site. This difference suggests distinct source emissions or secondary formation patterns between the two locations~~The diurnal patterns of $Abs_{BC,370}$ and $Abs_{BrC,370}$ at the GIG site, where enhanced at 10:00 and a stronger peak at 21:00, were slightly different than those at YBJ site, emphasizing the different source emission or secondary formation pattern for each study~~ (Fig. 4b and Fig. S~~8~~7b). Higher increase of NO_2/NO and CO at night in Guangzhou was also found, implying the potentially important contribution of vehicles and other combustion sources, e.g., biomass burning, at this urban site.

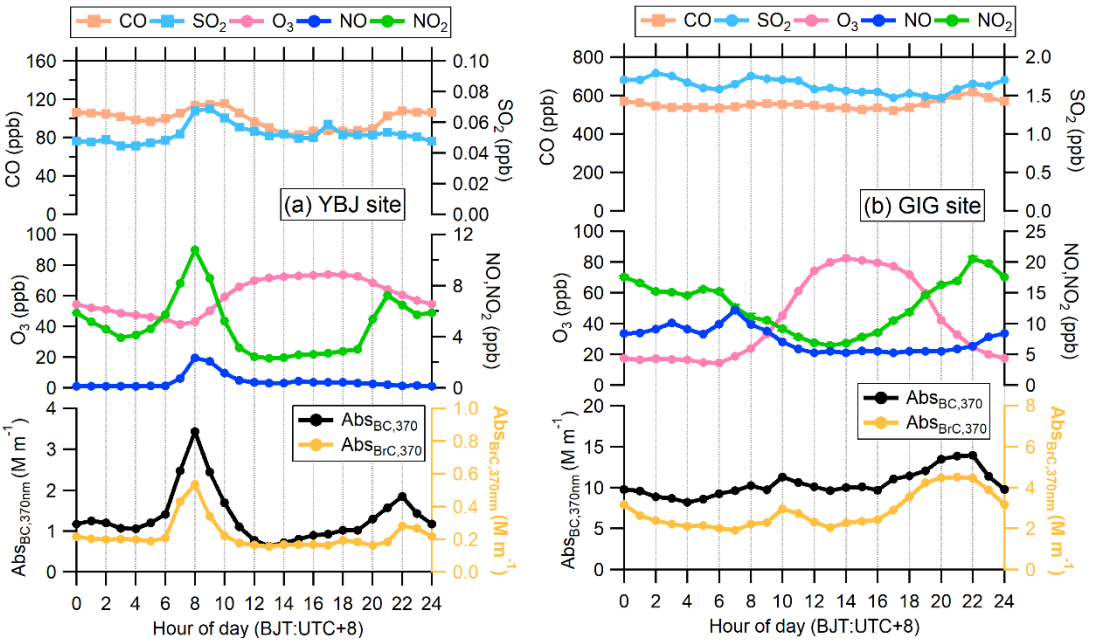

Figure 4. Diurnal variations of gas pollutants and BC/BrC light absorptions at 370 nm at (a) YBJ site and (b) GIG site.

3.2. Optical properties of source–specific BrC

To further identify the source of absorptive BrC in this study, we applied the multiple linear regression (MLR) method to attribute BrC light absorption at different wavelengths to OA components from various sources, based on the PMF analysis conducted at the YBJ and GIG sites. The detailed methodology is described in Sect.2.5.

At the YBJ site in Tibet, the MLR model identified BBOA (the sum of BBOA and Biofuel–OA, as defined in Sect.2.5.1 and Text S1), HOA, LO–OOA, and MO–OOA as the main contributors to BrC light absorption. As shown in Fig. 5a, secondary organic aerosol (SOA, comprising LO–OOA and MO–OOA) dominated the total OA mass concentration (67 %), followed by BBOA (22 %) and HOA (11 %). However, for BrC light absorption, POA (including BBOA and HOA) emerged as the most significant contributor, with BBOA contributing the most (40 %), followed by HOA (38 %) and SOA (22 %), signifying the key role played by biomass burning and vehicle emissions for BrC light absorption at the YBJ site. Indeed, both the BBOA (R = 0.77) and HOA (R = 0.64) show better correlations with BrC light absorption at 370 nm than other factors (Fig. ~~S9~~S10). A similar trend was observed at the GIG site in urban Guangzhou (Fig. 5d), where POA (including BBOA, HOA) represented only 29 % of the total OA mass concentration but contributed disproportionately to BrC light absorption (89 %). These findings highlight the critical role of primary BrC in light absorption during our measurement campaign. In the following, we will discuss each source contribution to BrC in detail.

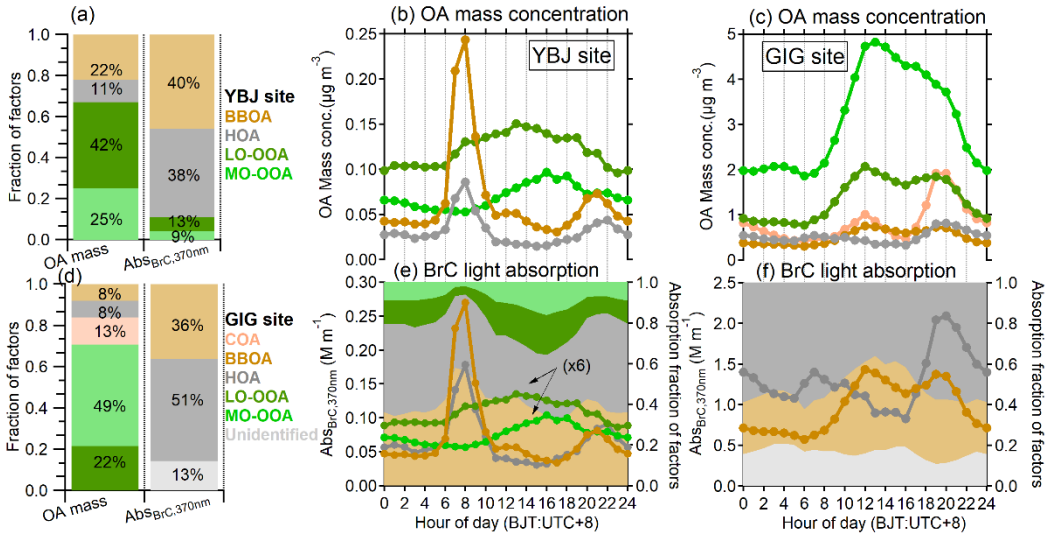

Figure 5. (a) The contributions of different OA factors to total OA (left bars) and contributions of different OA factors to BrC light absorption at 370 nm (right bars) at the YBJ site and GIG site. The diurnal variations of OA factors mass loading and the light absorption of different OA components at 370 nm at the YBJ site (b, e) and GIG site (c, d). The "x6" indicates the light absorption of LO-OOA and MO-OOA at 370 nm expanded by 6 times to better guide the eyes for the trend of diurnal patterns.

3.2.1. Optical properties of BBOA

The diurnal variations of the biomass burning OA (BBOA) light–absorbing coefficients at 370 nm for the YBJ site exhibited strong correlation with BBOA mass concentration (Fig. 5b, 5e), characterized by distinct peaks at 08:00 and 21:00 local time. This temporal pattern aligns with the observation reported in urban Lhasa, which exhibits a peak at 9:00 and 22:00, respectively (Zhao et al., 2022). The BBOA peaks at the YBJ site (central QTP) in the morning and night are primarily influenced by local anthropogenic activities, i.e., the traditional Weisang ritual. The Weisang activity, prevalent throughout Tibet, including the sparsely populated YBJ region, typically occurs twice daily in the morning and evening. Wherever Tibetans are living, almost all have a Weisang furnace. This cultural practice involves the combustion of specific organic materials, including wormwood, cypress branches, highland barley, ghee lamp, and zanba in dedicated stoves, generating characteristic mulberry smoke for religious purposes (Zhang et al., 2020b; Zhang et al., 2022a). Additionally, traditional residential solid biofuel combustion (primarily yak dung and wood) for cooking and space heating contributes significantly to BBOA loading in the plumes (Shen et al., 2021). The AMS spectral similarity between ambient BBOA and emissions from both Weisang activities and solid biofuel combustion (Zhang et al., 2022a), showing the highest signals of m/z 41, 43 and 55, and high abundance of hydrocarbon ions above m/z 60, provides further evidence for their dominant contributions to regional BBOA in Tibet. The hourly wind roses show that the wind direction at the YBJ site exhibits a regular diurnal pattern, with a gradual change from the north wind in the morning to the stronger southeast wind in the afternoon (Fig. ~~S10~~S11). Combining the Bivariate polar plots, the higher morning peak (6:00 to 11:00) of BBOA was from the nearby residential area under low wind speed condition (Figs. ~~S11~~S12, ~~12~~13), while the lower evening peak was due to the dilution of stronger wind speed in the evening (17:00 to 24:00) (Figs. ~~S11~~S12, ~~12~~13).

Compared to Tibet, the urban Guangzhou exhibited fundamentally different diurnal patterns in both BBOA mass concentration and BrC light absorption coefficients (Fig. 5c, 5f), where the BBOA peak

occurs around noon and nighttime, reflecting the different biomass burning activity between Tibet and Guangzhou. Previous literature (Cai et al., 2023; Wang et al., 2017) reported that the agriculture burning at the suburban areas likely dominated the BBOA mass concentration at Guangzhou areas.

The mass absorption coefficient (MAC, $m^2\ g^{-1}$), a crucial optical parameter for BrC characterization, quantifies the light absorption capacity per unit mass of OA. Our measured MAC values for BBOA (1.11–2.54 $m^2\ g^{-1}$ at YBJ vs. 1.91 ± 0.21 $m^2\ g^{-1}$ at GIG; Table 1, ~~S2~~S4) fall within the lower range of previously reported values (0.6–8 $m^2\ g^{-1}$; Fig. 6, Table ~~S7~~S10). This variability in MAC values from similar combustion sources, as documented in numerous studies (Budisulistiorini et al., 2017; Chen and Bond, 2010; Martinsson et al., 2015; Saleh et al., 2014), arises from multiple factors, including fuel composition, combustion conditions, and efficiency. The relatively low MAC values observed at both sites in this study can be attributed to several reasons: 1) Both studies were conducted in the summer time, which coincided with intense solar radiation and elevated oxidant concentrations, promoting photobleaching of chromophores in fresh BBOA (Sumlin et al., 2017). Recent experimental evidence (Hems et al., 2021) demonstrates rapid (minutes to hours), nonlinear photobleaching kinetics of fresh BrC, highlighting the complex nature of these atmospheric processes. Especially for the Guangzhou samples, BBOA from regional transport was likely subjected to a longer oxidation process, which led to a lower MAC at the GIG site.~~Especially for Guangzhou samples, BBOA from regional transport likely under longer oxidation process. which lead to a lower MAC from the GIG site.~~ 2) Combustion conditions and fuel type significantly influence MAC values (Martinsson et al., 2015). Zhang et al. (2022a) systematically characterized Tibetan biofuel emissions, revealing that Weisang materials and yak dung produce abundant OA with relatively low light absorption efficiency due to incomplete combustion. Similarly, Moschos et al. (2024) showed higher MAC values for hardwoods (0.8–1.6 $m^2\ g^{-1}$) versus animal dung (0.2–0.7 $m^2\ g^{-1}$); 3) At YBJ site, the multiple linear regression (MLR) model incorporates biofuel–OA, which contains cooking OA, typically characterized by weak/no absorption (Kasthuriarachchi et al., 2020a; Qin et al., 2018). The spectral similarity between COA and biofuel–OA prevents complete separation in PMF analyses. Sensitivity analyses (Sect.2.5.1 and Text S1; Table ~~S2~~S5) demonstrate MAC_{BBOA} variability (1.11–2.54 $m^2\ g^{-1}$) under different model assumptions, with maximum values (2.54 $m^2\ g^{-1}$) obtained when excluding biofuel–OA contributions.

3.2.2. Optical properties of HOA

The light–absorbing coefficient of HOA at the YBJ site exhibited a pronounced peak at 08:00 and a minor peak at 22:00 (Fig. 5b, 5e), aligning with the diurnal variation of HOA mass concentration. In the Tibetan Plateau region, heavy–duty diesel trucks, which are critical for transporting essential goods across this remote area, constitute a significant emission source alongside gasoline vehicles (Liu et al., 2021; Xiang et al., 2024). Our observation site is located less than 1 km (straight-line distance) from ~~is less than 1km from the direct distance of~~ the G6 Beijing–Tibet Expressway. The Bivariate polar plots also show that the HOA was affected by the wind direction, with the morning peak affected by the north and northeast plumes, while the evening peak was affected by the southeast and northeast plumes with stronger wind speed. The traffic emission during the night is more regional than that in the morning, which was supported by the fact that the NO mass concentration was only enhanced during the morning

(2.3 ppb) but not during the night, while an obvious NO_2 peak at both periods (10 ppb and 7.2 ppb) was observed (Fig. 4a). Combining the Rose plots and Bivariate polar plots (Fig. S12), the evening peak of HOA was also affected by the southeast and northeast traffic emissions plumes with stronger wind speed, which also supported the regional nature of evening HOA peak. At the urban GIG site in Guangzhou, HOA light absorption coefficients displayed a bimodal distribution with a moderate morning peak at 07:00 and a stronger evening peak at 20:00 (Figs. 5c, 5f), consistent with typical urban traffic emissions for rush hours (Chen et al., 2021). The much higher evening peak than the morning peak coincides with rush–hour traffic congestion, suggesting intensified vehicular emissions during these periods, as well as the effects of meteorological conditions (e.g., reduced boundary layer height). The different diurnal variation of light absorption on both HOA and BBOA between Tibetan and Guangzhou observations highlights the regionally specific emission drivers from different areas.

In our study, the MAC of HOA for Tibet (2.08 ± 0.3 $m^2\ g^{-1}$) and urban Guangzhou (2.57 ± 0.28 $m^2\ g^{-1}$) (Table 1) were in the higher ranges of HOA MAC values reported by other studies (0.4–2.04 $m^2\ g^{-1}$) (Table ~~S7~~S10). Note that since the OOA factors in Guangzhou were not considered in the BrC source apportionment due to collinearity with BBOA, the HOA reported here shall be an upper limit. The results of both observation sites show that the HOA MAC (2.08 $m^2\ g^{-1}$ at YBJ site vs. 2.57 $m^2\ g^{-1}$ at GIG site) is larger than the BBOA MAC (1.11–2.54 $m^2\ g^{-1}$ at YBJ vs. 1.91 ± 0.21 $m^2\ g^{-1}$ at GIG). To investigate whether the MAC from ambient BBOA or HOA is higher, we summarized the MAC results from different field studies in Fig. 6, yet no clear conclusion can be drawn. E.g., Higher HOA MAC than BBOA was observed for central Amazon study (De Sá et al., 2019) and Mexico study (Retama et al., 2022), while much higher BBOA MAC than HOA was found for Xianghe, Athens, Paris studies (Kaskaoutis et al., 2021; Wang et al., 2019b; Zhang et al., 2020c). For emission experiments, higher MAC for diesel exhaust than crop and wood have also been observed (Cheng et al., 2011; Du et al., 2014). In addition, very strong light absorption capacity (MAC; 5–6 $m^2\ g^{-1}$) (Table ~~S7~~S10) induced by coal combustion (Wang et al., 2019b; Zhang et al., 2022b) was found, which is comparable to these extreme MAC values reported from biomass burning (5–7.5 $m^2\ g^{-1}$) (Table ~~S7~~S10) (Kaskaoutis et al., 2021; Zhang et al., 2020c). The diversity of MAC from different combustion sources implies the complex influences on light absorption from multiple factors, e.g., ambient oxidation, combustion efficiency and fuel types. The comparable and diverse MAC between HOA and BBOA (Cappa et al., 2019; Zhong and Jang, 2014) warrants reevaluation of traffic aerosols' climate forcing and the necessity for clarifying MAC parameterizations for different sources.

3.2.3. Optical properties of SOA

Compared with the diurnal variation characteristics of BBOA and HOA from local emissions at YBJ site, light absorption coefficients of the less–oxidized oxygenated OA (LO–OOA) and more–oxidized oxygenated factor (MO–OOA) were characterized by high values during the day and low values at night (Fig. 5b, 5e). This day–enhanced temporal variation aligns with that of MO–OOA reported at NamCo (an observation station in central QTP) (Xu et al., 2018), which is influenced by the enhanced secondary BrC from photochemical oxidation during the day. In this study, the contribution of LO–OOA factor shows a broad increase to $Abs_{BrC,370nm}$ during the day and peaks around 14:00 (20 %), while MO–OOA

contribution (16 %) peaks approximately two hours later (16:00). The different diurnal variation of MO–OOA and LO–OOA suggests different formation pathways. In general, LO–OOA is characterized by freshly formed SOA showing a higher light absorption contribution (13 %) than that of MO–OOA (9 %), which more represents the regionally aging SOA (Figs. 5b, 5e). For the GIG site, the maximum direct light absorption contribution from SOA incorporated into case 2 (see Sect.2.5.1 and Text S1; Tables ~~S2~~ S4 and ~~S4~~S6) is 33 % (Fig. ~~S8~~S9).

The MAC of SOA (LO–OOA and MO–OOA) showed much lower values (0.15 and 0.18 $m^2\ g^{-1}$; Table 1, Fig. 6) than primary sources (e.g., BBOA and HOA), consistent with their higher degree of oxidation leading to the weaker light absorptivity of OA (Lee et al., 2014; Lambe et al., 2013). Lower MAC of SOA (0–4 $m^2\ g^{-1}$) (Table ~~S7~~S10) than POA (0.4–8 $m^2\ g^{-1}$) has also been observed in multiple other ambient (De Sá et al., 2019; Retama et al., 2022; Tian et al., 2023; Washenfelder et al., 2015; Zhang et al., 2021; Zhang et al., 2022b) and laboratory studies (Ni et al., 2021; Hems et al., 2021; Zhong and Jang, 2014).

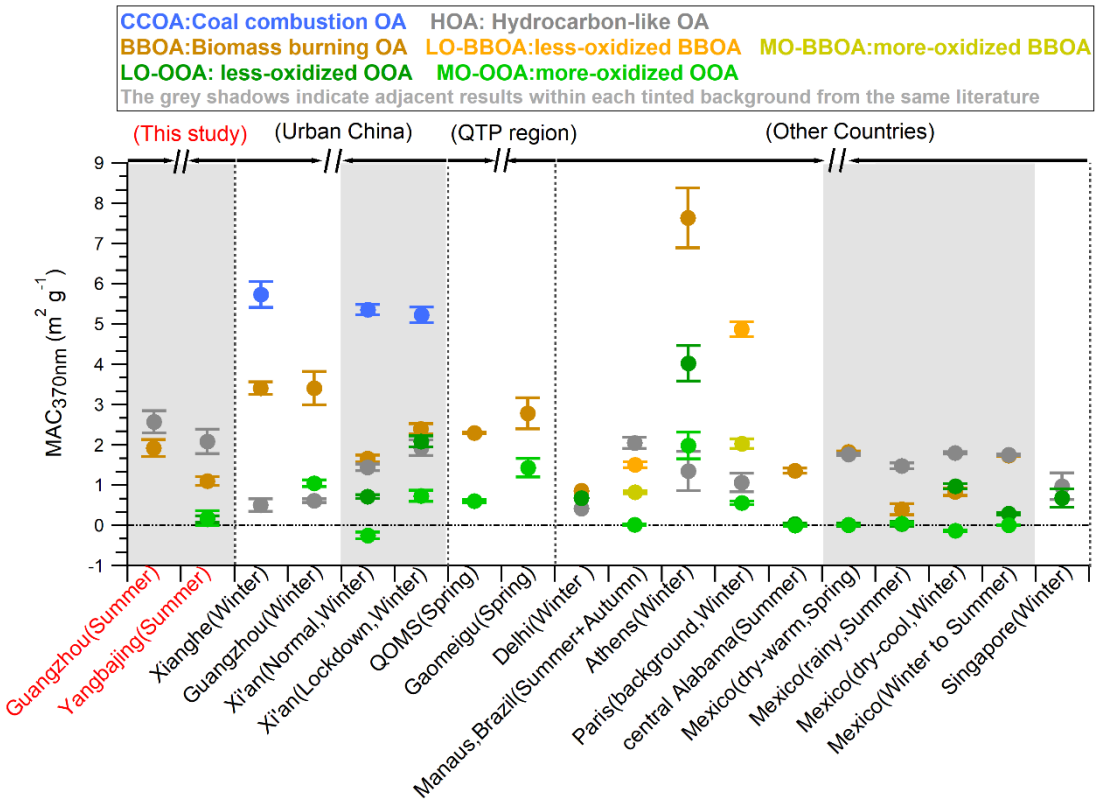

Figure 6. The literature summary of MAC from different BrC sources, which was obtained by the PMF–MLR method in different environments. All the results were categorized based on the locations of their observation sites (urban China, Qinghai–Tibet Plateau (QTP region), and other countries). Note the MO-OOA in Paris study represents OOA. Shadows indicate adjacent results within each tinted background from the same literature. The detailed information is provided in Table ~~S7~~S10.

3.2.4. Summarized source contribution to BrC in the field studies

Figs. 7 (detailed data in Table ~~S6~~S9) summarizes the light absorption contributions of OA from various sources across different regions, based on PMF and MLR analyses. Offline filter results are denoted by an asterisk in the pie chart. Based on this dataset, several features were found: 1) POA (primary organic aerosol) significantly influence ambient BrC light absorption on a global scale,

accounting for 30–95 % of the BrC light absorption except the extremely low fraction (8.3 %) in Xi'an during summer (Lei et al., 2019). In particular, 3 quarters of the summarized study (based on number, as shown in Fig. ~~S13~~S14) show that the POA contributes more than 50 % of BrC light absorption, signifying the important contribution of primary emission to total BrC. In the recent global model, Li et al. (2025) also found the primary emission dominated (77 %) the total light absorption from Nitrogen compounds. Note that the offline studies may underestimate the light absorption contribution of POA due to the application of soluble BrC~~due to soluble BrC was applied~~ (Bao et al., 2022; Chen et al., 2020; Lei et al., 2019; Zhong et al., 2023); 2) Key POA sources of BrC light absorption include coal combustion, biomass burning, and traffic emissions, with their light absorption contributions relative to total OA of -1–56 % (average: 33 %), 6–85 % (average: 38 %) and 4–83 % (average: 27 %), respectively (Fig. 7 and Table ~~S6~~S9); 3) Coal combustion is especially evident in northern China during winter, with light absorption contribution of 30–89 % relative to POA (Lei et al., 2019; Sun et al., 2021; Wang et al., 2019b; Zhang et al., 2022b). In areas not subject to coal combustion, the biomass burning and traffic emissions dominate primary BrC light absorption, which can contribute 11–100 % (53 % for average) and 5–98 % (43 % for average) of primary BrC, respectively (Retama et al., 2022; De Sá et al., 2019; Kaskaoutis et al., 2021; Kasthuriarachchi et al., 2020a; Singh et al., 2021; Washenfelder et al., 2015; Zhang et al., 2020c). 4) The light absorption contribution from different sources showed significant spatial and temporal differences, e.g., HOA shows extremely high light absorption contribution in Singapore during summer ~~winter~~ (83 %), and in Mexico in both winter (54 %) and summer (49 %), while biomass burning dominated in central Alabama (85 %) and Paris (74 %). Given the pronounced spatial and temporal variations in source–specific light absorption, it is essential to conduct region–specific and season–specific observational research for a better understanding of the BrC sources and to better understand BrC sources and to better validate model simulations.~~a better validate the model simulation.~~

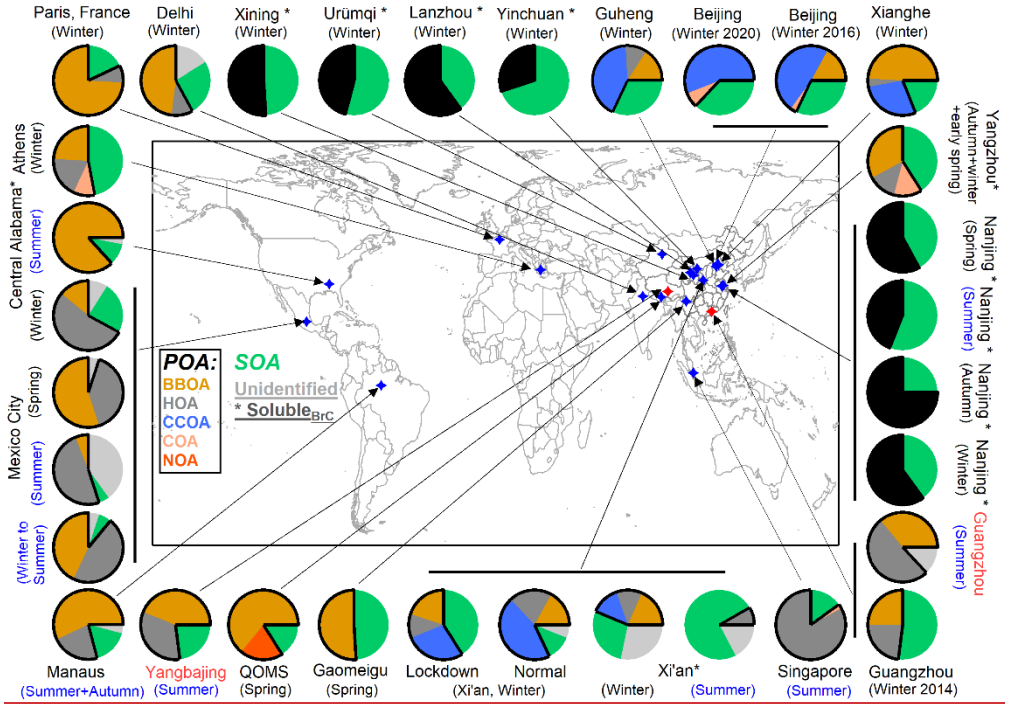

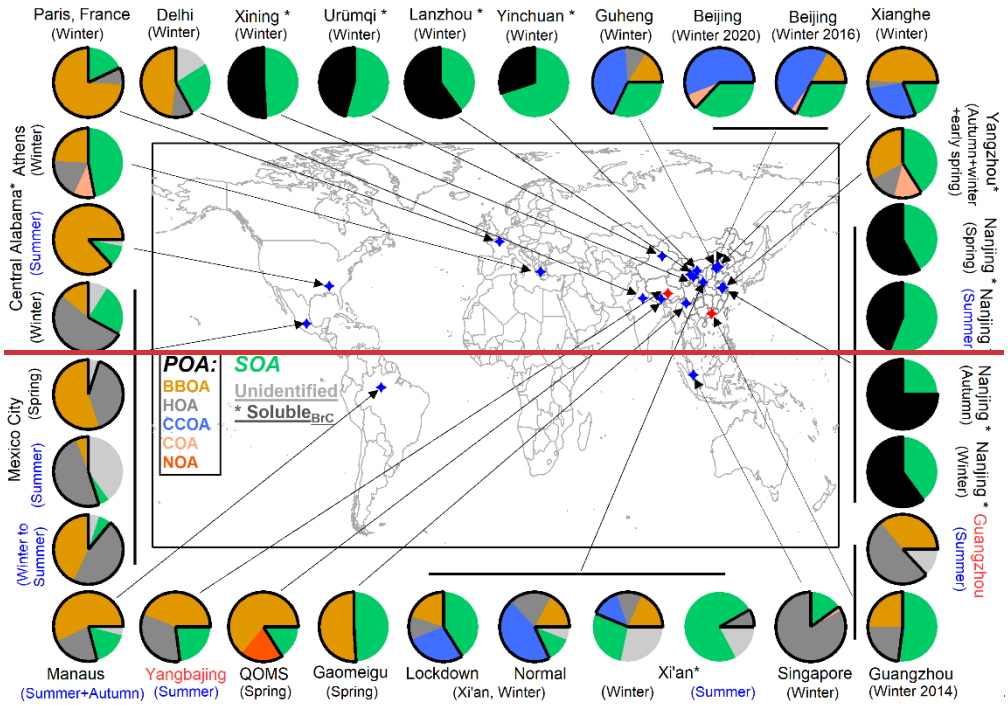

Figure 7. The summary of the contribution to BrC light absorption at 370 nm from different sources using the PMF–MLR method. The asterisks (*) represent the light absorption contributions of soluble BrC from different sources at 365nm. The sources include POA: biomass burning OA (BBOA), hydrocarbon–like OA (HOA), coal combustion OA(CCOA), cooking–related OA(COA), nitrogen-containing OA(NOA); The total SOA from oxygenated OA was used here. In addition, the unidentified fraction from the intercept of the MLR method was also shown. The detailed information on each pie is provided in Table ~~S6~~S9.

3.3. Radiative effect of BrC from different sources

The simple forcing efficiency (SFE) of different organic aerosol (OA) components at the YBJ and GIG sites was estimated using Eq. (4) as described in Sect.2.6. This methodology has been widely applied to evaluate the climate impact of brown carbon (BrC) (Tian et al., 2023; Wang et al., 2019b; Zhang et al., 2022b; Zhong et al., 2023). As illustrated in Fig. 8, black carbon (BC) emerged as the dominant light–absorbing component, exhibiting the highest integrated SFE values of 294.7 W g^{-1} at the YBJ site and 286.3 W g^{-1} at the GIG site. In contrast, the integrated total SFE (from total OA absorption) across the 370–660 nm wavelength range was 21.4 W g^{-1} at the YBJ site and 33.8 W g^{-1} at the GIG site, representing approximately 9–13 % of the BC values. This is consistent with the well–documented strong light–absorbing properties of BC (Gustafsson and Ramanathan, 2016), while also highlighting the significant role of BrC in short–term climate effects.

The SFE values for POA at the YBJ (19.2 W g^{-1}) and GIG (33.8 W g^{-1}) sites were comparable to those observed in other urban areas, such as Xi'an (approximately 33 W g^{-1} for HOA + BBOA + CCOA) during winter (Zhang et al., 2022b). POA, including BBOA and HOA, contributed significantly to the total BrC light absorption, accounting for over 80 % of the BrC-specific SFE ~~SFE~~ in this study. These findings underscore the substantial influence of anthropogenic emissions on aerosol radiative forcing and their implications for regional and global climate systems.

From an environmental and climatic perspective, these results emphasize the critical role of both BC and BrC in modulating atmospheric radiative balance. The higher SFE of BC underscores its potent

warming effect, while the non–negligible contribution of BrC, particularly from POA, highlights the importance of addressing anthropogenic sources. Further elucidating the fossil and non–fossil contribution, i.e., vehicle emission, coal vs. biomass burning combustion to the BrC, is vital for refining climate models, informing mitigation strategies, and developing policies aimed at reducing short–lived climate pollutants to mitigate near–term climate change and its associated environmental impacts.

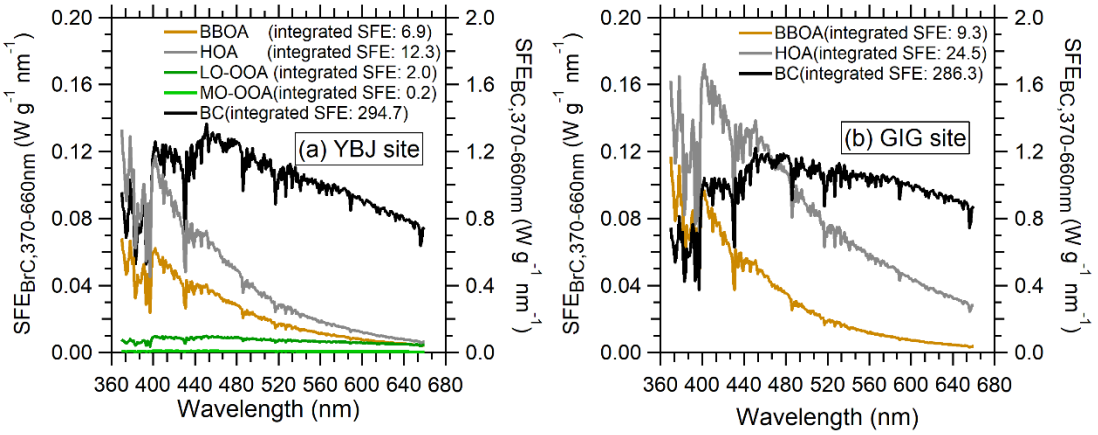

Figure 8. The Simple forcing efficiency (SFE) of BrC from different sources and BC from 370 to 660 nm at (a) YBJ and (b) GIG site.

4. Conclusions

To explore the optical properties, source contributions, and radiative effects of BrC in Qinghai–Tibet Plateau, the observations equipped with the AE33 and the SP–AMS were carried out in July 2022 in the Tibet background site (Yangbajing). For comparison, a simultaneous field observation was also conducted at the same periods in Guangzhou, a megacity with significant anthropogenic emissions. Our results reveal that the light absorption coefficient at 370nm from total aerosols (Abs_{total}, 1.6 ± 1.6 M m^{-1}) and BrC (Abs_{BrC}, 0.2 ± 0.3 M m^{-1}) in Tibet were approximately an order of magnitude lower than those in Guangzhou (Abs_{total}, 13.2 ± 7 M m^{-1}; Abs_{BrC}, 2.9 ± 2 M m^{-1}), consistent with the extremely low mass concentrations of total aerosols and organic aerosols (OA) observed at the Tibetan site. The minimal aerosol loading and weak light absorption in Tibet underscore its pristine atmospheric background.

Despite a large discrepancy in absolute light absorption coefficient, the BrC light absorption contribution to total aerosols (15 % and 21 %) is comparable between the two sites at 370 nm, highlighting BrC's significant contribution to total aerosol light absorption in Tibet. The summarized field studies demonstrate a positive correlation between BrC fraction in Abs_{total} as a function of POA/OA (R = 0.54), suggesting primary emissions contribute more effectively to BrC light absorption than BC, and POA is a more important source of BrC light absorption than SOA at these two sites. Source apportionment via the PMF–MLR method identified biomass–burning OA (BBOA) and hydrocarbon–like OA (HOA) from vehicles as the major contributors (> 80 %) to the BrC light absorption in both sites. The summarized field studies show that POA can account for 30–95 % of the BrC light absorption on a global scale. All these finding signifies the critical role of primary emission in OA light absorption. The main primary source for BrC includes biomass burning/biofuels, coal combustion, and vehicle emissions.

Diurnal variations of BrC and its sources exhibited distinct patterns with morning and nighttime peaks. Weisang activity and traffic rush hours in Tibet significantly influenced BrC levels, underscoring

even remote regions' vulnerability to anthropogenic activities. Notably, traffic–related BrC contributions remain substantial in Guangzhou and even in the Tibet background, which necessitates that explicit light absorption parameters for fossil-derived BrC (e.g., from vehicle emissions) be considered in model simulations.~~necessitating explicit BrC light absorption parameters from fossil fuel, e.g., vehicle emissions, shall be considered in the model simulation of BrC.~~ Current literature remains inconclusive regarding MAC differences between HOA and BBOA, though fuel type, combustion efficiency, and aging effects critically influence BrC MAC, emphasizing the need for enhanced field measurements and parameterization of source-specific MACs.

Based on this field study, the integrated total SFE of BrC across the 370–660 nm wavelength range can account for approximately 7 % and 12 % of the BC (294.7 W g^{-1} in Tibet and 286.3 W g^{-1} in Guangzhou). In total, primary emission contributes over 98 % of the total SFE at both sites. These findings reinforce the urgency of controlling primary emissions and call for regional–specific parameterizations in climate models to improve assessments of BrC's radiative effects. In general, our study promotes the understanding of BrC dynamic variation and its sources at clean background Tibet and typical urban areas, emphasizing the strong influences of anthropogenic to radiative forcing.

Data availability

The data shown in the paper are available on request from the corresponding authors (weiweihu@gig.ac.cn and shanhuang_eci@jnu.edu.cn).

Author contributions

WH, SH, PY, NM, BY, MS designed the research. SH, PY, NM, BY, WZ, ZL, LL, TP, TF, JW conducted the field measurements. GZ and XB supported the AE33 instrument. WZ, LL, ZL, and YC analyzed the data. LL and SH supported the SP-AMS data analysis and OA source analysis for the Tibet campaign. WZ wrote the paper. WH, SH, ZL, TP, TF, JW, YC, GZ, XB, and XW reviewed and commented on the paper.

Competing interests.

The authors declare that they have no conflict of interest.

Acknowledgments

This work has been supported by National Natural Science Foundation of China (Grant No 42375105), the second Tibetan Plateau Scientific Expedition and Research Program (Grant No. 2019QZKK0604), International Partnership Program of Chinese Academy of Sciences (Grant No.164GJHZ2023068FN, Guangdong Foundation for Program of Science and Technology Research (Grant No 2023B1212060049), Science Fund for Creative Research Groups of the National Natural Science Foundation of China (Grant No 42321003). We appreciate Xiaomin Chen from Jinan University for providing assistance regarding PMF analysis.

References

Andreae, M. O. and Gelencsér, A.: Black carbon or brown carbon? The nature of light-absorbing carbonaceous aerosols, Atmos. Chem. Phys., 6, 3131-3148, 10.5194/acp-6-3131-2006, 2006.

Bao, M., Zhang, Y.-L., Cao, F., Lin, Y.-C., Hong, Y., Fan, M., Zhang, Y., Yang, X., and Xie, F.: Light absorption and source apportionment of water soluble humic-like substances (HULIS) in PM2.5 at Nanjing, China, Environmental Research, 206, 10.1016/j.envres.2021.112554, 2022.

Barrett, T. E. and Sheesley, R. J.: Year-round optical properties and source characterization of Arctic organic carbon aerosols on the North Slope Alaska, Journal of Geophysical Research: Atmospheres, 122, 9319-9331, 10.1002/2016jd026194, 2017.

Bond, T. C. and Bergstrom, R. W.: Light Absorption by Carbonaceous Particles: An Investigative Review, Aerosol Science and Technology, 40, 27-67, 10.1080/02786820500421521, 2006.

Bond, T. C., Bergstrom, R. W. J. A. S., and Technology: Light Absorption by Carbonaceous Particles: An Investigative Review, 40, 27 - 67, 2006.

Brown, H., Liu, X., Feng, Y., Jiang, Y., Wu, M., Lu, Z., Wu, C., Murphy, S., and Pokhrel, R.: Radiative effect and climate impacts of brown carbon with the Community Atmosphere Model (CAM5), Atmospheric Chemistry and Physics, 18, 17745-17768, 10.5194/acp-18-17745-2018, 2018.

Budisulistiorini, S. H., Riva, M., Williams, M., Chen, J., Itoh, M., Surratt, J. D., and Kuwata, M.: Light-Absorbing Brown Carbon Aerosol Constituents from Combustion of Indonesian Peat and Biomass, Environ Sci Technol, 51, 4415-4423, 10.1021/acs.est.7b00397, 2017.

Cai, Y., Ye, C., Chen, W., Hu, W., Song, W., Peng, Y., Huang, S., Qi, J., Wang, S., Wang, C., Wu, C., Wang, Z., Wang, B., Huang, X., He, L., Gligorovski, S., Yuan, B., Shao, M., and Wang, X.: The important contribution of secondary formation and biomass burning to oxidized organic nitrogen (OON) in a polluted urban area: insights from in situ measurements of a chemical ionization mass spectrometer (CIMS), Atmospheric Chemistry and Physics, 23, 8855-8877, 10.5194/acp-23-8855-2023, 2023.

Canonaco, F., Crippa, M., Slowik, J. G., Baltensperger, U., and Prévôt, A. S. H.: SoFi, an IGOR-based interface for the efficient use of the generalized multilinear engine (ME-2) for the source apportionment: ME-2 application to aerosol mass spectrometer data, Atmospheric Measurement Techniques, 6, 3649-3661, 10.5194/amt-6-3649-2013, 2013.

Cappa, C. D., Zhang, X., Russell, L. M., Collier, S., Lee, A. K. Y., Chen, C. L., Betha, R., Chen, S., Liu,

J., Price, D. J., Sanchez, K. J., McMeeking, G. R., Williams, L. R., Onasch, T. B., Worsnop, D. R., Abbatt, J., and Zhang, Q.: Light Absorption by Ambient Black and Brown Carbon and its Dependence on Black Carbon Coating State for Two California, USA, Cities in Winter and Summer, Journal of Geophysical Research: Atmospheres, 124, 1550-1577, 10.1029/2018jd029501, 2019.

Cappa, C. D., Onasch, T. B., Massoli, P., Worsnop, D. R., Bates, T. S., Cross, E. S., Davidovits, P., Hakala, J., Hayden, K. L., Jobson, B. T., Kolesar, K. R., Lack, D. A., Lerner, B. M., Li, S.-M., Mellon, D., Nuaaman, I., Olfert, J. S., Petäjä, T., Quinn, P. K., Song, C., Subramanian, R., Williams, E. J., and Zaveri, R. A.: Radiative Absorption Enhancements Due to the Mixing State of Atmospheric Black Carbon, 337, 1078-1081, doi:10.1126/science.1223447, 2012.

Chelluboyina, G. S., Kapoor, T. S., and Chakrabarty, R. K.: Dark brown carbon from wildfires: a potent snow radiative forcing agent?, npj Climate and Atmospheric Science, 7, 10.1038/s41612-024-00738-7, 2024.

Chen, P., Kang, S., Hu, Y., Pu, T., Liu, Y., Wang, S., Rai, M., Wang, K., Tripathee, L., and Li, C.: South and Southeast Asia controls black carbon characteristics of Meili Snow Mountains in southeast Tibetan Plateau, Science of The Total Environment, 927, 10.1016/j.scitotenv.2024.172262, 2024.

Chen, W., Ye, Y., Hu, W., Zhou, H., Pan, T., Wang, Y., Song, W., Song, Q., Ye, C., Wang, C., Wang, B., Huang, S., Yuan, B., Zhu, M., Lian, X., Zhang, G., Bi, X., Jiang, F., Liu, J., Canonaco, F., Prevot, A. S. H., Shao, M., and Wang, X.: Real-Time Characterization of Aerosol Compositions, Sources, and Aging Processes in Guangzhou During PRIDE-GBA 2018 Campaign, Journal of Geophysical Research: Atmospheres, 126, 10.1029/2021jd035114, 2021.

Chen, Y. and Bond, T. C.: Light absorption by organic carbon from wood combustion, Atmos. Chem. Phys., 10, 1773-1787, 10.5194/acp-10-1773-2010, 2010.

Chen, Y., Xie, X., Shi, Z., Li, Y., Gai, X., Wang, J., Li, H., Wu, Y., Zhao, X., Chen, M., and Ge, X.: Brown carbon in atmospheric fine particles in Yangzhou, China: Light absorption properties and source apportionment, Atmospheric Research, 244, 10.1016/j.atmosres.2020.105028, 2020.

Cheng, Y., He, K. B., Zheng, M., Duan, F. K., Du, Z. Y., Ma, Y. L., Tan, J. H., Yang, F. M., Liu, J. M., Zhang, X. L., Weber, R. J., Bergin, M. H., and Russell, A. G.: Mass absorption efficiency of elemental carbon and water-soluble organic carbon in Beijing, China, Atmos. Chem. Phys., 11, 11497-11510, 10.5194/acp-11-11497-2011, 2011.

740 Chung, C. E., Ramanathan, V., and Decremer, D.: Observationally constrained estimates of carbonaceous
741 aerosol radiative forcing, Proc Natl Acad Sci U S A, 109, 11624-11629, 10.1073/pnas.1203707109,
742 2012.
743 Chylek, P. and Wong, J.: Effect of absorbing aerosols on global radiation budget, Geophysical Research
744 Letters, 22, 929-931, https://doi.org/10.1029/95GL00800, 1995.
745 Collaud Coen, M., Weingartner, E., Apituley, A., Ceburnis, D., Fierz-Schmidhauser, R., Flentje, H.,
746 Henzing, J. S., Jennings, S. G., Moerman, M., Petzold, A., Schmid, O., and Baltensperger, U.:
747 Minimizing light absorption measurement artifacts of the Aethalometer: evaluation of five
748 correction algorithms, Atmos. Meas. Tech., 3, 457-474, 10.5194/amt-3-457-2010, 2010.
749 Corr, C. A., Hall, S. R., Ullmann, K., Anderson, B. E., Beyersdorf, A. J., Thornhill, K. L., Cubison, M.
750 J., Jimenez, J. L., Wisthaler, A., and Dibb, J. E.: Spectral absorption of biomass burning aerosol
751 determined from retrieved single scattering albedo during ARCTAS, Atmos. Chem. Phys., 12,
752 10505-10518, 10.5194/acp-12-10505-2012, 2012.
753 de Sá, S. S., Rizzo, L. V., Palm, B. B., Campuzano-Jost, P., Day, D. A., Yee, L. D., Wernis, R., Isaacman-
754 VanWertz, G., Brito, J., Carbone, S., Liu, Y. J., Sedlacek, A., Springston, S., Goldstein, A. H.,
755 Barbosa, H. M. J., Alexander, M. L., Artaxo, P., Jimenez, J. L., and Martin, S. T.: Contributions of
756 biomass-burning, urban, and biogenic emissions to the concentrations and light-absorbing
757 properties of particulate matter in central Amazonia during the dry season, Atmos. Chem. Phys., 19,
758 7973-8001, 10.5194/acp-19-7973-2019, 2019.
759 Drinovec, L., Močnik, G., Zotter, P., Prévôt, A. S. H., Ruckstuhl, C., Coz, E., Rupakheti, M., Sciare, J.,
760 Müller, T., Wiedensohler, A., and Hansen, A. D. A.: The "dual-spot" Aethalometer: an improved
761 measurement of aerosol black carbon with real-time loading compensation, Atmos. Meas. Tech., 8,
762 1965-1979, 10.5194/amt-8-1965-2015, 2015.
763 Du, Z., He, K., Cheng, Y., Duan, F., Ma, Y., Liu, J., Zhang, X., Zheng, M., and Weber, R.: A yearlong
764 study of water-soluble organic carbon in Beijing II: Light absorption properties, Atmospheric
765 Environment, 89, 235-241, 10.1016/j.atmosenv.2014.02.022, 2014.
766 Efremenko, D. and Kokhanovsky, A.: Radiative Transfer Models, in: Foundations of Atmospheric
767 Remote Sensing, edited by: Efremenko, D., and Kokhanovsky, A., Springer International Publishing,
768 Cham, 149-232, 10.1007/978-3-030-66745-0_4, 2021.

769 Feng, Y., Ramanathan, V., and Kotamarthi, V. R.: Brown carbon: a significant atmospheric absorber of
770 solar radiation?, Atmos. Chem. Phys., 13, 8607-8621, 10.5194/acp-13-8607-2013, 2013.
771 Fröhlich, R., Cubison, M. J., Slowik, J. G., Bukowiecki, N., Prévôt, A. S. H., Baltensperger, U., Schneider,
772 J., Kimmel, J. R., Gonin, M., Rohner, U., Worsnop, D. R., and Jayne, J. T.: The ToF-ACSM: a
773 portable aerosol chemical speciation monitor with TOFMS detection, Atmospheric Measurement
774 Techniques, 6, 3225-3241, 10.5194/amt-6-3225-2013, 2013.
775 Gustafsson, O. and Ramanathan, V.: Convergence on climate warming by black carbon aerosols, Proc
776 Natl Acad Sci U S A, 113, 4243-4245, 10.1073/pnas.1603570113, 2016.
777 Hems, R. F. and Abbatt, J. P. D.: Aqueous Phase Photo-oxidation of Brown Carbon Nitrophenols:
778 Reaction Kinetics, Mechanism, and Evolution of Light Absorption, ACS Earth and Space Chemistry,
779 2, 225-234, 10.1021/acsearthspacechem.7b00123, 2018.
780 Hems, R. F., Schnitzler, E. G., Liu-Kang, C., Cappa, C. D., and Abbatt, J. P. D.: Aging of Atmospheric
781 Brown Carbon Aerosol, ACS Earth and Space Chemistry, 5, 722-748,
782 10.1021/acsearthspacechem.0c00346, 2021.
783 Hu, W., Hu, M., Hu, W., Jimenez, J. L., Yuan, B., Chen, W., Wang, M., Wu, Y., Chen, C., Wang, Z., Peng,
784 J., Zeng, L., and Shao, M.: Chemical composition, sources, and aging process of submicron aerosols
785 in Beijing: Contrast between summer and winter, Journal of Geophysical Research: Atmospheres,
786 121, 1955-1977, 10.1002/2015jd024020, 2016.
787 Hu, W. W., Hu, M., Yuan, B., Jimenez, J. L., Tang, Q., Peng, J. F., Hu, W., Shao, M., Wang, M., Zeng, L.
788 M., Wu, Y. S., Gong, Z. H., Huang, X. F., and He, L. Y.: Insights on organic aerosol aging and the
789 influence of coal combustion at a regional receptor site of central eastern China, Atmospheric
790 Chemistry and Physics, 13, 10095-10112, 10.5194/acp-13-10095-2013, 2013.
791 Huang, R.-J., Yuan, W., Yang, L., Yang, H., Cao, W., Guo, J., Zhang, N., Zhu, C., Wu, Y., and Zhang, R.:
792 Concentration, optical characteristics, and emission factors of brown carbon emitted by on-road
793 vehicles, Science of The Total Environment, 810, 10.1016/j.scitotenv.2021.151307, 2022.
794 Jacobson, M. Z.: Strong radiative heating due to the mixing state of black carbon in atmospheric aerosols,
795 Nature, 409, 695-697, 10.1038/35055518, 2001.
796 Jiang, H., Frie, A. L., Lavi, A., Chen, J. Y., Zhang, H., Bahreini, R., and Lin, Y.-H.: Brown Carbon
797 Formation from Nighttime Chemistry of Unsaturated Heterocyclic Volatile Organic Compounds,

798 Environmental Science & Technology Letters, 6, 184-190, 10.1021/acs.estlett.9b00017, 2019.
799 Kang, S., Zhang, Q., Qian, Y., Ji, Z., Li, C., Cong, Z., Zhang, Y., Guo, J., Du, W., Huang, J., You, Q.,
800 Panday, A. K., Rupakheti, M., Chen, D., Gustafsson, O., Thiemens, M. H., and Qin, D.: Linking
801 atmospheric pollution to cryospheric change in the Third Pole region: current progress and future
802 prospects, Natl Sci Rev, 6, 796-809, 10.1093/nsr/nwz031, 2019.
803 Kaskaoutis, D. G., Grivas, G., Stavroulas, I., Bougiatioti, A., Liakakou, E., Dumka, U. C., Gerasopoulos,
804 E., and Mihalopoulos, N.: Apportionment of black and brown carbon spectral absorption sources in
805 the urban environment of Athens, Greece, during winter, Science of The Total Environment, 801,
806 10.1016/j.scitotenv.2021.149739, 2021.
807 Kasthuriarachchi, N. Y., Rivellini, L. H., Adam, M. G., and Lee, A. K. Y.: Light Absorbing Properties of
808 Primary and Secondary Brown Carbon in a Tropical Urban Environment, Environ Sci Technol, 54,
809 10808-10819, 10.1021/acs.est.0c02414, 2020a.
810 Kasthuriarachchi, N. Y., Rivellini, L. H., Chen, X., Li, Y. J., and Lee, A. K. Y.: Effect of Relative Humidity
811 on Secondary Brown Carbon Formation in Aqueous Droplets, Environ Sci Technol, 54, 13207-
812 13216, 10.1021/acs.est.0c01239, 2020b.
813 Kirchstetter, T. W. and Thatcher, T. L.: Contribution of organic carbon to wood smoke particulate matter
814 absorption of solar radiation, Atmos. Chem. Phys., 12, 6067-6072, 10.5194/acp-12-6067-2012,
815 2012.
816 Kirchstetter, T. W., Novakov, T., and Hobbs, P. V.: Evidence that the spectral dependence of light
817 absorption by aerosols is affected by organic carbon, Journal of Geophysical Research: Atmospheres,
818 109, n/a-n/a, 10.1029/2004jd004999, 2004.
819 Lack, D. A. and Langridge, J. M.: On the attribution of black and brown carbon light absorption using
820 the Ångström exponent, Atmos. Chem. Phys., 13, 10535-10543, 10.5194/acp-13-10535-2013, 2013.
821 Lack, D. A., Moosmuller, H., McMeeking, G. R., Chakrabarty, R. K., and Baumgardner, D.:
822 Characterizing elemental, equivalent black, and refractory black carbon aerosol particles: a review
823 of techniques, their limitations and uncertainties, Anal Bioanal Chem, 406, 99-122,
824 10.1007/s00216-013-7402-3, 2014.
825 Lack, D. A., Richardson, M. S., Law, D., Langridge, J. M., Cappa, C. D., McLaughlin, R. J., and Murphy,
826 D. M.: Aircraft Instrument for Comprehensive Characterization of Aerosol Optical Properties, Part

827 2: Black and Brown Carbon Absorption and Absorption Enhancement Measured with Photo
828 Acoustic Spectroscopy, Aerosol Science and Technology, 46, 555-568,
829 10.1080/02786826.2011.645955, 2012.
830 Lambe, A. T., Cappa, C. D., Massoli, P., Onasch, T. B., Forestieri, S. D., Martin, A. T., Cummings, M. J.,
831 Croasdale, D. R., Brune, W. H., Worsnop, D. R., and Davidovits, P.: Relationship between oxidation
832 level and optical properties of secondary organic aerosol, Environ Sci Technol, 47, 6349-6357,
833 10.1021/es401043j, 2013.
834 Laskin, A., Laskin, J., and Nizkorodov, S. A.: Chemistry of atmospheric brown carbon, Chem Rev, 115,
835 4335-4382, 10.1021/cr5006167, 2015.
836 Laskin, J., Laskin, A., Nizkorodov, S. A., Roach, P., Eckert, P., Gilles, M. K., Wang, B., Lee, H. J., and
837 Hu, Q.: Molecular selectivity of brown carbon chromophores, Environ Sci Technol, 48, 12047-
838 12055, 10.1021/es503432r, 2014.
839 Lee, H. J., Aiona, P. K., Laskin, A., Laskin, J., and Nizkorodov, S. A.: Effect of Solar Radiation on the
840 Optical Properties and Molecular Composition of Laboratory Proxies of Atmospheric Brown
841 Carbon, Environmental Science & Technology, 48, 10217-10226, 10.1021/es502515r, 2014.
842 Lei, Y., Shen, Z., Zhang, T., Lu, D., Zeng, Y., Zhang, Q., Xu, H., Bei, N., Wang, X., and Cao, J.: High
843 time resolution observation of PM2.5 Brown carbon over Xi'an in northwestern China: Seasonal
844 variation and source apportionment, Chemosphere, 237, 10.1016/j.chemosphere.2019.124530,
845 2019.
846 Li, C., He, Q., Hettiyadura, A. P. S., Kafer, U., Shmul, G., Meidan, D., Zimmermann, R., Brown, S. S.,
847 George, C., Laskin, A., and Rudich, Y.: Formation of Secondary Brown Carbon in Biomass Burning
848 Aerosol Proxies through NO(3) Radical Reactions, Environ Sci Technol, 54, 1395-1405,
849 10.1021/acs.est.9b05641, 2020.
850 Li, X., Kang, S., He, X., Qu, B., Tripathee, L., Jing, Z., Paudyal, R., Li, Y., Zhang, Y., Yan, F., Li, G., and
851 Li, C.: Light-absorbing impurities accelerate glacier melt in the Central Tibetan Plateau, Sci Total
852 Environ, 587-588, 482-490, 10.1016/j.scitotenv.2017.02.169, 2017.
853 Li, Y., Fu, T.-M., Yu, J. Z., Zhang, A., Yu, X., Ye, J., Zhu, L., Shen, H., Wang, C., Yang, X., Tao, S., Chen,
854 Q., Li, Y., Li, L., Che, H., and Heald, C. L.: Nitrogen dominates global atmospheric organic aerosol
855 absorption, 387, 989-995, doi:10.1126/science.adr4473, 2025.

Liu, D., Whitehead, J., Alfarra, M. R., Reyes-Villegas, E., Spracklen, Dominick V., Reddington, Carly L., Kong, S., Williams, Paul I., Ting, Y.-C., Haslett, S., Taylor, Jonathan W., Flynn, Michael J., Morgan, William T., McFiggans, G., Coe, H., and Allan, James D.: Black-carbon absorption enhancement in the atmosphere determined by particle mixing state, Nature Geoscience, 10, 184-188, 10.1038/ngeo2901, 2017.

Liu, Y., Wang, Y., Cao, Y., Yang, X., Zhang, T., Luan, M., Lyu, D., Hansen, A. D. A., Liu, B., and Zheng, M.: Impacts of COVID-19 on Black Carbon in Two Representative Regions in China: Insights Based on Online Measurement in Beijing and Tibet, Geophys Res Lett, 48, e2021GL092770, 10.1029/2021GL092770, 2021.

Luo, B., Kuang, Y., Huang, S., Song, Q., Hu, W., Li, W., Peng, Y., Chen, D., Yue, D., Yuan, B., and Shao, M.: Parameterizations of size distribution and refractive index of biomass burning organic aerosol with black carbon content, Atmos. Chem. Phys., 22, 12401-12415, 10.5194/acp-22-12401-2022, 2022.

Martinsson, J., Eriksson, A. C., Nielsen, I. E., Malmborg, V. B., Ahlberg, E., Andersen, C., Lindgren, R., Nystrom, R., Nordin, E. Z., Brune, W. H., Svenningsson, B., Swietlicki, E., Boman, C., and Pagels, J. H.: Impacts of Combustion Conditions and Photochemical Processing on the Light Absorption of Biomass Combustion Aerosol, Environ Sci Technol, 49, 14663-14671, 10.1021/acs.est.5b03205, 2015.

Middlebrook, A. M., Bahreini, R., Jimenez, J. L., and Canagaratna, M. R.: Evaluation of Composition-Dependent Collection Efficiencies for the Aerodyne Aerosol Mass Spectrometer using Field Data, Aerosol Science and Technology, 46, 258-271, 10.1080/02786826.2011.620041, 2012.

Ming, J., Xiao, C., Du, Z., and Yang, X.: An overview of black carbon deposition in High Asia glaciers and its impacts on radiation balance, Advances in Water Resources, 55, 80-87, 10.1016/j.advwatres.2012.05.015, 2013.

Mo, Y., Li, J., Liu, J., Zhong, G., Cheng, Z., Tian, C., Chen, Y., and Zhang, G.: The influence of solvent and pH on determination of the light absorption properties of water-soluble brown carbon, Atmospheric Environment, 161, 90-98, 10.1016/j.atmosenv.2017.04.037, 2017.

Moschos, V., Christensen, C., Mouton, M., Fiddler, M. N., Isolabella, T., Mazzei, F., Massabò, D., Turpin, B. J., Bililign, S., and Surratt, J. D.: Quantifying the Light-Absorption Properties and Molecular

Composition of Brown Carbon Aerosol from Sub-Saharan African Biomass Combustion, Environmental Science & Technology, 10.1021/acs.est.3c09378, 2024.

Ni, H., Huang, R. J., Pieber, S. M., Corbin, J. C., Stefenelli, G., Pospisilova, V., Klein, F., Gysel-Beer, M., Yang, L., Baltensperger, U., Haddad, I. E., Slowik, J. G., Cao, J., Prevot, A. S. H., and Dusek, U.: Brown Carbon in Primary and Aged Coal Combustion Emission, Environ Sci Technol, 55, 5701-5710, 10.1021/acs.est.0c08084, 2021.

Onasch, T. B., Trimborn, A., Fortner, E. C., Jayne, J. T., Kok, G. L., Williams, L. R., Davidovits, P., and Worsnop, D. R.: Soot Particle Aerosol Mass Spectrometer: Development, Validation, and Initial Application, Aerosol Science and Technology, 46, 804-817, 10.1080/02786826.2012.663948, 2012.

Peng, J., Hu, M., Guo, S., Du, Z., Zheng, J., Shang, D., Levy Zamora, M., Zeng, L., Shao, M., Wu, Y. S., Zheng, J., Wang, Y., Glen, C. R., Collins, D. R., Molina, M. J., and Zhang, R.: Markedly enhanced absorption and direct radiative forcing of black carbon under polluted urban environments, Proc Natl Acad Sci U S A, 113, 4266-4271, 10.1073/pnas.1602310113, 2016.

Phillips, S. M., Bellcross, A. D., and Smith, G. D.: Light Absorption by Brown Carbon in the Southeastern United States is pH-dependent, Environ Sci Technol, 51, 6782-6790, 10.1021/acs.est.7b01116, 2017.

Powelson, M. H., Espelien, B. M., Hawkins, L. N., Galloway, M. M., and De Haan, D. O.: Brown carbon formation by aqueous-phase carbonyl compound reactions with amines and ammonium sulfate, Environ Sci Technol, 48, 985-993, 10.1021/es4038325, 2014.

Qin, Y. M., Tan, H. B., Li, Y. J., Li, Z. J., Schurman, M. I., Liu, L., Wu, C., and Chan, C. K.: Chemical characteristics of brown carbon in atmospheric particles at a suburban site near Guangzhou, China, Atmospheric Chemistry and Physics, 18, 16409-16418, 10.5194/acp-18-16409-2018, 2018.

Retama, A., Ramos-Cerón, M., Rivera-Hernández, O., Allen, G., and Velasco, E.: Aerosol optical properties and brown carbon in Mexico City, Environmental Science: Atmospheres, 2, 315-334, 10.1039/d2ea00006g, 2022.

Saleh, R.: From Measurements to Models: Toward Accurate Representation of Brown Carbon in Climate Calculations, Current Pollution Reports, 6, 90-104, 10.1007/s40726-020-00139-3, 2020.

Saleh, R., Robinson, E. S., Tkacik, D. S., Ahern, A. T., Liu, S., Aiken, A. C., Sullivan, R. C., Presto, A. A., Dubey, M. K., Yokelson, R. J., Donahue, N. M., and Robinson, A. L.: Brownness of organics in

aerosols from biomass burning linked to their black carbon content, Nature Geoscience, 7, 647-650, 10.1038/ngeo2220, 2014.

Shen, G., Xiong, R., Cheng, H., and Tao, S.: Rural residential energy carrier structure and primary PM_{2.5} emissions from the Qinghai-Tibet Plateau, Chinese Science Bulletin, 66, 1900-1911, 10.1360/tb-2020-0408, 2021.

Singh, A., Rastogi, N., Kumar, V., Slowik, J. G., Satish, R., Lalchandani, V., Thamban, N. M., Rai, P., Bhattu, D., Vats, P., Ganguly, D., Tripathi, S. N., and Prévôt, A. S. H.: Sources and characteristics of light-absorbing fine particulates over Delhi through the synergy of real-time optical and chemical measurements, ATMOSPHERIC ENVIRONMENT, 252, 10.1016/j.atmosenv.2021.118338, 2021.

Sumlin, B. J., Pandey, A., Walker, M. J., Pattison, R. S., Williams, B. J., and Chakrabarty, R. K.: Atmospheric Photooxidation Diminishes Light Absorption by Primary Brown Carbon Aerosol from Biomass Burning, Environmental Science & Technology Letters, 4, 540-545, 10.1021/acs.estlett.7b00393, 2017.

Sun, J., Xie, C., Xu, W., Chen, C., Ma, N., Xu, W., Lei, L., Li, Z., He, Y., Qiu, Y., Wang, Q., Pan, X., Su, H., Cheng, Y., Wu, C., Fu, P., Wang, Z., and Sun, Y.: Light absorption of black carbon and brown carbon in winter in North China Plain: comparisons between urban and rural sites, Science of The Total Environment, 770, 10.1016/j.scitotenv.2020.144821, 2021.

Tang, J., Li, J., Su, T., Han, Y., Mo, Y., Jiang, H., Cui, M., Jiang, B., Chen, Y., Tang, J., Song, J., Peng, P. a., and Zhang, G.: Molecular compositions and optical properties of dissolved brown carbon in biomass burning, coal combustion, and vehicle emission aerosols illuminated by excitation–emission matrix spectroscopy and Fourier transform ion cyclotron resonance mass spectrometry analysis, Atmospheric Chemistry and Physics, 20, 2513-2532, 10.5194/acp-20-2513-2020, 2020.

Tang, S., Li, F., Lv, J., Liu, L., Wu, G., Wang, Y., Yu, W., Wang, Y., and Jiang, G.: Unexpected molecular diversity of brown carbon formed by Maillard-like reactions in aqueous aerosols, Chem Sci, 13, 8401-8411, 10.1039/d2sc02857c, 2022.

Tian, J., Wang, Q., Ma, Y., Wang, J., Han, Y., and Cao, J.: Impacts of biomass burning and photochemical processing on the light absorption of brown carbon in the southeastern Tibetan Plateau, Atmospheric Chemistry and Physics, 23, 1879-1892, 10.5194/acp-23-1879-2023, 2023.

Ulbrich, I. M., Canagaratna, M. R., Zhang, Q., Worsnop, D. R., and Jimenez, J. L.: Interpretation of

943 organic components from Positive Matrix Factorization of aerosol mass spectrometric data,
944 Atmospheric Chemistry and Physics, 9, 2891-2918, 10.5194/acp-9-2891-2009, 2009.
945 Usha, K. H., Nair, V. S., and Babu, S. S.: Effects of Aerosol–Induced Snow Albedo Feedback on the
946 Seasonal Snowmelt Over the Himalayan Region, Water Resources Research, 58,
947 10.1029/2021wr030140, 2022.
948 Wang, D., Shen, Z., Zhang, Q., Lei, Y., Zhang, T., Huang, S., Sun, J., Xu, H., and Cao, J.: Winter brown
949 carbon over six of China's megacities: light absorption, molecular characterization, and improved
950 source apportionment revealed by multilayer perceptron neural network, Atmospheric Chemistry
951 and Physics, 22, 14893-14904, 10.5194/acp-22-14893-2022, 2022a.
952 Wang, L. Y., Qu, Y., Wang, N., Shi, J. L., Zhou, Y., Cao, Y., Yang, X. L., Shi, Y. Q., Liu, S. X., Zhu, C.
953 S., and Cao, J. J.: Long-term spatial distribution and implication of black and brown carbon in the
954 Tibetan Plateau, Sci Total Environ, 945, 174093, 10.1016/j.scitotenv.2024.174093, 2024.
955 Wang, Q., Zhou, Y., Ma, N., Zhu, Y., Zhao, X., Zhu, S., Tao, J., Hong, J., Wu, W., Cheng, Y., and Su, H.:
956 Review of Brown Carbon Aerosols in China: Pollution Level, Optical Properties, and Emissions,
957 Journal of Geophysical Research: Atmospheres, 127, 10.1029/2021jd035473, 2022b.
958 Wang, Q., Han, Y., Ye, J., Liu, S., Pongpiachan, S., Zhang, N., Han, Y., Tian, J., Wu, C., Long, X., Zhang,
959 Q., Zhang, W., Zhao, Z., and Cao, J.: High Contribution of Secondary Brown Carbon to Aerosol
960 Light Absorption in the Southeastern Margin of Tibetan Plateau, Geophysical Research Letters, 46,
961 4962-4970, 10.1029/2019gl082731, 2019a.
962 Wang, Q., Ye, J., Wang, Y., Zhang, T., Ran, W., Wu, Y., Tian, J., Li, L., Zhou, Y., Hang Ho, S. S., Dang,
963 B., Zhang, Q., Zhang, R., Chen, Y., Zhu, C., and Cao, J.: Wintertime Optical Properties of Primary
964 and Secondary Brown Carbon at a Regional Site in the North China Plain, Environmental Science
965 & Technology, 53, 12389-12397, 10.1021/acs.est.9b03406, 2019b.
966 Wang, X., Heald, C. L., Liu, J., Weber, R. J., Campuzano-Jost, P., Jimenez, J. L., Schwarz, J. P., and
967 Perring, A. E.: Exploring the observational constraints on the simulation of brown carbon,
968 Atmospheric Chemistry and Physics, 18, 635-653, 10.5194/acp-18-635-2018, 2018.
969 Wang, X., Chakrabarty, R. K., Schwarz, J. P., Murphy, S. M., Levin, E. J. T., Howell, S. G., Guo, H.,
970 Campuzano-Jost, P., and Jimenez, J. L.: Dark brown carbon from biomass burning contributes to
971 significant global-scale positive forcing, One Earth, 10.1016/j.oneear.2025.101205, 2025.

Wang, Y., Hu, M., Lin, P., Guo, Q., Wu, Z., Li, M., Zeng, L., Song, Y., Zeng, L., Wu, Y., Guo, S., Huang, X., and He, L.: Molecular Characterization of Nitrogen-Containing Organic Compounds in Humic-like Substances Emitted from Straw Residue Burning, Environmental Science & Technology, 51, 5951-5961, 10.1021/acs.est.7b00248, 2017.

Wang, Y. Q.: An Open Source Software Suite for Multi-Dimensional Meteorological Data Computation and Visualisation, Journal of Open Research Software, 7, 10.5334/jors.267, 2019.

Washenfelder, R. A., Attwood, A. R., Brock, C. A., Guo, H., Xu, L., Weber, R. J., Ng, N. L., Allen, H. M., Ayres, B. R., Baumann, K., Cohen, R. C., Draper, D. C., Duffey, K. C., Edgerton, E., Fry, J. L., Hu, W. W., Jimenez, J. L., Palm, B. B., Romer, P., Stone, E. A., Wooldridge, P. J., and Brown, S. S.: Biomass burning dominates brown carbon absorption in the rural southeastern United States, Geophysical Research Letters, 42, 653-664, https://doi.org/10.1002/2014GL062444, 2015.

Wong, J. P. S., Nenes, A., and Weber, R. J.: Changes in Light Absorptivity of Molecular Weight Separated Brown Carbon Due to Photolytic Aging, Environ Sci Technol, 51, 8414-8421, 10.1021/acs.est.7b01739, 2017.

Xiang, Y., Li, X., Zhang, T., Cheng, Q., Yan, C., Liu, X., Liu, Y., Wang, Y., Kang, S., Ding, X., and Zheng, M.: Characteristics and Sources of Organic Aerosol in PM2.5 at Yangbajing in Tibetan Plateau, Atmospheric Environment, 333, 10.1016/j.atmosenv.2024.120662, 2024.

Xie, M., Hays, M. D., and Holder, A. L.: Light-absorbing organic carbon from prescribed and laboratory biomass burning and gasoline vehicle emissions, Sci Rep, 7, 7318, 10.1038/s41598-017-06981-8, 2017.

Xu, J., Zhang, Q., Shi, J., Ge, X., Xie, C., Wang, J., Kang, S., Zhang, R., and Wang, Y.: Chemical characteristics of submicron particles at the central Tibetan Plateau: insights from aerosol mass spectrometry, Atmospheric Chemistry and Physics, 18, 427-443, 10.5194/acp-18-427-2018, 2018.

Xu, L., Lin, G., Liu, X., Wu, C., Wu, Y., and Lou, S.: Constraining Light Absorption of Brown Carbon in China and Implications for Aerosol Direct Radiative Effect, Geophysical Research Letters, 51, 10.1029/2024gl109861, 2024.

Yao, T., Thompson, L. G., Mosbrugger, V., Zhang, F., Ma, Y., Luo, T., Xu, B., Yang, X., Joswiak, D. R., Wang, W., Joswiak, M. E., Devkota, L. P., Tayal, S., Jilani, R., and Fayziev, R.: Third Pole Environment (TPE), Environmental Development, 3, 52-64, 10.1016/j.envdev.2012.04.002, 2012.

Yu, L., Smith, J., Laskin, A., George, K. M., Anastasio, C., Laskin, J., Dillner, A. M., and Zhang, Q.: Molecular transformations of phenolic SOA during photochemical aging in the aqueous phase: competition among oligomerization, functionalization, and fragmentation, Atmospheric Chemistry and Physics, 16, 4511-4527, 10.5194/acp-16-4511-2016, 2016.

Yue, S., Bikkina, S., Gao, M., Barrie, L. A., Kawamura, K., and Fu, P.: Sources and Radiative Absorption of Water-Soluble Brown Carbon in the High Arctic Atmosphere, Geophysical Research Letters, 46, 14881-14891, 10.1029/2019gl085318, 2019.

Yue, S., Zhu, J., Chen, S., Xie, Q., Li, W., Li, L., Ren, H., Su, S., Li, P., Ma, H., Fan, Y., Cheng, B., Wu, L., Deng, J., Hu, W., Ren, L., Wei, L., Zhao, W., Tian, Y., Pan, X., Sun, Y., Wang, Z., Wu, F., Liu, C.-Q., Su, H., Penner, J. E., Pöschl, U., Andreae, M. O., Cheng, Y., and Fu, P.: Brown carbon from biomass burning imposes strong circum-Arctic warming, One Earth, 5, 293-304, 10.1016/j.oneear.2022.02.006, 2022.

Zhai, J., Yang, X., Li, L., Bai, B., Liu, P., Huang, Y., Fu, T.-M., Zhu, L., Zeng, Z., Tao, S., Lu, X., Ye, X., Wang, X., Wang, L., and Chen, J.: Absorption Enhancement of Black Carbon Aerosols Constrained by Mixing-State Heterogeneity, Environmental Science & Technology, 56, 1586-1593, 10.1021/acs.est.1c06180, 2022.

Zhang, Q., Jimenez, J. L., Canagaratna, M. R., Ulbrich, I. M., Ng, N. L., Worsnop, D. R., and Sun, Y.: Understanding atmospheric organic aerosols via factor analysis of aerosol mass spectrometry: a review, Anal Bioanal Chem, 401, 3045-3067, 10.1007/s00216-011-5355-y, 2011.

Zhang, Q., Shen, Z., Zhang, L., Zeng, Y., Ning, Z., Zhang, T., Lei, Y., Wang, Q., Li, G., Sun, J., Westerdahl, D., Xu, H., and Cao, J.: Investigation of Primary and Secondary Particulate Brown Carbon in Two Chinese Cities of Xi'an and Hong Kong in Wintertime, Environmental Science & Technology, 54, 3803-3813, 10.1021/acs.est.9b05332, 2020a.

Zhang, X., Xu, J., and Kang, S.: Chemical characterization of submicron particulate matter (PM1) emitted by burning highland barley in the northeastern part of the Qinghai–Tibet Plateau, Atmospheric Environment, 224, 10.1016/j.atmosenv.2020.117351, 2020b.

Zhang, X., Xu, J., Zhai, L., and Zhao, W.: Characterization of Aerosol Properties from the Burning Emissions of Typical Residential Fuels on the Tibetan Plateau, Environ Sci Technol, 10.1021/acs.est.2c04211, 2022a.

Zhang, X., Xu, J., Kang, S., Sun, J., Shi, J., Gong, C., Sun, X., Du, H., Ge, X., and Zhang, Q.: Regional Differences in the Light Absorption Properties of Fine Particulate Matter Over the Tibetan Plateau: Insights From HR-ToF-AMS and Aethalometer Measurements, Journal of Geophysical Research: Atmospheres, 126, 10.1029/2021jd035562, 2021.

Zhang, Y., Wang, Q., Tian, J., Li, Y., Liu, H., Ran, W., Han, Y., Prévôt, A. S. H., and Cao, J.: Impact of COVID-19 lockdown on the optical properties and radiative effects of urban brown carbon aerosol, Geoscience Frontiers, 13, 101320, https://doi.org/10.1016/j.gsf.2021.101320, 2022b.

Zhang, Y., Albinet, A., Petit, J.-E., Jacob, V., Chevrier, F., Gille, G., Pontet, S., Chrétien, E., Dominik-Sègue, M., Levigoureux, G., Močnik, G., Gros, V., Jaffrezo, J.-L., and Favez, O.: Substantial brown carbon emissions from wintertime residential wood burning over France, Science of The Total Environment, 743, 10.1016/j.scitotenv.2020.140752, 2020c.

Zhao, R., Lee, A. K. Y., Huang, L., Li, X., Yang, F., and Abbatt, J. P. D.: Photochemical processing of aqueous atmospheric brown carbon, Atmospheric Chemistry and Physics, 15, 6087-6100, 10.5194/acp-15-6087-2015, 2015.

Zhao, W., Zhang, X., Zhai, L., Shen, X., and Xu, J.: Chemical characterization and sources of submicron aerosols in Lhasa on the Qinghai–Tibet Plateau: Insights from high-resolution mass spectrometry, Science of The Total Environment, 152866, 10.1016/j.scitotenv.2021.152866, 2022.

Zhao, Z., Cao, J., Shen, Z., Xu, B., Zhu, C., Chen, L.-W. A., Su, X., Liu, S., Han, Y., Wang, G., and Ho, K.: Aerosol particles at a high-altitude site on the Southeast Tibetan Plateau, China: Implications for pollution transport from South Asia, 118, 11,360-311,375, https://doi.org/10.1002/jgrd.50599, 2013.

Zhong, M. and Jang, M.: Dynamic light absorption of biomass-burning organic carbon photochemically aged under natural sunlight, Atmos. Chem. Phys., 14, 1517-1525, 10.5194/acp-14-1517-2014, 2014.

Zhong, M., Xu, J., Wang, H., Gao, L., Zhu, H., Zhai, L., Zhang, X., and Zhao, W.: Characterizing water-soluble brown carbon in fine particles in four typical cities in northwestern China during wintertime: integrating optical properties with chemical processes, Atmos. Chem. Phys., 23, 12609-12630, 10.5194/acp-23-12609-2023, 2023.

Zhu, C.-S., Qu, Y., Huang, H., Shi, J.-L., Dai, W.-T., Zhang, N.-N., Wang, N., Wang, L.-Y., Ji, S.-S., and Cao, J.-J.: Brown Carbon From Biomass Burning Reinforces the Himalayas and Tibetan Plateau Warming, Geophysical Research Letters, 51, e2023GL107269,

https://doi.org/10.1029/2023GL107269, 2024.

Zhu, C.-S., Cao, J.-J., Hu, T.-F., Shen, Z.-X., Tie, X.-X., Huang, H., Wang, Q.-Y., Huang, R.-J., Zhao, Z.-Z., Močnik, G., and Hansen, A. D. A.: Spectral dependence of aerosol light absorption at an urban and a remote site over the Tibetan Plateau, Science of The Total Environment, 590-591, 14-21, https://doi.org/10.1016/j.scitotenv.2017.03.057, 2017.

Zhu, C. S., Qu, Y., Huang, H., Chen, J., Dai, W. T., Huang, R. J., and Cao, J. J.: Black Carbon and Secondary Brown Carbon, the Dominant Light Absorption and Direct Radiative Forcing Contributors of the Atmospheric Aerosols Over the Tibetan Plateau, Geophysical Research Letters, 48, 10.1029/2021gl092524, 2021.

Supplement of

Strong Primary contribution to Brown Carbon light absorption in Tibet and urban areas: insights based on in situ measurement

Wenhui Zhao et al.

Correspondence to: Weiwei Hu (E-mail：weiweihu@gig.ac.cn)； Shan Huang (Email: shanhuang_eci@jnu.edu.cn)

Supplementary Information Contents:

Text S1. Positive matrix factorization (PMF) analysis

SP-AMS is based on the design of a high-resolution time-of-flight aerosol mass spectrometer (HR-ToF-AMS) (Decarlo et al., 2006), while SP-AMS has an additional Nd-YAG intra-cavity infrared (IR) laser module at the wavelength of 1064nm (Onasch et al., 2012). In this study, the SP-AMS at YBJ site was operated at 4 min alternating intervals between tungsten-only vaporizer mode (TV mode) and dual-vaporizer mode (DV mode), implemented by alternately activating (IR laser-on, i.e., dual vaporizers) and deactivating the laser vaporizer (IR laser-off, i.e., tungsten vaporizer only). In TV mode, the SP-AMS performs identically to the HR-ToF-AMS, providing continuous high-resolution mass concentration and mass spectral data for non-refractory submicron particulate matter (NR-PM_1). In DV mode, simultaneous use of both vaporizers enables real-time quantification of refractory black carbon (rBC) and NR-PM_1. rBC absorbs strongly at 1064nm and consequently heats up to ～ 4000 ℃ for rBC vaporization (Onasch et al., 2012). The term rBC is operationally defined, referring to BC particles detected by SP-AMS. However, the data for the PMF analysis in this study originated exclusively from the tungsten-vaporizer mode (the data for dual-vaporizer mode will be discussed in Liang et al. in preparation). Thus, the positive matrix factorization (PMF) was performed on the high-resolution mass spectra of organic aerosol (OA) of the SP-AMS operated with tungsten-only vaporizer at the YBJ site. Figure S2 is the standard determination panel for separating the PMF factors. The solutions of factor 1–8 with fpeak varied from -1 to 1 were run. The Q/Q_{exp}, scaled residuals, comparison between mass spectra of individual factors, diurnal variation of each factor, and comparison of the temporal evolution of every factor with corresponding external tracers were used to identify the best correlation for determining the optimum number of factors. The detailed steps were listed in a previous study (Zhang et al., 2011). The sharp decrease of Q/Q_{exp} suggest there are mass was not resolved out when 2-factor solutions were chosen. Values of $Q/Q_{exp} >> 1$ indicate either an underestimation of the errors or the presence of variability in the factor mass spectra that cannot be adequately modeled by the sum of the given number of factors. $Q/Q_{exp} << 1$ indicates overestimation of the errors of the input data (Ulbrich et al., 2009). In this study, Q/Q_{exp} =0.82 under the final PMF result of 5-factor solution is within an acceptable range. Table S1 summarized the descriptions of PMF solutions. In general, the 5-factor solution is the optimum solution. For 4-factor solution, we found mixed factor between BBOA and Biofuel OA. For 6-10 factor solution, we found there is an extra factor with unexplained peak (m/z 77) in their spectrum. As shown in Fig. S2, 5–factors solution (fpeak = 0) is the best solution, including biomass burning OA (BBOA), hydrocarbon-like OA (HOA), BBOA mixed with cooking-related OA (COA) (biofuel–OA), less-oxidized oxygenated OA (LO-OOA), and more-oxidized oxygenated OA (MO-OOA) (Fig. S4).

At the GIG site, unconstrained PMF (factor 1–8 with fpeak varied from -1 to 1) was also first performed on the OA measured by the ToF–ACSM (Fig. S2). However, we didn't find the best solution due to the ambiguous factor3 (mixed with BBOA and COA) in the 5 factor-solution as shown in Fig. S2. For UMR spectrum, multiple studies show that the BBOA and COA is hard to separate with unconstrained-PMF (Zhang et al., 2019b). Especially, when the BBOA contribution is

less than 10%, their good separation in the unconstrained-PMF is unachievable. However, we know that the Guangzhou sampling site (GIG site) was impacted by the biomass burning from surrounding areas based the results from previous study (Cai et al., 2023; Jiang et al., 2021; Jiang et al., 2022). In addition, in Fig. 1 we show fire spots data during our observation period. The back trajectory data indicates our observation site might impacted by the fire plumes from surrounding. To resolve out the contribution of BBOA, Multilinear Engine 2 (ME-2; SoFi 6.8) (Canonaco et al., 2013) was applied here. Previous study proved that using the standard BBOA spectrum, the BBOA can be efficiently resolved out in the UMR dataset (Crippa et al., 2014; Lanz et al., 2007).– We constrained BBOA by applying the standard BBOA mass spectra (Hu et al., 2016; Hu et al., 2013) with a wide range of a value (e.g., a value = 0–1) ~~based on Multilinear Engine 2 (ME-2; SoFi 6.8) (Canonaco et al., 2013)~~. Finally, we selected an optimum solution of 5 factors in ME-2 with a value=0 (Figs. S3 and S4), including COA, BBOA, HOA, LO-OOA, and MO-OOA.

Biomass burning OA (BBOA) and Biofuel–OA

The BBOA component was identified at the YBJ site with an obvious peak at m/z 60 ($C_2H_4O_2^+$) and 73 ($C_3H_5O_2^+$) signals in the MS (Fig. S4), which are usually considered as a recognized tracer emitted from biomass burning (Alfarra et al., 2007). Different from the BBOA factor in other cities in eastern China, which is mainly from burning of residual straw or wood for heating, the BBOA in Tibet was mainly from wormwood, cypress branches, highland barley, yak butter, zanba, and so on (Cui et al., 2018; Zhang et al., 2020b). The diurnal variation in BBOA therefore (Fig. S4) showed a unique diurnal pattern with two peaks in the morning (~ 8:00) and evening (20:00–21:00). This pattern was mainly related to the lifecycle of residents in Tibet, who routinely perform "Weisang" activity during the morning and evening each day. The BBOA component identified at GIG site showed different diurnal variation with enhanced afternoon and nighttime peaks likely reflect regional transport of biomass burning emissions from agricultural activities in the Pearl River Delta region during summer (Cai et al., 2023; Wang et al., 2017).

The Biofuel-OA component at the YBJ site was characterized by the highest m/z 55 ($C_3H_3O^+$) signal and a higher ratio of m/z 55/57 compared with HOA (Zhang et al., 2011), as well as the m/z 73 ($C_3H_5O_2^+$) signal. The time series of biofuel-OA component showed a close correlation with emissions of tracking ions fragments $C_3H_3O^+$ (R=0.8) and $C_6H_{10}O^+$ (R=0.93) (Fig. S~~5~~6), which were also highly correlated with the emissions of biomass burning fragments $C_2H_4O_2^+$ (R=0.93). These findings demonstrated that this factor was associated with emissions of biomass burning and cooking. In this study at YBJ site, the diurnal variation in COA showed three notable peaks corresponding to breakfast time (8:00), lunchtime (13:00), and dinner time (21:00) in Tibet, while peaks occurred at 7:00, 12:00 and 19:00 for GIG site, which coincided with different schedules between urban Guangzhou and remote Tibet.

Hydrocarbon-like OA (HOA)

The HOA component identified at the YBJ site, sourced from traffic emissions and/or other fossil fuel burning activities, presented a high-resolution mass spectrum (Fig. S4) resembling that of former research (Zhang et al., 2011; Ulbrich et al., 2009; Hu et al., 2016; Xu et al., 2014). The hydrocarbon ion series of $C_xH_y^+$ dominated the MS of HOA; therein $C_3H_5^+$, $C_3H_7^+$, $C_4H_7^+$, $C_4H_9^+$,

$C_5H_9^+$ and $C_5H_{11}^+$ (m/z = 41, 43, 55, 57, 69, 71) were the main constituents (Ng et al., 2011; Zhang et al., 2005b; Xu et al., 2014; Zhang et al., 2019a). The O/C ratio of HOA in this study was 0.11, suggesting its fresh property. The tight correlation between HOA versus BC and $C_4H_9^+$ (R = 0.53 and 0.92; Fig. ~~S5A~~6a) also indicated that the source of HOA was from traffic emissions. In addition, two distinct peaks of HOA occurred in the morning (8:00-9:00) and evening (20:00-21:00) rush hours (Fig. 4). All these characteristics suggested a reasonable decomposition for HOA. At the GIG site, HOA displayed a bimodal distribution with a moderate morning peak at 07:00 and a stronger evening peak at 20:00 (Fig. 4), consistent with typical urban HOA diurnal patterns. The enhanced evening peak coincides with rush-hour traffic congestion, suggesting intensified vehicular emissions during these periods. Notably, the evening peak magnitude exceeds morning levels, potentially reflecting combined effects of meteorological conditions (e.g., reduced boundary layer height) and emission intensity.

Despite the three POA factors, i.e., HOA, BBOA, and Biofuel OA show similar peak in the morning, their night peaks are different with HOA peaked later an hour than BBOA and Biofuel OA, supporting their different origins based on their time series (e.g., the Pearson correlation coefficient between BBOA and HOA is only 0.41 (Fig. S6a)).

For the POA factors mass spectra, scatter plots showed correlation coefficients between BBOA and HOA, Biofuel-OA and HOA, BBOA and Biofuel-OA were 0.52, 0.85 and 0.64, respectively (Fig. S5), suggesting the BBOA spectra shows distinct differences with HOA and biofuel-OA, however, biofuel-OA and HOA have similarity. Despite the similarity between biofuel-OA and HOA, we can still distinguish them based on their relatively unique and abundant "tracer ions". As shown in Table S2, the most obvious difference between Biofuel-OA and HOA lies in the fact that Biofuel-OA has an obvious higher ratio of m/z 55/57 (2.6) than that of HOA (with m/z 55/57 = 0.9) (Zhang et al., 2011), as well as the higher m/z 60 ($C_2H_4O_2^+$) and 73 ($C_3H_5O_2^+$) signals. Different mass spectra characteristics prove that HOA and biofuel OA have significantly different sources.

Oxygenated OA (OOA)

The mass spectra of MO-OOA and LO-OOA at the YBJ site were characterized by high peaks at m/z 44 (mostly CO_2^+) and LO-OOA had a larger peak at m/z 43 (mostly $C_2H_3O^+$) as well (Crippa et al., 2013; Hu et al., 2016; Lanz et al., 2007; Sun et al., 2010; Zhang et al., 2005a). As a highly oxidizing species, MO-OOA is consistent with the time variation of sulfate (R=0.74; Fig. ~~S5a~~S6a). Among all OA factors, MO-OOA had the highest O/C (0.78) and the lowest H/C (1.40), indicating a high oxidation degree of this factor, while LO-OOA had the lower O/C (0.55). There is a good correlation between the LO-OOA factor time series and the characteristic ion fragments $C_2H_3O^+$ and $C_3H_3O^+$ with R of 0.95 and 0.75 (Fig. ~~S5a~~S6a), respectively. The diurnal variation of LO-OOA and MO-OOA was characterized by high values during the day and low values at night, with the fact that MO-OOA concentrations (6:00) increased approximately two hours later than LO-OOA (8:00) during the daytime, indicating different degrees of photochemical aging of local or regional aerosols under strong solar radiation. At the GIG site, the mass spectrum of the MO-OOA was similar to the MO-OOA of the YBJ site, with high peaks at m/z 44 and the diurnal pattern, demonstrating that

MO-OOA was significantly influenced by aging processes, in particular photochemistry. The concentration of MO-OOA showed a better correlation with that of sulfate (R = 0.87) than with nitrate (R = 0.7) (Fig. ~~S5b~~S6b), which is likely attributed to similarly high oxidation degrees of both MO-OOA and sulfate. The LO-OOA component identified at the GIG site is also characterized by a high m/z 44 signal but lower than that of MO-OOA, indicating its relatively fresh Features.

Text S2. Uncertainty analysis for the MLR method.

Before the MLR method was applied, the correlations between the BrC absorption coefficients at 370nm ($Abs_{BrC,370nm}$) and the mass loadings of OA factors were evaluated as shown in Fig. S10~~9~~. Results show that BBOA and HOA concentrations were well correlated with $Abs_{BrC,370nm}$ (R = 0.77 and R = 0.64). A moderate correlation (R = 0.31) was also found between $Abs_{BrC,370nm}$ and the LO-OOA mass concentration. The correlation for MO-OOA was near zero, indicating that aging may have reduced the absorption capacity. In addition, the correlation coefficient of each PMF factor was also performed for each campaign. At the YBJ site, it shows that the BBOA factor correlated strongly with the biofuel-OA factor (R = 0.89; Fig. S6~~5~~a), which caused multicollinearity issues. To solve this issue, we set four different cases via combining or removing the latent collinearity factors to test the sensitivity of the MLR method, including considering all five individual factors (case 1), removing biofuel-OA (case 2), combining BBOA and biofuel-OA (case 3), and removing BBOA (case 4), as shown in Table ~~S2~~S5.

At the GIG site, due to the strong similarity among time series of each factor (while different mass spectral profiles as shown in Fig. S4), the factors, except HOA, showed varying degrees of strong correlation with each other, as shown in Fig. S6~~5~~b. And all OA factors were well or moderately correlated with $Abs_{BrC,370nm}$ (Fig. S10~~9~~). Based on these problems, we set up three scenarios to test the sensitivity of the MLR method, including considering all five individual factors (case 1) and combining all collinearity factors except HOA (case 2). In addition, we also consider the hypothesis that only BBOA and HOA are absorptive (case 3).

To get the best final solution, we calculated the total uncertainty of the MLR regression coefficients (i.e., MAC) for each case using Monte Carlo. For the Monte Carlo calculation input, the uncertainty of the PMF factor mass concentration needs to be evaluated. A bootstrap analysis (100 iterations; (Ulbrich et al., 2009) was applied, which shows a 9–36 % uncertainty for the PMF factors at the YBJ site and 3 – 9 % at the GIG site, as shown in Table ~~S3~~S6. The uncertainty for the coefficient of BrC at 370 nm calculated using $AAE_{BC} = 1$ was estimated to be 43 % for the YBJ site and 36 % for the GIG site based on the lower (0.8) and upper limit of (1.2) previously reported AAE_{BC} range. The total uncertainties of each coefficient for each PMF factor were then calculated by Monte Carlo with 10,000 simulations.

Monte Carlo results show a high total uncertainty (Table ~~S4~~S7) of the factors when we don't deal with collinearity at all (i.e., case 1) at both sites, indicating that the collinearity problem among the factors does increase the uncertainty of the MLR regression coefficients (i.e., MAC).

Combining or removing collinearity factors (i.e., case 2–4 for the YBJ site or case 2–3 for the GIG

site) can effectively reduce the uncertainty.

Considering that biomass burning is widely reported as an important source of BrC light absorption and regarded as a warming agent affecting global climate (Wang et al., 2025), we consider all biomass burning related contributing sources when run the MLR model in the case of eliminating the collinearity problemin in this study. As previously reported in the literature (Kasthuriarachchi et al., 2020; Qin et al., 2018), the MAC of COA is nearly zero. Thus, the absorption of light by COA was not considered in this study. For the YBJ site, we finally combined the BBOA factor and the biofuel-OA factor as BBOA (case3). The final results show an uncertainty of BBOA (26.4 %), HOA (20.8 %), LO–OOA (56.3 %), and MO-OOA (57.9%), as shown in Table ~~S4~~S7. For the GIG site, we consider only including BBOA and HOA as input variables (case 3) for MLR at the GIG site. And the final results show an uncertainty of HOA (5.8 %), BBOA (6.8 %), and intercept (21.6 %).

We also evaluate the lower and upper limits of the proportion of different sources contributing to the BrC light absorption under all case scenarios. At the YBJ site, the lower limit of MAC is 1.11, 2.04. 0.07 and 0.07 $m^2 g^{-1}$ for BBOA, HOA, LO–OOA, and MO–OOA, while the upper limit of MAC is 2.54, 2.36, 0.23, and 0.29 $m^2 g^{-1}$ for BBOA, HOA, LO–OOA, and MO–OOA. At the GIG site, the lower limit of MAC is 1.91 and 2.57 $m^2 g^{-1}$ for BBOA and HOA, while the upper limit is 2.63 and 0.16 $m^2 g^{-1}$ for HOA and BBOA+LO–OOA+MO–OOA. As shown in Fig. S~~9~~8, at the YBJ site, BBOA was the significant contributor to BrC light absorption (46 %–54 %), followed by HOA (26 %–43 %) and SOA (11 %–20 %). At the GIG site, HOA was the significant contributor to BrC light absorption (50–54 %), followed by BBOA (36 %) and SOA (0–33 %). Regardless of the case, BBOA is still the dominant absorption contributor at the YBJ site, while HOA is the dominant absorption contributor at the GIG site, as well as the dominant contribution of POA to BrC light absorption in both sites, indicating the robust conclusion in this study.

Table S1. Descriptions of PMF solutions obtained at YBJ site and GIG site.

Factor number	**Fpeak**	**Q/Q_{exp}**	**Solution Description from Free PMF (YBJ site)**
1-3	0	1.4 to 0.93	Too few factors, large residuals at time periods and key m/z's. Q/Q_{exp} decreases very fast.
4	0	0.9	Except MO-OOA, LO-OOA and HOA, the characteristics of one factor is not clear. It seems that BBOA mixed with Biofuel OA.
5	**0**	**0.82**	**Optimum choices for PMF factors (MO-OOA, LO-OOA, HOA, BBOA and Biofuel OA). Time series and diurnal variations of PMF factors are consistent with the external tracers. The spectra of 5 factors are consistent with the source spectra in AMS spectra database.**
6	0	0.8	showed over-split factors without an explicit physical meaning
5	-1 to 1	0.873 to 0.892	Under the 5-factor solution, the factor contributions obtained by different fpeak are relatively stable, clarifying the stability and interpretability of the five-factor solution.
Factor number	**Fpeak/ a value**	**Q/Q_{exp}**	**Solution Description from free PMF and ME2 (GIG site)**
1-3	0	1.96-1.21	Too few factors, large residuals at time periods and key m/z's. Q/Q_{exp} decreases very fast.
4	0	1.15	Too few factors. Factors are mixed based on the time series and spectra.
5	0	1.1	Relatively reasonable profiles and time series under a fully unconstrained condition. However, BBOA was still mixed in other factors.
6	0	1.01	Factor split, e.g., COA was split into two factors with similar spectra, however, different time series.
5	-1 to 1	1.104 to 1.112	Under the 5-factor solution, factor MS and time series are nearly identical and the factor contributions obtained by different fpeaks are relatively stable, clarifying the stability and interpretability of the five-factor solution.
Factor number	**a value**	**Q/Q_{exp}**	**Solution Description from ME2 (GIG site)**
5	**a value: 0**	**1.05**	**Optimum choices for PMF factors (MO-OOA, LO-OOA, HOA, BBOA and COA) resolved by ME2. Time series and diurnal variations of PMF factors are consistent with the external tracers. The spectra of 5 factors are consistent with the source spectra in AMS spectra database.**
5	a value: 0 to 0.8	1.03 to 1.05	Under the 5-factor solution, factor MS and time series are nearly identical under different a value (Fig. S3)

Table S2. The main mass spectra characteristics of PMF factors at YBJ site and GIG site.

Factor	Main mass spectra characteristics (YBJ site)
HOA	dominated by alkyl fragments ($C_nH_{2n+1}^+$ and $C_nH_{2n-1}^+$). The O/C ratio of HOA in this study was 0.11, suggesting its fresh property. The tight correlation between HOA versus BC and $C_4H_9^+$ (R = 0.53 and 0.92; Fig. S6a) also indicated that the source of HOA was from traffic emissions.
BBOA	characterized by an obvious peak at m/z 60 ($C_2H_4O_2^+$) and 73 ($C_3H_5O_2^+$) signals in the MS (Fig. S4), which are usually considered as a recognized tracer emitted from biomass burning.
Biofuel OA	characterized by the highest m/z 55 ($C_3H_3O^+$) signal and a higher ratio of m/z 55/57 (2.6) compared with HOA (0.9) (Zhang et al., 2011), as well as the m/z 73 ($C_3H_5O_2^+$) signal. The time series of biofuel OA component showed a close correlation with emissions of tracking ions fragments $C_3H_3O^+$ (R=0.8) and $C_6H_{10}O^+$ (R=0.93) (Fig. S6), which were also highly correlated with the emissions of biomass burning fragments $C_2H_4O_2^+$ (R=0.93). These findings demonstrated that this factor was associated with emissions of biomass burning and cooking.
LO-OOA	characterized by high peaks at m/z 44 (mostly CO_2^+) and had a larger peak at m/z 43 (mostly $C_2H_3O^+$) than MO-OOA as well. LO-OOA had a lower O/C (0.55) than MO-OOA. There is a good correlation between the LO-OOA factor time series and the characteristic ion fragments $C_2H_3O^+$ and $C_3H_3O^+$ with R of 0.95 and 0.75 (Fig. S6a), respectively.
MO-OOA	characterized by high peaks at m/z 44 (mostly CO_2^+) and the time series was consistent with sulfate (R=0.74; Fig. S6a). MO-OOA had the highest O/C (0.78) and the lowest H/C (1.40), indicating a high oxidation degree of this factor
Factor	**Mass spectra characteristics (GIG site)**
HOA	dominated by alkyl fragments ($C_nH_{2n+1}^+$ and $C_nH_{2n-1}^+$). HOA displayed a bimodal distribution with a moderate morning peak at 07:00 and a stronger evening peak at 20:00 (Fig. S4), consistent with typical urban HOA diurnal patterns.
BBOA	characterized by an obvious peak at m/z 60 and 73 signals and showed different diurnal variation with enhanced afternoon and nighttime peaks likely reflect regional transport of biomass burning emissions from agricultural activities in the Pearl River Delta region during summer.
COA	characterized by the highest m/z 55 signal and a higher ratio of m/z 55/57 compared with HOA. The diurnal variation showed three notable peaks (7:00, 12:00 and 19:00), corresponding to breakfast time, lunchtime, and dinner time.
LO-OOA	characterized by a high m/z 44 signal but lower than that of MO-OOA, indicating its relatively fresh features.
MO-OOA	characterized by high peaks at m/z 44. The concentration of MO-OOA showed a better correlation with that of sulfate (R = 0.87) than with nitrate (R = 0.7) (Fig. S6b), which is likely attributed to similarly high oxidation degrees of both MO-OOA and sulfate.

Table S3. The AAE_{BC} values used to separate BC and BrC light absorption in other studies.

Observation sites	AAE_{BC}	Reference
Qomolangma Station	1.187	(Zhang et al., 2021b)
Nam Co Station	1.086	
Waliguan Station	1.042	
Lhasa	1	(Zhu et al., 2017)
Lulang	1	
Gaomeigu	1.1	(Tian et al., 2023)
Xianghe	1.1	(Wang et al., 2019)
Beijing 2016	1	(Xie et al., 2019)
Beijing 2020	1	(Sun et al., 2021)
Gucheng	1	
Xian	1	(Zhang et al., 2020a)
Hong Kong	1	
Singapore	0.99 to 1.04	(Kasthuriarachchi et al., 2020)

Table ~~S1~~S4. The summary of BrC light absorption coefficients and the contributions at 370 nm, as well as the OA mass concentration and primary OA fraction, are based on the literature results. The results were categorized according to the locations of their observation sites (Arctic region, Qinghai–Tibet Plateau (QTP region), Southern China, and Northern China).

Sites	$Fraction_{BrC}$ (%)	Abs_{BrC} (M m^{-1})	OA (μg m^{-3})	$Fraction_{POA}$ (%)	References
Arctic region					
circum–Arctic		0.1			(Yue et al., 2022)
Alert		0.04			(Yue et al., 2019)
Utqiagvik, Alaska		0.2			(Barrett and Sheesley, 2017)
QTP region					
Lhasa (Autumn)	8	4.2			(Zhu et al., 2017)
Beiluhe (Summer)	12.0	1.6			(Zhu et al., 2021)
Beiluhe (Autumn)	15.2	2.4			(Zhu et al., 2021)
YBJ site (Summer; **This study**)	15.4	0.2	0.7	34	
Beiluhe (Spring)	16.2	1.9			(Zhu et al., 2021)
Beiluhe (1 year)	18.0	2.0			(Zhu et al., 2021)
NamCo (Spring+Summer)	21.3	0.7			(Zhang et al., 2021b)
WLG(Summer)	22.4	0.6			(Zhang et al., 2021b)
Beiluhe (winter)	25.9	2.1			(Zhu et al., 2021)
Ngari (Autumn)	27.4	7.6			(Zhu et al., 2021)
Ngari (Summer)	31.4	5.9			(Zhu et al., 2021)
Lulang (Autumn)	32.0	4.8			(Zhu et al., 2017)
QOMS (Spring)	33.1	4.4	2.4	86	(Zhang et al., 2021b)
Qinghai Lake (Summer)	33.9	4.1			(Zhu et al., 2021)
Ngari (one year)	35.0	7.3			(Zhu et al., 2021)
Ngari (Spring)	36.7	6.1			(Zhu et al., 2021)
Gaomeigu (Spring)	37.0	12.3			(Tian et al., 2023)
Qinghai Lake (Spring)	38.6	9.3			(Zhu et al., 2021)
Ngari (winter)	40.7	10.7			(Zhu et al., 2021)
Qinghai Lake (winter)	43.0	9.6			(Zhu et al., 2021)
Qinghai Lake (1 year)	44.0	9.1			(Zhu et al., 2021)

Qinghai Lake (Autumn)	54.4	14.9			(Zhu et al., 2021)
Southern China					
Hong Kong (Winter)	11.0	6.3			(Zhang et al., 2020a)
Nanjing (Summer)	14.4	26.5			(Bao et al., 2022)
Nanjing (Spring)	16.1	29.7			(Bao et al., 2022)
Nanjing (3 years)	16.7	6.3			(Wang et al., 2018)
Nanjing (Autumn)	17.0	37.3			(Bao et al., 2022)
Nanjing (Winter)	19.6	51			(Bao et al., 2022)
GIG site (Summer; **This study**)	21.0	2.9	6.9	29	
Guangzhou, Panyu (Winter)	23.6	13.7	20	40	(Qin et al., 2018)
Wuhan (Winter)	28.7				(Zhang et al., 2021a)
Northern China					
Xian (Winter, Normal)	29.0	49.4	43.3	49	(Zhang et al., 2022)
Beijing (Winter 2020)	36.0	24	11.25	56.3	(Sun et al., 2021)
Shanghai (Winter)	37.6				(Zhang et al., 2021a)
Gucheng (Winter)	38.0	66.5	21.33	51.2	(Sun et al., 2021)
Harbin (Winter)	40.6				(Zhang et al., 2021a)
Beijing (Winter 2016)	46.0			77	(Xie et al., 2019)
Xian (Winter, Lockdown)	49.0	47.7	29.4	44	(Zhang et al., 2022)
Xianghe (Winter)	58.0	61.8			(Wang et al., 2019)

Table ~~S2~~S5. Regression coefficients (MAC) of the multiple linear regression (MLR) at 370,470, 520, 590, and 660 nm at the YBJ site and GIG site.—

YBJ site

		Wavelength (nm)				
		370nm	470nm	520nm	590nm	660nm
Case1	BBOA	2.54±0.53	0.66±0.25	0.25±0.18	0.11±0.11	0±0.13
	HOA	2.36±0.31	1.16±0.14	0.20±0.1	0.16±0.06	0±0.08
	LO–OOA	0.07±0.08	0.13±0.04	0.06±0.03	0.04±0.02	0±0.02
	MO–OOA	0.29±0.19	0.20±0.09	0±0.06	0.02±0.04	0±0.05
	biofuel–OA	0±0.42	0.22±0.20	0±0.14	0.10±0.09	0±0.1
	intercept	0±0.02	0.02±0.01	0.04±0.01	0.02±0	0.03±0
Case2	biofuel–OA	1.80±0.19	0.70±0.09	0.18±0.06	0.18±0.04	0±0.04
	HOA	2.04±0.32	1.08±0.14	0.17±0.1	0.15±0.06	0±0.07
	LO–OOA	0.23±0.08	0.17±0.03	0.08±0.02	0.05±0.01	0.01±0.02
	MO–OOA	0.07±0.19	0.15±0.09	0±0.06	0.01±0.04	0±0.04
	intercept	0±0.02	0.02±0.01	0.04±0.01	0.02±0	0.03±0
Case3	BBOA+ biofuel–OA	1.11±0.11	0.42±0.05	0.11±0.03	0.11±0.02	0±0.03
	HOA	2.08±0.30	1.11±0.14	0.18±0.1	0.16±0.06	0±0.07
	LO–OOA	0.15±0.08	0.14±0.03	0.07±0.02	0.04±0.02	0.01±0.02
	MO–OOA	0.18±0.18	0.19±0.08	0±0.06	0.02±0.04	0±0.04
	intercept	0±0.02	0.02±0.01	0.04±0.01	0.02±0	0.03±0
Case4	BBOA	2.54±0.23	0.92±0.11	0.25±0.08	0.23±0.05	0±0.06
	HOA	2.36±0.28	1.24±0.13	0.20±0.09	0.20±0.06	0±0.07
	LO–OOA	0.07±0.08	0.12±0.04	0.06±0.03	0.04±0.02	0±0.02
	MO–OOA	0.29±0.18	0.22±0.09	0±0.06	0.03±0.04	0±0.04
	intercept	0±0.02	0.02±0.01	0.04±0.01	0.02±0	0.03±0

GIG site

		Wavelength (nm)				
		370nm	470nm	520nm	590nm	660nm
Case1	COA	0.78±0.39	0.17±0.19	0.05±0.11	0.04±0.08	0±0.04
	BBOA	0±3.23	0±1.51	0±0.87	0±0.63	0±0.31
	HOA	1.67±0.48	1.32±0.24	0.72±0.14	0.40±0.1	0.17±0.05
	LO–OOA	0±0.35	0±0.17	0±0.09	0±0.07	0±0.03
	MO–OOA	0.19±0.34	0.11±0.16	0.04±0.07	0.05±0.07	0.03±0.03
	intercept	0.57±0.19	0.22±0.09	0.43±0.05	0.17±0.04	0.11±0.02
Case2	HOA	2.93±0.27	1.57±0.12	0.79±0.07	0.45±0.05	0.16±0.03
	BBOA+LO–OOA+MO–OOA	0.16±0.02	0.08±0.01	0.03±0	0.03±0	0.02±0
	intercept	0.34±0.17	0.17±0.08	0.41±0.05	0.16±0.03	0.11±0.02
Case3	HOA	2.57±0.28	1.40±0.13	0.72±0.07	0.38±0.06	0.13±0.03
	BBOA	1.91±0.21	0.90±0.10	0.35±0.06	0.40±0.04	0.20±0.02
	intercept	0.37±0.17	0.18±0.08	0.42±0.04	0.17±0.03	0.11±0.02

Table ~~S3~~S6. Quantitative assessment of the uncertainty of the PMF factors was made by bootstrapping analysis with 100 iterations.

YBJ site	Uncertainty	GIG site	Uncertainty
BBOA	23%	BBOA	5%
HOA	36%	HOA	4%
biofuel–OA	23%	COA	4%
LO–OOA	9%	MO–OOA	3%
MO–OOA	15%	LO–OOA	5%
BBOA+ biofuel–OA	33%	BBOA+MO–OOA+LO–OOA	8%
$Abs_{BrC,370nm}$	43%	$Abs_{BrC,370nm}$	36%

Table ~~S4~~S7. The uncertainty of multiple linear regression (MLR) at 370 nm using Monte Carlo simulations at the YBJ site and GIG site.

YBJ site

CASE		Mean	Standard deviation	Uncertainty (%) (100*std/mean)
Case1	BBOA	2.06	0.81	39.3
	HOA	2.07	0.39	19.0
	LO–OOA	0.10	0.09	88.1
	MO–OOA	0.27	0.11	42.7
	biofuel–OA	0.43	0.49	114.3
	intercept	0	0	
Case2	biofuel–OA	1.78	0.43	24.2
	HOA	1.91	0.42	22.0
	LO–OOA	0.22	0.07	33.2
	MO–OOA	0.11	0.09	83.5
	intercept	0	0	
Case3	BBOA+ biofuel–OA	1.06	0.28	26.4
	HOA	2.02	0.42	20.8
	LO–OOA	0.16	0.09	56.2
	MO–OOA	0.19	0.11	57.9
	intercept	0	0	
Case4	BBOA	2.55	0.60	23.4
	HOA	2.22	0.37	16.7
	LO–OOA	0.09	0.09	97.2
	MO–OOA	0.29	0.11	37.6
	intercept	0	0	

GIG site

CASE		Mean	Standard deviation	Uncertainty (%) (100*std/mean)
Case1	COA	0.74	0.14	19.5
	BBOA	0.23	0.49	216.4
	MO–OOA	0.16	0.06	37.5
	HOA	1.72	0.26	15.1
	LO–OOA	0.00	0.02	552.3
	intercept	0.57	0.08	14.8
Case2	BBOA+MO–OOA+LO–OOA	0.16	0.01	6.2
	HOA	2.98	0.18	6.0
	intercept	0.35	0.08	23.5
Case3	BBOA	1.87	0.11	5.8
	HOA	2.62	0.18	6.8
	intercept	0.38	0.08	21.6

Table ~~S5~~S8. The summary of campaign–averaged light absorption coefficients (M m^{-1}) of total aerosols, BC, and BrC, as well as the BrC contribution to the total absorption of particles (f_{BrC}, %).

Average ± SD		370nm	470nm	520nm	590nm	660nm	880nm
YBJ	Total	1.59±1.59	1.19±1.24	1.01± 1.05	0.88± 0.92	0.76±0.80	0.58±0.60
	BC	1.34±1.46	1.06±1.15	0.96±1.04	0.84±0.92	0.75±0.82	0.58±0.60
	BrC	0.22±0.32	0.13±0.17	0.05±0.08	0.03± 0.05	0.02±0.03	0
	f_{BrC}	15.4±14.0	13.0±13.2	8.5±13.4	6.4±11.5	5.2±11.8	0
GIG	Total	13.2±7.0	9.5±5.1	8.1±4.4	7.1±3.7	6.1±3.3	4.4±2.4
	BC	10.5±5.6	8.3±4.4	7.5±4.0	6.6±3.5	5.9±3.1	4.4±2.4
	BrC	2.9±2.0	1.5±0.9	1.1±0.5	0.6± 0.4	0.3± 0.2	0
	f_{BrC}	21.0±7.8	14.9±6.2	12.5±7.8	8.5±4.3	5.1±3.4	0

Table ~~S6~~S9. The summary of OA factors contributing to BrC absorption at 370 nm using the PMF–MLR method. The asterisks (*) represent the absorption contributions of soluble BrC from different sources at 365nm. The sources include POA (primary OA) (BBOA (biomass burning OA), HOA (hydrocarbon–like OA), CCOA (coal combustion OA), COA (cooking–related OA), NOA (nitrogen-containing OA); If other types of BrC primary sources exist in the literature, they are unified as POA and SOA (secondary OA).

Sites	BBOA	HOA	CCOA	COA	NOA	*POA	*SOA*	Unidentified	References
China									
Gucheng (winter)	(16%)	(10%)	(42%)				(52%)		(Sun et al., 2021)
Beijing (winter 2016)	(17%)		(48%)	(3%)			(32%)		(Xie et al., 2019)
Beijing (winter 2020)			(56%)	(7%)			(37%)		(Sun et al., 2021)
Xianghe (winter)	(49%)	(4%)	(28%)				(19%)		(Wang et al., 2019)
$Xian_{lockdown}$ (winter)	(20%)	(11%)	(28%)				(40%)	(1%)	(Zhang et al., 2022)
$Xian_{normal}$ (winter)	(17%)	(20%)	(45%)				LO–OOA (12%)	(6%)	
Guangzhou(summer; **This study**)	(36%)	(51%)						(13%)	
Guangzhou (Winter 2014)	(25%)	(23%)					LV–OOA (52%)		(Qin et al., 2018)
QTP region									
Gaomeigu (Spring)	(51%)						po–OOA (49%)		(Tian et al., 2023)
QOMS (Spring)	(64%)				(20%)		MO–OOA (16%)		(Zhang et al., 2021b)
YBJ (Summer; **This study**)	(40%)	(38%)					(22%)		
Other countries									
Paris (winter)	(74%)	(8%)					OOA (18%)		(Zhang et al., 2020c)
Delhi (winter)	(48%)	(10%)					SV–OOA (26%)	(16%)	(Singh et al., 2021)
Athens (winter)	(33%)	(13%)		(13%)			(41%)		(Kaskaoutis et al., 2021)
Singapore (winter)		(83%)		(2%)			LO–OOA (15%)		(Kasthuriarachchi et al., 2020)
Manaus (Summer+Autumn)	(57%)	(22%)					(17%)	(4%)	(De Sá et al., 2019)
Mexico (winter)	(14%)	(54%)					(24%)		
Mexico (Spring)	(55%)	(40%)					(0.2%)	(4.8%)	(Retama et al., 2022)
Mexico (Summer)	(6%)	(49%)					(5%)	(40%)	
Mexico (Winter to summer)	(43%)	(46%)					(6%)	(5%)	
***Soluble BrC a 365nm**									
*Central Alabama (Summer)	(85%)						LO–OOA (10%)	(3%)	(Washenfelder et al., 2015)
*Urumqi (Winter)						(46%)	(54%)		
*Xining (Winter)						(51%)	(49%)		(Zhong et al., 2023)
*Lanzhou (Winter)						(60%)	(40%)		
*Yinchuan (Winter)						(30%)	(70%)		
*Xian (Winter)	(19%)	(12%)	(13%)				OOA (28%)	(28%)	(Lei et al., 2019)
*Xian (Summer)		(7%)	(1%)				OOA (75%)	(17%)	
*Yangzhou (Autumn to early Spring)	(24%)	(19%)					(47%)		(Chen et al., 2020)

*Nanjing (Spring)	(58%)	(42%)	
*Nanjing (Summer)	(44%)	(56%)	(Bao et al., 2022)
*Nanjing (Autumn)	(75%)	(25%)	
*Nanjing (Winter)	(60%)	(40%)	

Note:

**Nanjing SOA = anthropogenic SOA+ biogenic SOA + secondary nitrate and sulfate formation*

**Urumqi Xining Lanzhou Yinchuan SOA = HO–OOA1 + HO–OOA2 + LO–OOA*

Mexico SOA = LO–OOA+MO–OOA

**Yangzhou SOA = LO–OOA+MO–OOA*

Paris BBOA = LO–BBOA+MO–BBOA

Manaus BBOA = LO–BBOA+MO–BBOA—

Manaus SOA = MO–OOA+LO–OOA+IEPOX–SOA

Athens SOA = SV–OOA+LV–OOA

Singapore HOA = HOA+O–HOA

Beijing CCOA = FFOA

Beijing (winter 2016)–SOA = aqOOA + OPOA+OOA

Beijing (winter 2020)–SOA = LO–OOA+MO–OOA

$Xian_{lockdown}$ SOA = LO–OOA + MO–OOA

Table ~~S7~~S10. The literature summary of MAC ($m^2\ g^{-1}$) from different BrC sources, which was obtained by the PMF–MLR method in different environments. All the results were categorized based on the locations of their observation sites (urban China, Qinghai–Tibet Plateau (QTP region), and other countries).

Sites	BBOA	HOA	CCOA	LO–OOA	MO–OOA	References
Urban China						
Xianghe (winter)	3.40±0.16	0.50±0.16	5.73±0.32			(Wang et al., 2019)
Guangzhou (Winter 2014)	3.40±0.41	0.61±0.05			1.04±0.08	(Qin et al., 2018)
$Xian_{normal}$ (winter)	1.66±0.08	1.44±0.08	5.35±0.13	0.71±0.05	–0.26±0.08	(Zhang et al., 2022)
$Xian_{lockdown}$ (winter)	2.39±0.13	1.92±0.19	5.22±0.19	2.08±0.14	0.73±0.14	
Guangzhou (Summer; **This study**)	1.91±0.21	2.57±0.28				
QTP region						
Gaomeigu (Spring)	2.78±0.39				1.43±0.23	(Tian et al., 2023)
QOMS (Spring)	2.29±0.02				0.60±0.03	(Zhang et al., 2021b)
YBJ (Summer; **This study**)	1.11–2.54	2.08±0.30		0.15±0.08	0.18±0.08	
Other countries						
Delhi (winter)	0.86	0.42		0.67		(Singh et al., 2021)
Manaus (Summer+Autumn)	(LO–BBOA) 1.5±0.07 (MO–BBOA) 0.82±0.01	2.04±0.14		0.01±0.02	0.01±0.02	(De Sá et al., 2019)
Athens (winter)	7.63±0.74	1.34±0.49		4.02±0.44	1.98±0.33	(Kaskaoutis et al., 2021)
Paris (winter)	(LOBBOA) 4.86±0.18 (MO–BBOA) 2.02 ±0.12	1.06±0.23		(OOA) 0.55±0.05		(Zhang et al., 2020c)
Central Alabama (Summer)	1.35±0.06			0.03±0.02	–0.01±0.01	(Washenfelder et al., 2015)
Mexico (Spring)	1.82±0.02	1.76±0.03		0.01±0.04	0±0.01	(Retama et al., 2022)
Mexico (Summer)	0.4±0.14	1.47±0.07		0.03±0.06	0.04±0.03	
Mexico (winter)	0.83±0.09	1.79±0.03		0.97±0.06	–0.14±0.02	
Mexico (Winter to summer)	1.73±0.02	1.75±0.02		0.29±0.03	0±0.01	
Singapore (winter)		0.97±0.33		0.67±0.23		(Kasthuriarachchi et al., 2020)

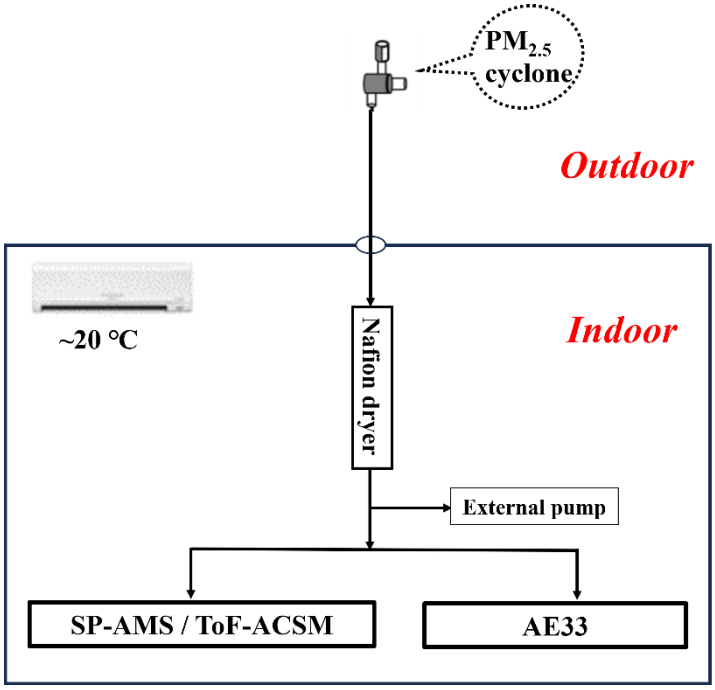

Figure S1. The setup diagram of instruments during campaign in Yangbajing and Guangzhou.

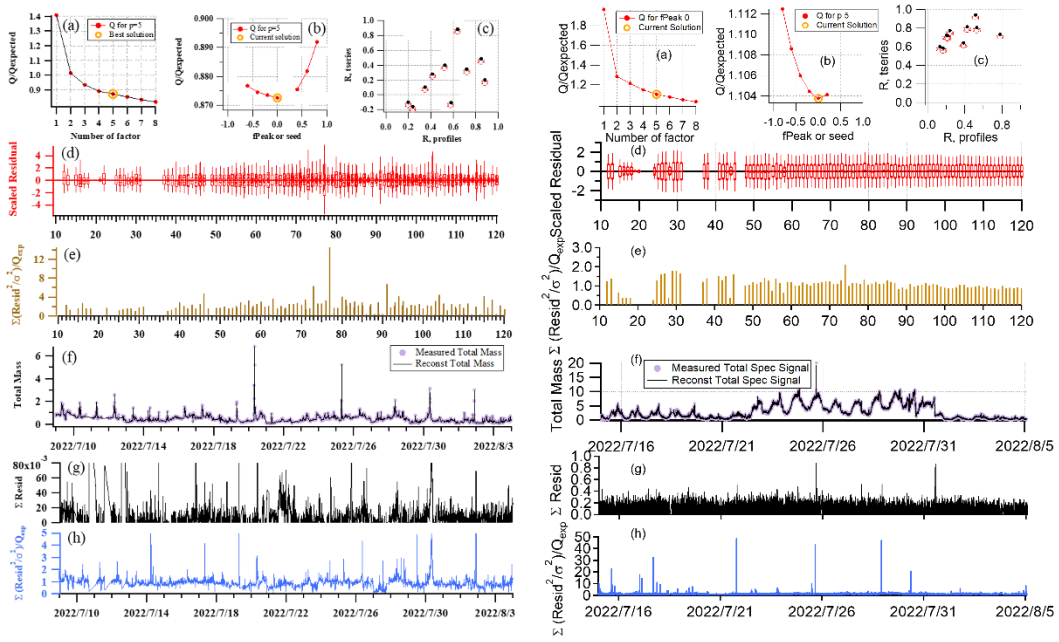

Figure S2. Diagnostics plots of factor selections in the unconstrained PMF at the YBJ site (left) and the GIG site (right).

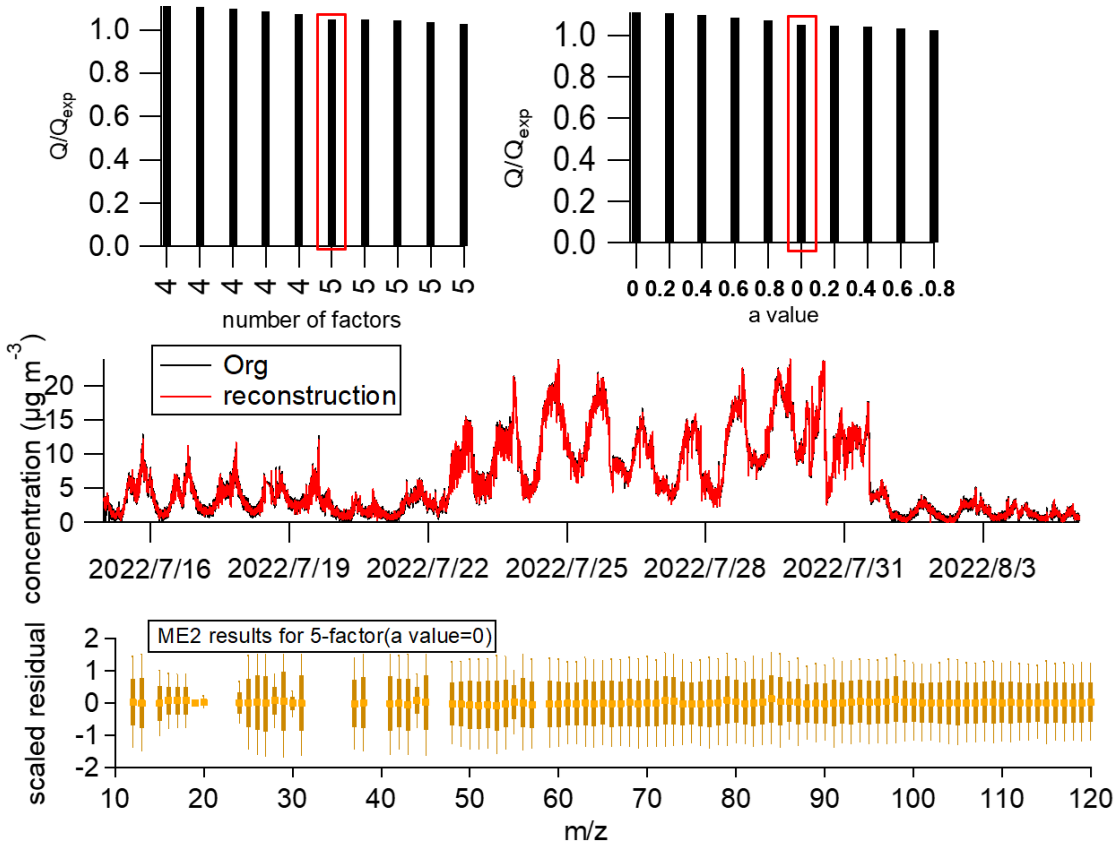

Figure S3. ME2-Diagnostics plots of factor selections at the GIG site.

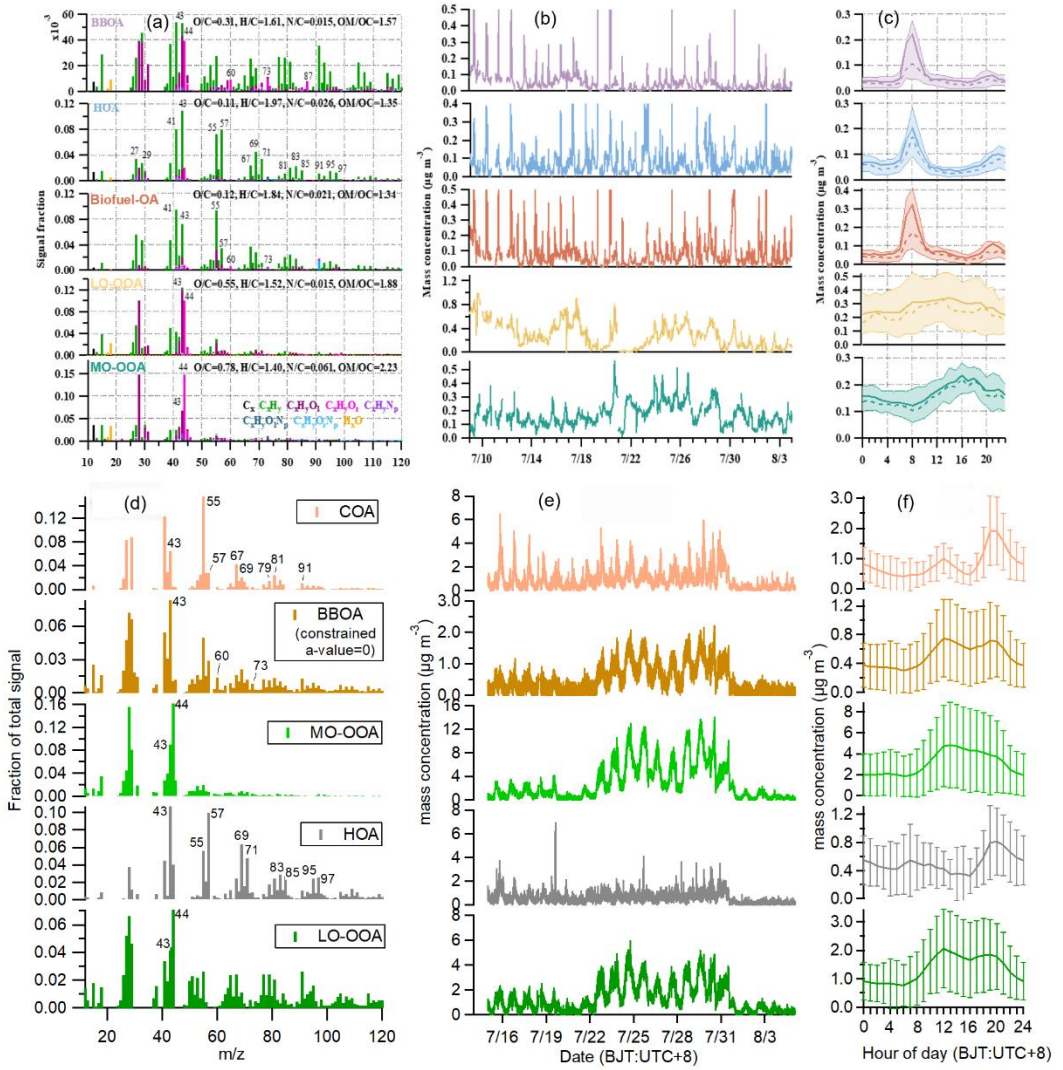

Figure S4. The final optimum solution for OA sources at the YBJ site and the GIG site. The mass spectrum was plotted in the form of UMR, and each peak was colored on the basis of the contributions of 8 ion categories: C_x^+, $C_xH_v^+$, $C_xH_vO_1^+$, $C_xH_vO_z^+$, $C_xH_vN_p^+$, $C_xH_vO_1N_p^+$, $C_xH_vO_zN_p^+$, H_xO^+.

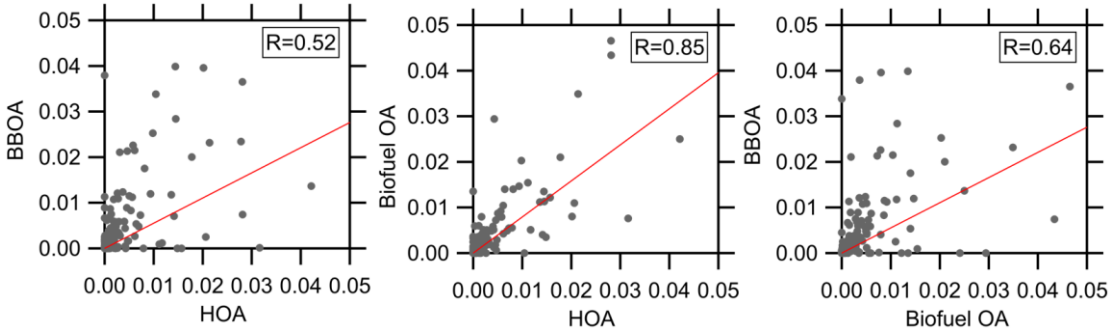

Figure S5. Mass spectra scatter plots among BBOA, HOA and Biofuel-OA at YBJ site.

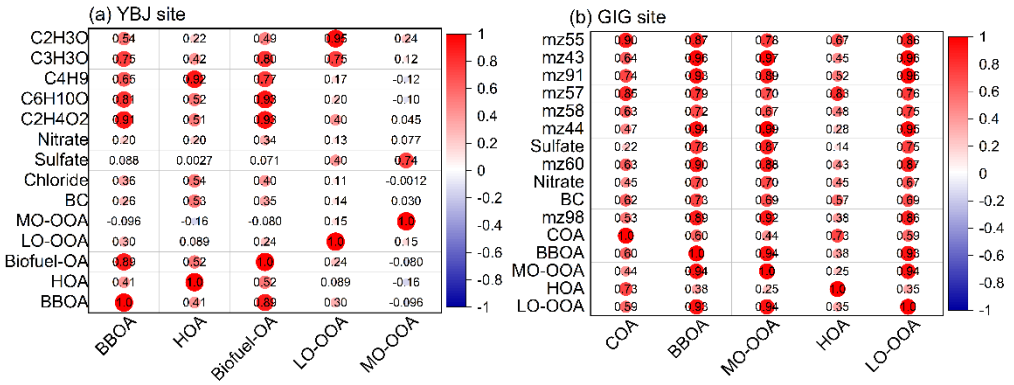

Figure ~~S5~~S6. The Pearson's correlation coefficient (R) between the OA factor and tracers at the YBJ site and the GIG site.

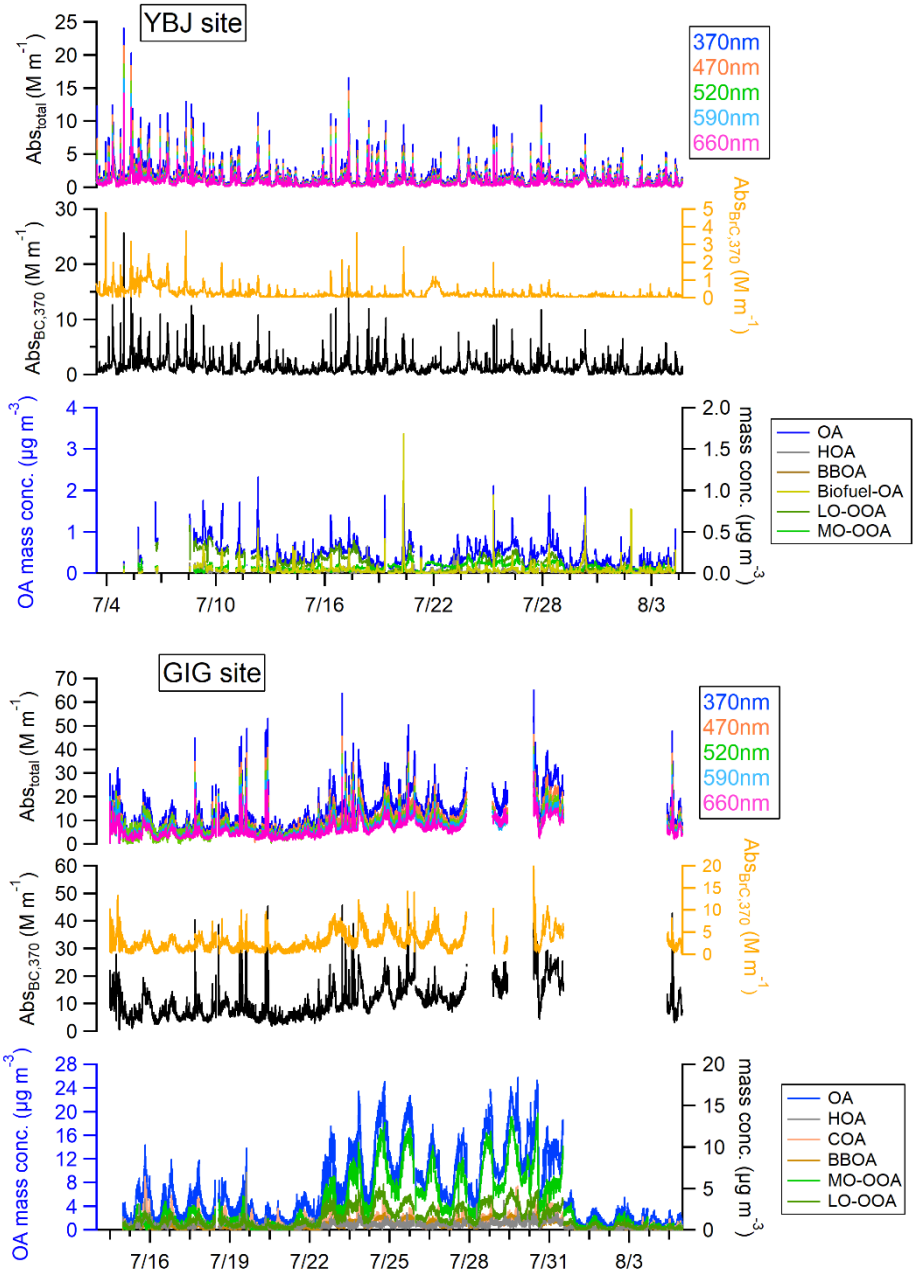

Figure ~~S6~~S7. The time series of OA mass concentration and BrC light absorption coefficients at 370, 470, 520, 590, and 660 nm at the YBJ site and GIG site.

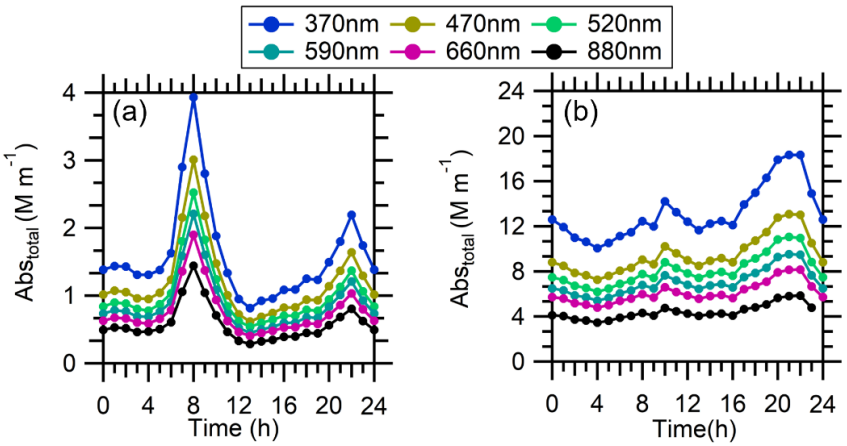

Figure ~~S7~~S8. Diurnal variations of light absorption of total aerosol at seven wavelengths at the YBJ site (a) and the GIG site (b).

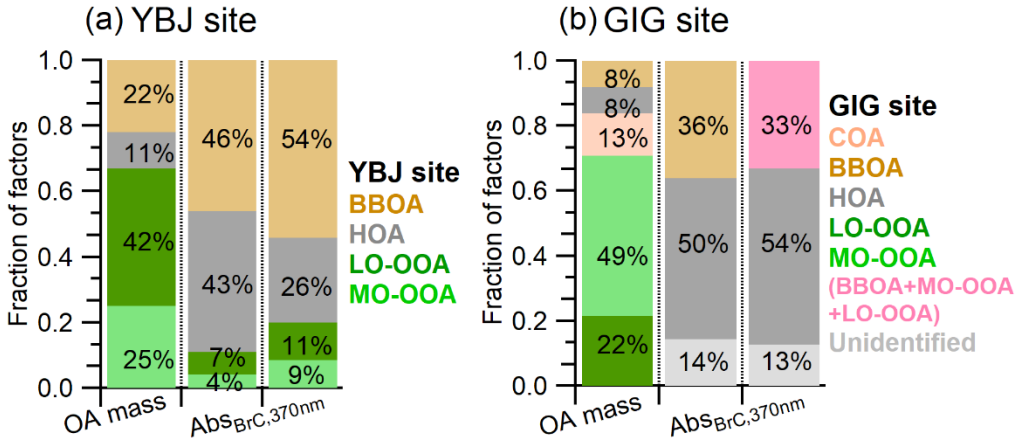

Figure ~~S8~~S9. (a) The contributions of different OA factors to total OA (left) and contributions of different OA factors to BrC light absorption at 370 nm (Center and right; represent a upper and lower bound based on the different cases discussed in Section 2.5.1 and Text S2) at YBJ site (a) and GIG site (b).

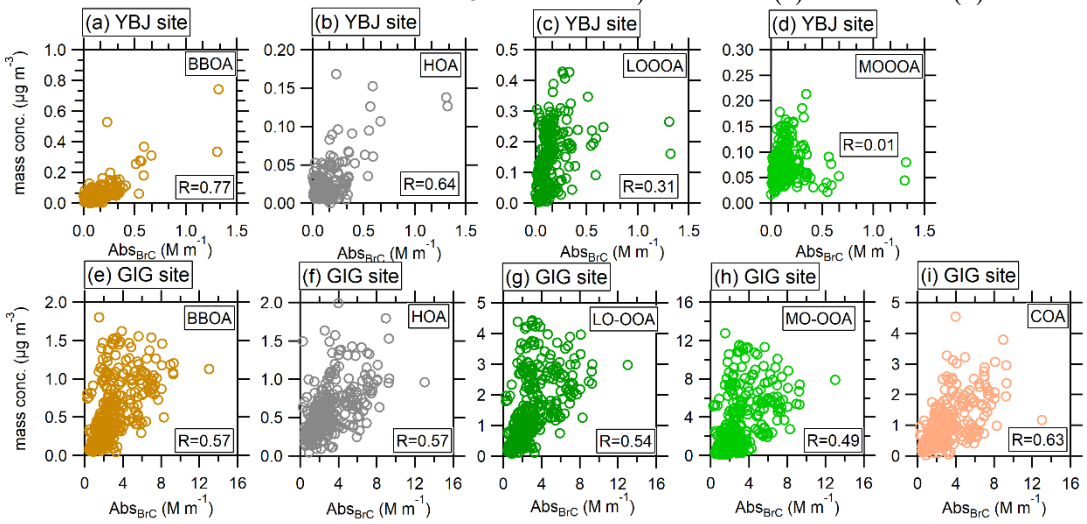

Figure ~~S9~~S10. Scatter plots of brown carbon absorption at 370 nm versus the mass concentrations of OA factors during the campaign.

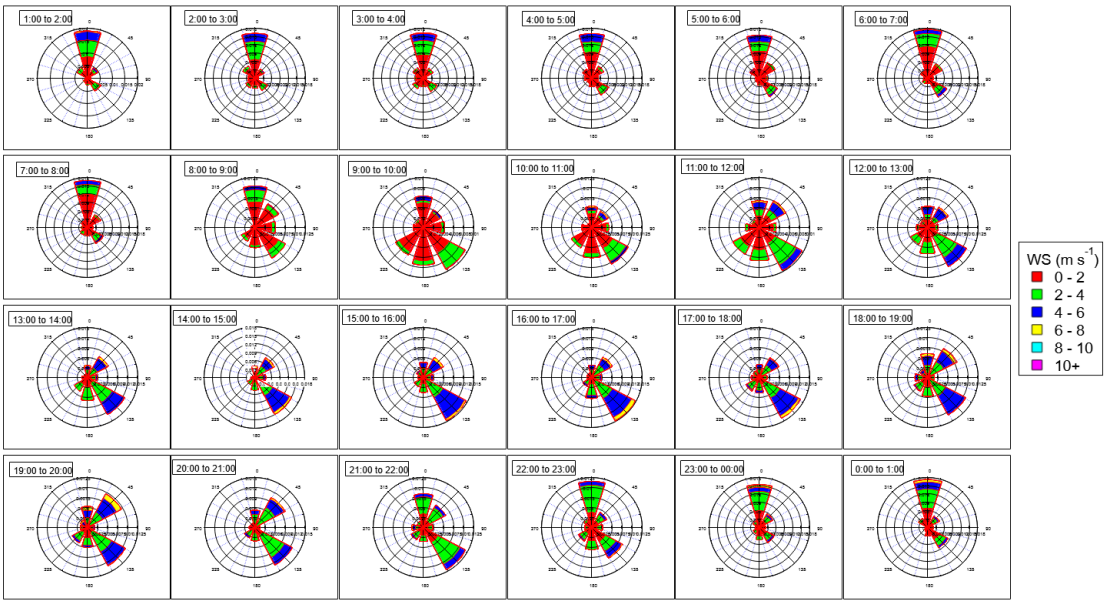

Figure ~~S10~~S11. Hourly rose plots at the YBJ site.

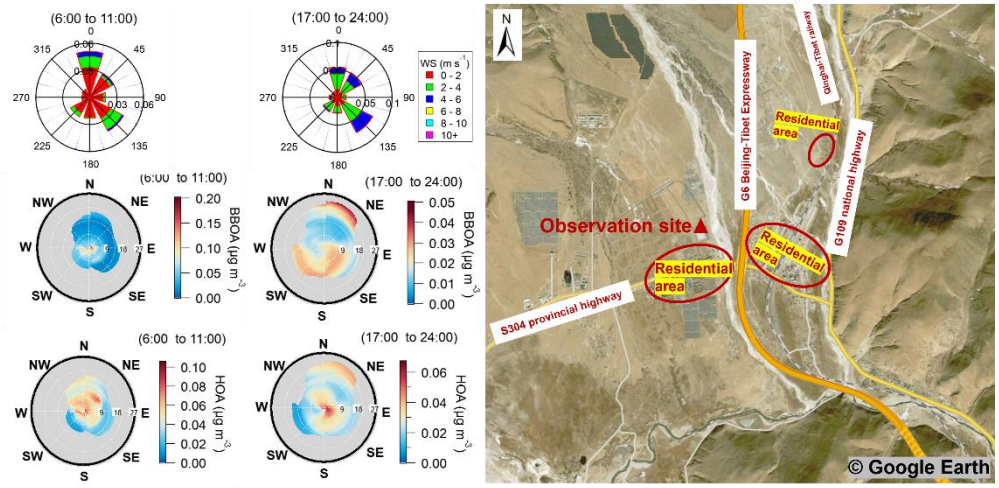

Figure ~~S11~~S12. Rose plots and Bivariate polar plots of HOA and BBOA during morning peak (6:00 to 11:00) and evening peak (17:00 to 24:00). The unit of wind speed is km h^{-1} in the Bivariate polar plots.

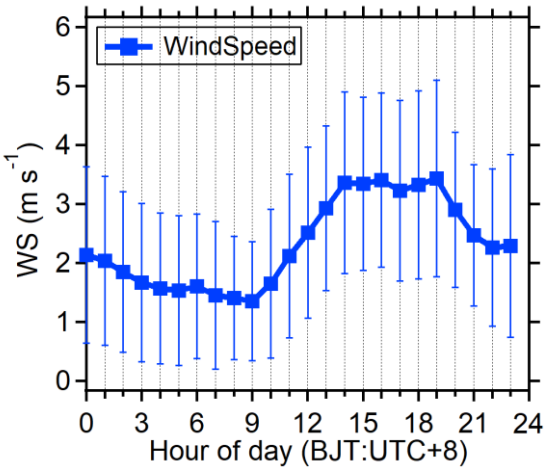

Figure ~~S12~~S13. The diurnal variations of wind speed at the YBJ site

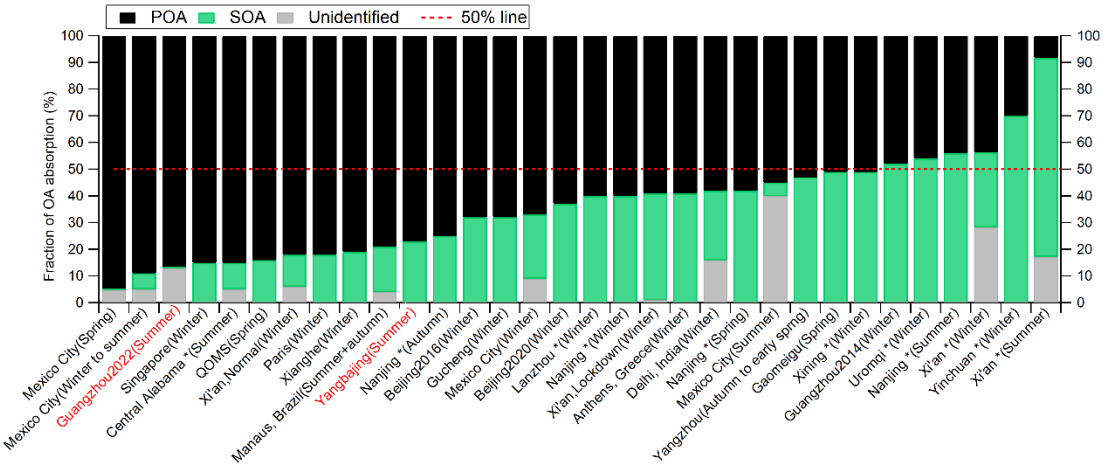

Figure ~~S13~~S14~~.~~ The summary of the contribution of organic aerosols from different sources to BrC absorption at 370 nm using the PMF–MLR method. The asterisks (*) represent the absorption contributions of soluble BrC from different sources at 365nm. The sources include POA (primary OA) and SOA (secondary OA). The dashed line represents 50% of BrC absorption.

Reference

Alfarra, M. R., Prevot, A. S. H., Szidat, S., Sandradewi, J., Weimer, S., Lanz, V. A., Schreiber, D., Mohr, M., and Baltensperger, U.: Identification of the Mass Spectral Signature of Organic Aerosols from Wood Burning Emissions, Environmental Science & Technology, 41, 5770-5777, 10.1021/es062289b, 2007.

Bao, M., Zhang, Y.-L., Cao, F., Lin, Y.-C., Hong, Y., Fan, M., Zhang, Y., Yang, X., and Xie, F.: Light absorption and source apportionment of water soluble humic-like substances (HULIS) in PM2.5 at Nanjing, China, Environmental Research, 206, 10.1016/j.envres.2021.112554, 2022.

Barrett, T. E. and Sheesley, R. J.: Year-round optical properties and source characterization of Arctic organic carbon aerosols on the North Slope Alaska, Journal of Geophysical Research: Atmospheres, 122, 9319-9331, 10.1002/2016jd026194, 2017.

Cai, Y., Ye, C., Chen, W., Hu, W., Song, W., Peng, Y., Huang, S., Qi, J., Wang, S., Wang, C., Wu, C., Wang, Z., Wang, B., Huang, X., He, L., Gligorovski, S., Yuan, B., Shao, M., and Wang, X.: The important contribution of secondary formation and biomass burning to oxidized organic nitrogen (OON) in a polluted urban area: insights from in situ measurements of a chemical ionization mass spectrometer (CIMS), Atmospheric Chemistry and Physics, 23, 8855-8877, 10.5194/acp-23-8855-2023, 2023.

Canonaco, F., Crippa, M., Slowik, J. G., Baltensperger, U., and Prévôt, A. S. H.: SoFi, an IGOR-based interface for the efficient use of the generalized multilinear engine (ME-2) for the source apportionment: ME-2 application to aerosol mass spectrometer data, Atmospheric Measurement Techniques, 6, 3649-3661, 10.5194/amt-6-3649-2013, 2013.

Chen, Y., Xie, X., Shi, Z., Li, Y., Gai, X., Wang, J., Li, H., Wu, Y., Zhao, X., Chen, M., and Ge, X.: Brown carbon in atmospheric fine particles in Yangzhou, China: Light absorption properties and source apportionment, Atmospheric Research, 244, 10.1016/j.atmosres.2020.105028, 2020.

Crippa, M., Decarlo, P. F., Slowik, J. G., Mohr, C., Heringa, M. F., Chirico, R., Poulain, L., Freutel, F., Sciare, J., Cozic, J., Di Marco, C. F., Elsasser, M., Nicolas, J. B., Marchand, N., Abidi, E., Wiedensohler, A., Drewnick, F., Schneider, J., Borrmann, S., Nemitz, E., Zimmermann, R., Jaffrezo, J. L., Prévôt, A. S. H., and Baltensperger, U.: Wintertime aerosol chemical composition and source apportionment of the organic fraction in the metropolitan area of Paris, Atmospheric Chemistry and Physics, 13, 961-981, 10.5194/acp-13-961-2013, 2013.

Crippa, M., Canonaco, F., Lanz, V. A., Äijälä, M., Allan, J. D., Carbone, S., Capes, G., Ceburnis, D., Dall'Osto, M., Day, D. A., DeCarlo, P. F., Ehn, M., Eriksson, A., Freney, E., Hildebrandt Ruiz, L., Hillamo, R., Jimenez, J. L., Junninen, H., Kiendler-Scharr, A., Kortelainen, A. M., Kulmala, M., Laaksonen, A., Mensah, A. A., Mohr, C., Nemitz, E., O'Dowd, C., Ovadnevaite, J., Pandis, S. N., Petäjä, T., Poulain, L., Saarikoski, S., Sellegri, K., Swietlicki, E., Tiitta, P., Worsnop, D. R., Baltensperger, U., and Prévôt, A. S. H.: Organic aerosol components derived from 25 AMS data sets across Europe using a consistent ME-2 based source apportionment approach, Atmospheric Chemistry and Physics, 14, 6159-6176, 10.5194/acp-14-6159-2014, 2014.

Cui, Y. Y., Liu, S., Bai, Z., Bian, J., Li, D., Fan, K., McKeen, S. A., Watts, L. A., Ciciora, S. J., and Gao, R.-S.: Religious burning as a potential major source of atmospheric fine aerosols in summertime Lhasa on the Tibetan Plateau, Atmospheric Environment, 181, 186-191, 10.1016/j.atmosenv.2018.03.025, 2018.

de Sá, S. S., Rizzo, L. V., Palm, B. B., Campuzano-Jost, P., Day, D. A., Yee, L. D., Wernis, R., Isaacman-VanWertz, G., Brito, J., Carbone, S., Liu, Y. J., Sedlacek, A., Springston, S., Goldstein, A. H., Barbosa, H. M. J., Alexander, M. L., Artaxo, P., Jimenez, J. L., and Martin, S. T.: Contributions of biomass-burning, urban, and biogenic emissions to the concentrations and light-absorbing properties of particulate matter in central Amazonia during the dry season, Atmos. Chem. Phys., 19, 7973-8001, 10.5194/acp-19-7973-2019, 2019.

DeCarlo, P. F., Kimmel, J. R., Trimborn, A., Northway, M. J., Jayne, J. T., Aiken, A. C., Gonin, M., Fuhrer, K., Horvath, T., Docherty, K. S., Worsnop, D. R., and Jimenez, J. L.: Field-Deployable, High-Resolution, Time-of-Flight Aerosol Mass Spectrometer, Analytical Chemistry, 78, 8281-8289, 10.1021/ac061249n, 2006.

Hu, W., Hu, M., Hu, W., Jimenez, J. L., Yuan, B., Chen, W., Wang, M., Wu, Y., Chen, C., Wang, Z., Peng, J., Zeng, L., and Shao, M.: Chemical composition, sources, and aging process of submicron aerosols in Beijing: Contrast between summer and winter, Journal of Geophysical Research: Atmospheres, 121, 1955-1977, 10.1002/2015jd024020, 2016.

Hu, W. W., Hu, M., Yuan, B., Jimenez, J. L., Tang, Q., Peng, J. F., Hu, W., Shao, M., Wang, M., Zeng, L. M., Wu, Y. S., Gong, Z. H., Huang, X. F., and He, L. Y.: Insights on organic aerosol aging and the influence of coal combustion at a regional receptor site of central eastern China, Atmospheric Chemistry and Physics, 13, 10095-10112, 10.5194/acp-13-10095-2013, 2013.

Jiang, H., Li, J., Sun, R., Tian, C., Tang, J., Jiang, B., Liao, Y., Chen, C. E., and Zhang, G.: Molecular Dynamics and Light Absorption Properties of Atmospheric Dissolved Organic Matter, Environ Sci Technol, 55, 10268-10279, 10.1021/acs.est.1c01770, 2021.

Jiang, H., Li, J., Tang, J., Zhao, S., Chen, Y., Tian, C., Zhang, X., Jiang, B., Liao, Y., and Zhang, G.: Factors Influencing the Molecular Compositions and Distributions of Atmospheric Nitrogen-Containing Compounds, Journal of Geophysical Research: Atmospheres, 127, 10.1029/2021jd036284, 2022.

Kaskaoutis, D. G., Grivas, G., Stavroulas, I., Bougiatioti, A., Liakakou, E., Dumka, U. C., Gerasopoulos, E., and Mihalopoulos, N.: Apportionment of black and brown carbon spectral absorption sources in the urban environment of Athens, Greece, during winter, Science of The Total Environment, 801, 10.1016/j.scitotenv.2021.149739, 2021.

Kasthuriarachchi, N. Y., Rivellini, L. H., Adam, M. G., and Lee, A. K. Y.: Light Absorbing Properties of Primary and Secondary Brown Carbon in a Tropical Urban Environment, Environ Sci Technol, 54, 10808-10819, 10.1021/acs.est.0c02414, 2020.

Lanz, V. A., Alfarra, M. R., Baltensperger, U., Buchmann, B., Hueglin, C., and Prévôt, A. S. H.: Source apportionment of submicron organic aerosols at an urban site by factor analytical modelling of aerosol mass spectra, Atmospheric Chemistry and Physics, 7, 1503-1522, 10.5194/acp-7-1503-2007, 2007.

Lei, Y., Shen, Z., Zhang, T., Lu, D., Zeng, Y., Zhang, Q., Xu, H., Bei, N., Wang, X., and Cao, J.: High time resolution observation of PM2.5 Brown carbon over Xi'an in northwestern China: Seasonal variation and source apportionment, Chemosphere, 237, 10.1016/j.chemosphere.2019.124530, 2019.

Ng, N. L., Canagaratna, M. R., Jimenez, J. L., Chhabra, P. S., Seinfeld, J. H., and Worsnop, D. R.: Changes in organic aerosol composition with aging inferred from aerosol mass spectra, Atmospheric Chemistry and Physics, 11, 6465-6474, 10.5194/acp-11-6465-2011, 2011.

Onasch, T. B., Trimborn, A., Fortner, E. C., Jayne, J. T., Kok, G. L., Williams, L. R., Davidovits, P., and Worsnop, D. R.: Soot Particle Aerosol Mass Spectrometer: Development, Validation, and Initial Application, Aerosol Science and Technology, 46, 804-817, 10.1080/02786826.2012.663948, 2012.

Qin, Y. M., Tan, H. B., Li, Y. J., Li, Z. J., Schurman, M. I., Liu, L., Wu, C., and Chan, C. K.: Chemical characteristics of brown carbon in atmospheric particles at a suburban site near Guangzhou, China, Atmospheric Chemistry and Physics, 18, 16409-16418, 10.5194/acp-18-16409-2018, 2018.

Retama, A., Ramos-Cerón, M., Rivera-Hernández, O., Allen, G., and Velasco, E.: Aerosol optical properties and brown carbon in Mexico City, Environmental Science: Atmospheres, 2, 315-334, 10.1039/d2ea00006g, 2022.

Singh, A., Rastogi, N., Kumar, V., Slowik, J. G., Satish, R., Lalchandani, V., Thamban, N. M., Rai, P., Bhattu, D., Vats, P., Ganguly, D., Tripathi, S. N., and Prévôt, A. S. H.: Sources and characteristics of light-absorbing fine particulates over Delhi through the synergy of real-time optical and chemical measurements, ATMOSPHERIC ENVIRONMENT, 252, 10.1016/j.atmosenv.2021.118338, 2021.

Sun, J., Zhang, Q., Canagaratna, M. R., Zhang, Y., Ng, N. L., Sun, Y., Jayne, J. T., Zhang, X., Zhang, X., and Worsnop, D. R.: Highly time- and size-resolved characterization of submicron aerosol particles in Beijing using an Aerodyne Aerosol Mass Spectrometer, Atmospheric Environment, 44, 131-140, 10.1016/j.atmosenv.2009.03.020, 2010.

Sun, J., Xie, C., Xu, W., Chen, C., Ma, N., Xu, W., Lei, L., Li, Z., He, Y., Qiu, Y., Wang, Q., Pan, X., Su, H., Cheng, Y., Wu, C., Fu, P., Wang, Z., and Sun, Y.: Light absorption of black carbon and brown carbon in winter in North China Plain: comparisons between urban and rural sites, Science of The Total Environment, 770, 10.1016/j.scitotenv.2020.144821, 2021.

Tian, J., Wang, Q., Ma, Y., Wang, J., Han, Y., and Cao, J.: Impacts of biomass burning and photochemical processing on the light absorption of brown carbon in the southeastern Tibetan Plateau, Atmospheric Chemistry and Physics, 23, 1879-1892, 10.5194/acp-23-1879-2023, 2023.

Ulbrich, I. M., Canagaratna, M. R., Zhang, Q., Worsnop, D. R., and Jimenez, J. L.: Interpretation of organic components from Positive Matrix Factorization of aerosol mass spectrometric data, Atmospheric Chemistry and Physics, 9, 2891-2918, 10.5194/acp-9-2891-2009, 2009.

Wang, J., Nie, W., Cheng, Y., Shen, Y., Chi, X., Wang, J., Huang, X., Xie, Y., Sun, P., Xu, Z., Qi, X., Su, H., and Ding, A.: Light absorption of brown carbon in eastern China based on 3-year multi-wavelength aerosol optical property observations and an improved absorption Ångström exponent segregation method, Atmospheric Chemistry and Physics, 18, 9061-9074, 10.5194/acp-18-9061-2018, 2018.

Wang, Q., Ye, J., Wang, Y., Zhang, T., Ran, W., Wu, Y., Tian, J., Li, L., Zhou, Y., Hang Ho, S. S., Dang, B., Zhang, Q., Zhang, R., Chen, Y., Zhu, C., and Cao, J.: Wintertime Optical Properties of Primary and Secondary Brown Carbon at a Regional Site in the North China Plain, Environmental Science

& Technology, 53, 12389-12397, 10.1021/acs.est.9b03406, 2019.
Wang, X., Chakrabarty, R. K., Schwarz, J. P., Murphy, S. M., Levin, E. J. T., Howell, S. G., Guo, H., Campuzano-Jost, P., and Jimenez, J. L.: Dark brown carbon from biomass burning contributes to significant global-scale positive forcing, One Earth, 10.1016/j.oneear.2025.101205, 2025.
Wang, Y., Hu, M., Lin, P., Guo, Q., Wu, Z., Li, M., Zeng, L., Song, Y., Zeng, L., Wu, Y., Guo, S., Huang, X., and He, L.: Molecular Characterization of Nitrogen-Containing Organic Compounds in Humic-like Substances Emitted from Straw Residue Burning, Environmental Science & Technology, 51, 5951-5961, 10.1021/acs.est.7b00248, 2017.
Washenfelder, R. A., Attwood, A. R., Brock, C. A., Guo, H., Xu, L., Weber, R. J., Ng, N. L., Allen, H. M., Ayres, B. R., Baumann, K., Cohen, R. C., Draper, D. C., Duffey, K. C., Edgerton, E., Fry, J. L., Hu, W. W., Jimenez, J. L., Palm, B. B., Romer, P., Stone, E. A., Wooldridge, P. J., and Brown, S. S.: Biomass burning dominates brown carbon absorption in the rural southeastern United States, Geophysical Research Letters, 42, 653-664, https://doi.org/10.1002/2014GL062444, 2015.
Xie, C., Xu, W., Wang, J., Wang, Q., Liu, D., Tang, G., Chen, P., Du, W., Zhao, J., Zhang, Y., Zhou, W., Han, T., Bian, Q., Li, J., Fu, P., Wang, Z., Ge, X., Allan, J., Coe, H., and Sun, Y.: Vertical characterization of aerosol optical properties and brown carbon in winter in urban Beijing, China, Atmospheric Chemistry and Physics, 19, 165-179, 10.5194/acp-19-165-2019, 2019.
Xu, J., Zhang, Q., Chen, M., Ge, X., Ren, J., and Qin, D.: Chemical composition, sources, and processes of urban aerosols during summertime in northwest China: insights from high-resolution aerosol mass spectrometry, Atmospheric Chemistry and Physics, 14, 12593-12611, 10.5194/acp-14-12593-2014, 2014.
Yue, S., Bikkina, S., Gao, M., Barrie, L. A., Kawamura, K., and Fu, P.: Sources and Radiative Absorption of Water-Soluble Brown Carbon in the High Arctic Atmosphere, Geophysical Research Letters, 46, 14881-14891, 10.1029/2019gl085318, 2019.
Yue, S., Zhu, J., Chen, S., Xie, Q., Li, W., Li, L., Ren, H., Su, S., Li, P., Ma, H., Fan, Y., Cheng, B., Wu, L., Deng, J., Hu, W., Ren, L., Wei, L., Zhao, W., Tian, Y., Pan, X., Sun, Y., Wang, Z., Wu, F., Liu, C.-Q., Su, H., Penner, J. E., Pöschl, U., Andreae, M. O., Cheng, Y., and Fu, P.: Brown carbon from biomass burning imposes strong circum-Arctic warming, One Earth, 5, 293-304, 10.1016/j.oneear.2022.02.006, 2022.
Zhang, Q., Worsnop, D. R., Canagaratna, M. R., and Jimenez, J. L.: Hydrocarbon-like and oxygenated organic aerosols in Pittsburgh: Insights into sources and processes of organic aerosols, Atmos. Chem. Phys., 5, 3289, 2005a.
Zhang, Q., Canagaratna, M. R., Jayne, J. T., Worsnop, D. R., and Jimenez, J. L.: Time and size-resolved chemical composition of submicron particles in Pittsburgh - Implications for aerosol sources and processes, J. Geophys. Res., 110, 10, 2005b.
Zhang, Q., Jimenez, J. L., Canagaratna, M. R., Ulbrich, I. M., Ng, N. L., Worsnop, D. R., and Sun, Y.: Understanding atmospheric organic aerosols via factor analysis of aerosol mass spectrometry: a review, Anal Bioanal Chem, 401, 3045-3067, 10.1007/s00216-011-5355-y, 2011.
Zhang, Q., Shen, Z., Zhang, L., Zeng, Y., Ning, Z., Zhang, T., Lei, Y., Wang, Q., Li, G., Sun, J., Westerdahl, D., Xu, H., and Cao, J.: Investigation of Primary and Secondary Particulate Brown Carbon in Two Chinese Cities of Xi'an and Hong Kong in Wintertime, Environmental Science & Technology, 54, 3803-3813, 10.1021/acs.est.9b05332, 2020a.
Zhang, Q., Shen, Z., Zhang, T., Kong, S., Lei, Y., Wang, Q., Tao, J., Zhang, R., Wei, P., Wei, C., Cui, S., Cheng, T., Ho, S. S. H., Li, Z., Xu, H., and Cao, J.: Spatial distribution and sources of winter black carbon and brown carbon in six Chinese megacities, Science of The Total Environment, 762, 143075, https://doi.org/10.1016/j.scitotenv.2020.143075, 2021a.
Zhang, X., Xu, J., and Kang, S.: Chemical characterization of submicron particulate matter (PM1) emitted by burning highland barley in the northeastern part of the Qinghai–Tibet Plateau, Atmospheric Environment, 224, 10.1016/j.atmosenv.2020.117351, 2020b.
Zhang, X., Xu, J., Kang, S., Zhang, Q., and Sun, J.: Chemical characterization and sources of submicron aerosols in the northeastern Qinghai–Tibet Plateau: insights from high-resolution mass spectrometry, Atmospheric Chemistry and Physics, 19, 7897-7911, 10.5194/acp-19-7897-2019, 2019a.
Zhang, X., Xu, J., Kang, S., Sun, J., Shi, J., Gong, C., Sun, X., Du, H., Ge, X., and Zhang, Q.: Regional Differences in the Light Absorption Properties of Fine Particulate Matter Over the Tibetan Plateau: Insights From HR-ToF-AMS and Aethalometer Measurements, Journal of Geophysical Research: Atmospheres, 126, 10.1029/2021jd035562, 2021b.
Zhang, Y., Wang, Q., Tian, J., Li, Y., Liu, H., Ran, W., Han, Y., Prévôt, A. S. H., and Cao, J.: Impact of COVID-19 lockdown on the optical properties and radiative effects of urban brown carbon aerosol, Geoscience Frontiers, 13, 101320, https://doi.org/10.1016/j.gsf.2021.101320, 2022.
Zhang, Y., Favez, O., Petit, J.-E., Canonaco, F., Truong, F., Bonnaire, N., Crenn, V., Amodeo, T., Prévôt,

A. S. H., Sciare, J., Gros, V., and Albinet, A.: Six-year source apportionment of submicron organic aerosols from near-continuous highly time-resolved measurements at SIRTA (Paris area, France), Atmospheric Chemistry and Physics, 19, 14755-14776, 10.5194/acp-19-14755-2019, 2019b.

Zhang, Y., Albinet, A., Petit, J.-E., Jacob, V., Chevrier, F., Gille, G., Pontet, S., Chrétien, E., Dominik-Sègue, M., Levigoureux, G., Močnik, G., Gros, V., Jaffrezo, J.-L., and Favez, O.: Substantial brown carbon emissions from wintertime residential wood burning over France, Science of The Total Environment, 743, 10.1016/j.scitotenv.2020.140752, 2020c.

Zhong, M., Xu, J., Wang, H., Gao, L., Zhu, H., Zhai, L., Zhang, X., and Zhao, W.: Characterizing water-soluble brown carbon in fine particles in four typical cities in northwestern China during wintertime: integrating optical properties with chemical processes, Atmos. Chem. Phys., 23, 12609-12630, 10.5194/acp-23-12609-2023, 2023.

Zhu, C.-S., Cao, J.-J., Hu, T.-F., Shen, Z.-X., Tie, X.-X., Huang, H., Wang, Q.-Y., Huang, R.-J., Zhao, Z.-Z., Močnik, G., and Hansen, A. D. A.: Spectral dependence of aerosol light absorption at an urban and a remote site over the Tibetan Plateau, Science of The Total Environment, 590-591, 14-21, https://doi.org/10.1016/j.scitotenv.2017.03.057, 2017.

Zhu, C. S., Qu, Y., Huang, H., Chen, J., Dai, W. T., Huang, R. J., and Cao, J. J.: Black Carbon and Secondary Brown Carbon, the Dominant Light Absorption and Direct Radiative Forcing Contributors of the Atmospheric Aerosols Over the Tibetan Plateau, Geophysical Research Letters, 48, 10.1029/2021gl092524, 2021.